Investigating the properties of glioma-associated microglia/macrophages

Dissertation zur Erlangung des akademischen Grades des

Doktors der Naturwissenschaften (Dr. rer. nat.)

Eingereicht im

Fachbereich Biologie, Chemie, Pharmazie der Freien Universität Berlin

vorgelegt von

Frank Szulzewsky

aus Rüdersdorf

2014

Diese Arbeit wurde am Max-Delbrück Zentrum für Molekulare Medizin von September 2011 bis Dezember 2014 unter der Leitung von Prof. Helmut Kettenmann angefertigt.

1. Gutachter: Prof. Helmut Kettenmann
2. Gutachter: Prof. Fritz Rathjen

Tag der Disputation: 26.3.2015

Acknowledgements

I would like to thank Professor Helmut Kettenmann for the opportunity to perform my PhD in his lab and for his support and the possibilities he offered me during this time.

I would also like to thank Dr. Susanne Wolf and Dr. Vitali Matyash for their guidance and input during this time.

Special thanks to Prof. Fritz Rathjen who agreed to supervise my PhD at the FU Berlin.

I would also like to thank my collaboration partners during this time without whom I would not have been able to complete this project: Prof. Dolores Hambardzumyan, Dr. Xi Feng, and Dr. Ilaria Tamagno from the Cleveland Clinic, Prof. Erik Boddeke and Inge Holtman from the Groningen University, Prof. Thomas Langmann, Dr. Michael Synowitz, and Dr. Darko Markovic.

I would also like to thank my former student Andreas Pelz and my current student Nina Schwendinger for their hard work and for their patience during my first attempts at teaching.

Special thanks also to our lab technicians who made my life so much easier: Regina Piske, Irene Haupt, Hanna Schmidt, and Nadine Scharek. Special thanks also to Birgit Jarchow.

Furthermore, I would like to thank my current and former colleagues and friends for their support and the fun times: Petya Georgieva, Philipp Jordan, Nadine Richter, Daniele Mattei, Maria Pannell, Felipe Sassi, Feng Hu, Min Chi Ku, and everyone else I couldn't mention.

Last but not least, I would like to thank my parents who supported me during all those years of studies!

Thank you!

Table of Contents

List of Figures

List of Tables

List of Abbreviations

Adenosine triphosphate (ATP)
Base pair (bp)
Complementary DNA (cDNA)
Central Nervous System (CNS)
Cluster of differentiation (CD)
Complementary RNA (cRNA)
Deoxyribonucleic acid (DNA)
Ethylenediaminetetraacetic acid (EDTA)
Enhanced green fluorescent protein (*eGFP*)
For example, exempla gratia (e.g.)
Fluorescence activated cell sorting (FACS)
Fetal calf serum (FCS)
Gravital force (g)
Glioma-associated microglia/ macrophages (GAMs)
Glioblastoma multiforme (GBM)
Gene expression dynamic inspector (GEDI)
Gene ontology (GO)
Hour (h)
Intra-peritoneal (i.p.)
Magnetic-activated cell sorting (MACS)
Minute (min)
Natural killer cells (NK cells)
Postnatal day (P)
Polymerase Chain Reaction (PCR)
Platelet-derived growth factor b (*PDGFb*)
Quantitative reverse transcription PCR (qRT-PCR)
Red fluorescent protein (*RFP*)
Ribonucleic acid (RNA)
Room temperature (RT)
Rounds per minute (rpm)
The Cancer Genome Atlas (TCGA)
Uridine triphosphate (UTP)
Weighted gene coexpression network analysis (WGCNA)
Wild-type (WT)

1. Introduction

1.1. Glioblastoma multiforme

Malignant glioma (WHO grade III and IV) are highly aggressive types of brain tumors and account for almost 80% of all malignant brain neoplasms (Dolecek, Propp et al. 2012). Each year 14,000 new cases of malignant glioma are diagnosed in the U.S. alone. The most aggressive and most common form of glioma is the grade IV glioma, also called glioblastoma multiforme (GBM). As of today no successful treatment exists, offering GBM patients an average survival time of about 12-15 months after diagnosis, despite surgical tumor resection, radio-, and chemotherapy (Wen and Kesari 2008).

Reasons for the failure of GBM treatment are diverse. One feature of GBM is the highly invasive growth pattern into the brain parenchyma which prevents complete surgical resection of the tumor. Even though GBM can be visualized on MRI as mass lesions with enhanced contrast, tumor cells migrate deep into the brain parenchyma and far beyond the visualized tumor area. Recurring GBM after surgical resection often reappear close to the margins of the resected primary tumor, but also at locations distant from the original tumor location and can also cross over to the contra-lateral hemisphere (Figure 1) (Holland 2000).

Another cause for the failure of treatment is the genetic and cellular inter- and intra-tumor heterogeneity of GBMs (Phillips, Kharbanda et al. 2006; Brennan, Momota et al. 2009; Chen, McKay et al. 2012; Sottoriva, Spiteri et al. 2013; Francis, Zhang et al. 2014; Patel, Tirosh et al. 2014). Several different subtypes of GBM have been proposed, classifying tumors according to the mutated and activated genes and pathways that drive tumor growth. However, even within one tumor different subpopulations/subclones of tumor cells exist that differ in the acquired mutations and activated, tumor-driving pathways.

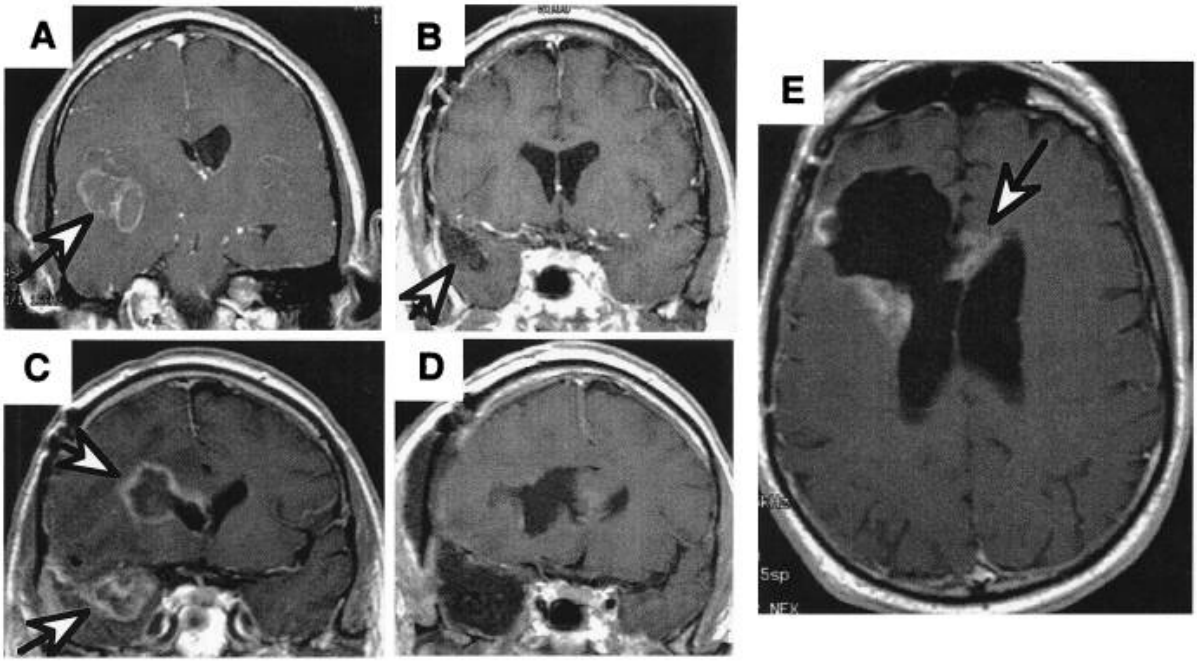

Figure 1 – Series of consecutive MRI scans of a patient with GBM showing recurrence after standard of care treatment.
(*A*) Presurgical scan. (*B*) Scan after ''gross total resection'' showing resection cavity, and (*C*) six months later, showing recurrence at the primary tumor location (arrow) as well as a second focus (arrow). (*D*) Postresection scans of both recurrent tumors. (*E*) 3 months later, scan showing the tumor recurring at the resection margin and crossing to the contralateral hemisphere (arrow). Image taken from (Holland 2000).

Furthermore, GBMs are heterogeneous with regard to their cellular composition. In addition to the actual neoplastic tumor cells, the tumor also comprises a multitude of cells from the microenvironment that interact with the tumor cells in various ways and influence the efficacy and efficiency of glioma therapy. In addition to rapidly dividing tumor bulk cells that account for the majority of the tumor cells, increasing evidence supports the existence of quiescent glioma-initiating cells that are resistant to chemo- and radiotherapy and thereby responsible for tumor relapse. Among others, the tumor microenvironment includes entrapped cells of the CNS and invading immune cells, such as CNS-specific microglia and blood born peripheral macrophages and monocytes. The focus of this work is directed towards the interaction of glioma cells with innate immune cells, specifically with brain-resident microglia and peripheral macrophages/monocytes (Charles, Holland et al. 2011; Jones and Holland 2012).

1.1.1. Histological classification of glioma

Glioma are classified based on a histological resemblance of the tumor cells compared to cell types in the healthy brain tissue. They are histologically heterogeneous tumors and comprise all brain tumors with tumor cells morphologically resembling glial (-like) cell types including astrocytomas, oligodendrocyctomas, and ependymomas (Louis, Ohgaki et al. 2007; Wen and Kesari 2008). Glioma can be graded according to their malignancy into the WHO grade I-IV, with IV being the most malignant. Grade I glioma (e.g. pilocytic astrocytoma) are non-infiltrating tumors with low cell proliferation that can be cured by resection alone. Grade II glioma (e.g. diffuse astrocytoma, well-differentiated oligodendrogliomas, and oligoastrocytomas) are more infiltrative and are likely to recur after surgery. The cell proliferation of the tumor cells is still relatively low. Both grade 1 and 2 are termed low-grade glioma. Grade III glioma (e.g. anaplastic astrocytoma, anaplastic oligodendrogliomas, and anaplastic oligoastrocytomas) are malignant tumors with a high proliferative potential and characterized by nuclear atypia. Grade IV glioma (GBM) are the most aggressive forms of brain tumors; they are highly proliferative and invasive and the tumor cells are pleomorphic and morphologically undifferentiated. GBM typically display necrosis and microvasculature proliferation (Figure 2) (Wen and Kesari 2008).

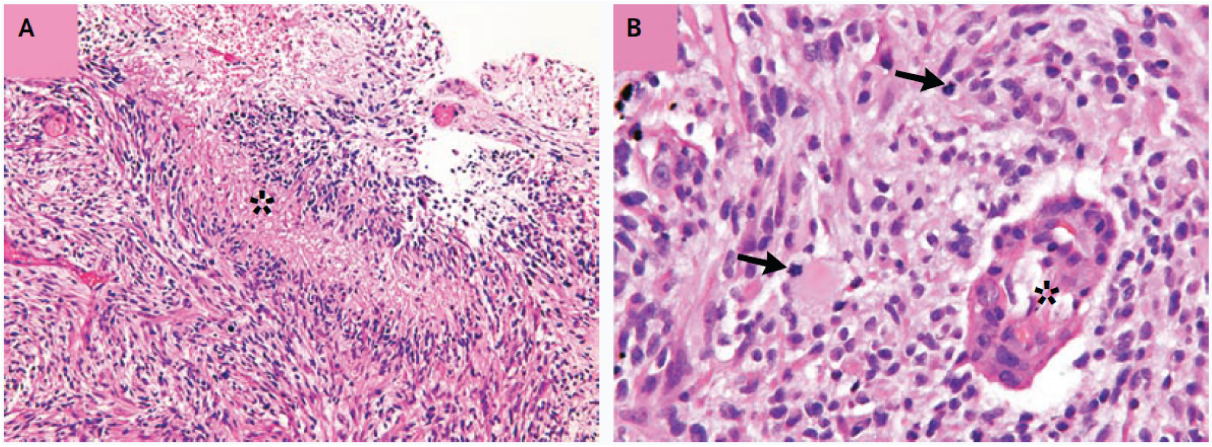

Figure 2 – Histological features of GBM.
GBM tissue stained with hematoxylin and eosin depicting typical features of GBM, such as nuclear pleomorphism, dense cellularity, and pseudopalisading necrosis (asterisk) (A), as well as vascular endothelial proliferation (asterisk) and mitotic figures (arrows) (B). Image modified from (Wen and Kesari 2008).

1.1.2. Genetic classification of GBM

GBM can be divided into primary and secondary GBM. The majority of the cases are primary GBM (around 90%), that develop "de novo", without evidence of a less malignant precursor. In contrast, secondary GBM gradually evolve from an initially lower-grade glioma (grade II or III) into GBM (Ohgaki and Kleihues 2009). Histologically, primary and secondary GBM are indistinguishable, however, they develop via different genetic lesions and have a different epidemiology (Figure 3). Patients suffering from secondary GBM tend to be younger (average of 40 years old versus 55 years of age for patients with primary GBM) and have a slightly better prognosis and overall survival time (Wen and Kesari 2008; Wilson, Karajannis et al. 2014).

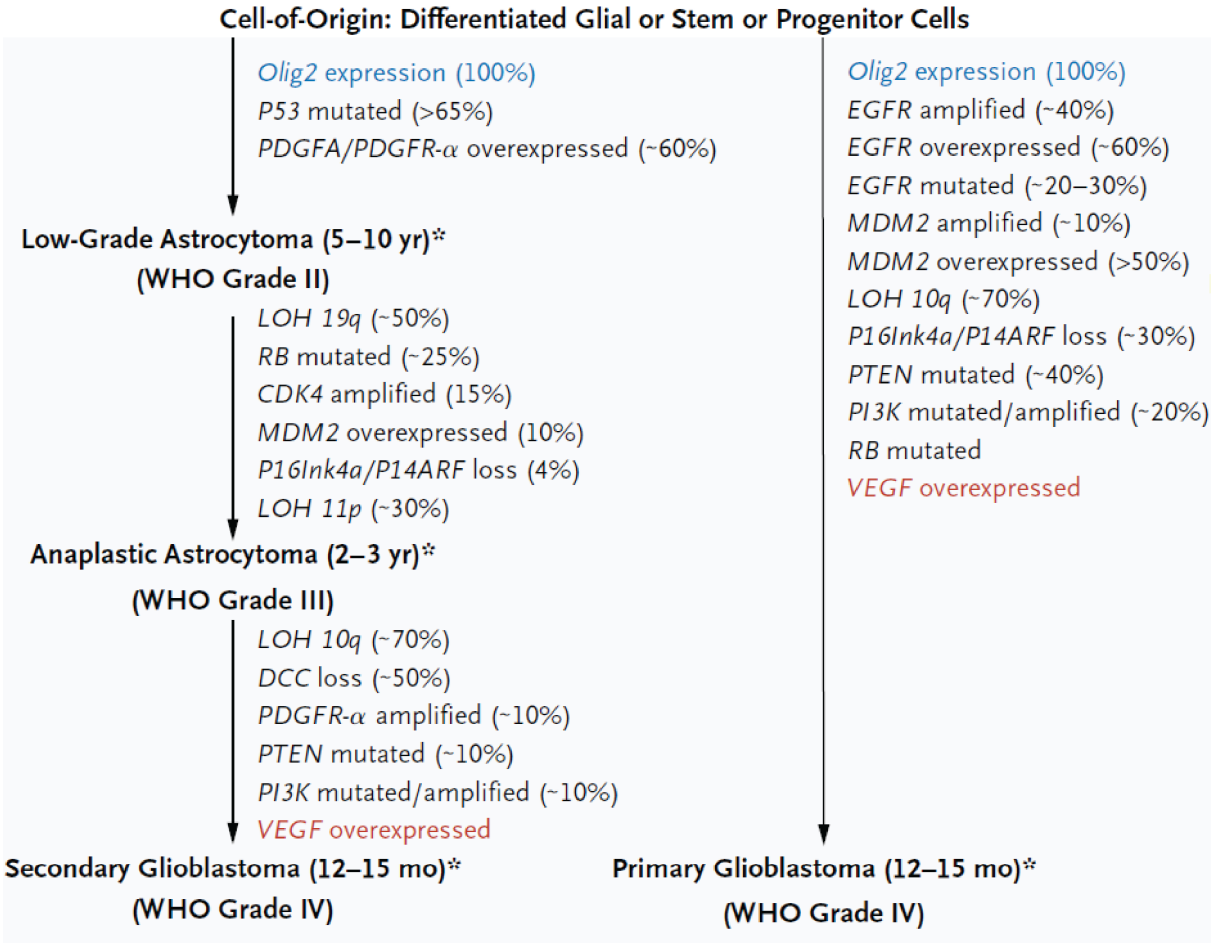

Figure 3 – Frequent mutations in the development of primary and secondary GBM. Image modified from (Wen and Kesari 2008).

Apart from the histological classification, which focuses on the morphological appearance of the tumor cells, malignant glioma are also grouped according to the underlying genetic lesions (Phillips, Kharbanda et al. 2006; Brennan, Momota et al. 2009; Guan, Vengoechea et al. 2014; Patel, Tirosh et al. 2014). GBM can be grouped into 4 different subtypes: classical, mesenchymal, proneural, and neural. The classical subtype is characterized by amplification of chromosome 7, leading to *EGFR* overexpression, paired with loss of chromosome 10. There is a lack of mutations of *TP53* in this subtype, however, *CDKN2A* is frequently deleted. Classical tumors show high expression of astrocytic markers. The mesenchymal subtype is characterized by deletions of the *NF1* and *PTEN* gene. These tumors also express astrocytic markers, however also display higher expression of mesenchymal markers (e.g. CD44). This may be due to increased infiltration of mesenchymal cells into these tumors. The proneural subtype is characterized by alterations in *TP53*, *PDGFR*, and *IDH1*. This subtype shows high expression levels of genes associated with oligodendrocytic developmental genes, such as *PDGFRA*, *OLIG2*, and *NKX2-2*. The neural subtype is characterized by gene expression pattern similar to normal brain tissue and the expression of neuron markers, such as *NEFL*, *GABRA1*, *SYT1*, and *SLC12A5* (Phillips, Kharbanda et al. 2006; TheCancerGenomeAtlas 2008; Brennan, Momota et al. 2009; Verhaak, Hoadley et al. 2010).

These different subtypes have different clinical prognosis and react differently to treatment. The proneural subtype is associated with better prognosis and increased survival compared to the other subtypes. However, aggressive treatment with chemotherapy and radiotherapy has been shown to significantly prolong survival in patients with classical or mesenchymal GBM, but no survival benefit has been observed in proneural GBM (Verhaak, Hoadley et al. 2010). A recent publication investigated the localization of different subtypes across different areas within the tumor (Gill, Pisapia et al. 2014). They found that the contrast-enhancing core of GBM samples predominantly clustered into the proneural, classical, or mesenchymal subtype, whereas non-contrast-enhancing tumor-margins predominantly clustered into the neural subtype. These tumor margin areas contained a significantly higher percentage of neurons and oligodendrocytes when compared to central tumor areas, which might be in part responsible for the high expression of neuronal genes in the neural subtype.

Recent reports showed that there is a large degree of heterogeneity even within a single GBM tumor. Analysis of different tumor parts and single cell analysis of GBM cells has shown that tumor cells within one tumor can have different subtypes. This possibly reflects the evolution of the tumor cells that stepwise acquire different mutations that give them a higher survival benefit. Cells in different locations probably originate from an earlier ancestor, which co-evolved and gained different mutations during disease progression (Sottoriva, Spiteri et al. 2013; Francis, Zhang et al. 2014; Patel, Tirosh et al. 2014). This intra-tumor heterogeneity is one of the biggest obstacles for successful glioma therapy.

1.1.3. Cellular hierarchy in GBM

Similar to non-neoplastic stem cells in adult tissues, glioma stem (-like) cells, also termed glioma-initiating cells, are defined by their ability to give rise to all cell types of the tumor – with the exception of non-neoplastic stromal cells – and their ability to self-renew. The concept of the cancer stem cell in glioma emerged when it was shown that $CD133^+$ cells, isolated from human brain tumor samples, could be cultured under stem-cell promoting conditions *in vitro*, demonstrated multipotency, the ability to self-renew, and to reform tumors that resembled the original tumor upon consecutive (re)transplantations into immunodeficient mice (Singh, Clarke et al. 2003; Singh, Hawkins et al. 2004). However, to date there is still a dispute about the actual population of glioma stem cells and potential markers for the isolation and definition of these cells (Gilbert and Ross 2009).

The concept of the glioma stem cell is of critical clinical relevance, as these cells seem to be resistant to the current standard of care for GBM patients and could explain the resistance of these tumors to treatment and subsequent relapse. In contrast to the rapidly dividing tumor bulk cells that are susceptible to radio- and chemotherapy, the quiescent stem cells have been shown to be resistant to these therapies (Dean, Fojo et al. 2005; Bao, Wu et al. 2006; Liu, Yuan et al. 2006; Bleau, Hambardzumyan et al. 2009).

1.1.4. Cell of origin for glioma

By the time a tumor has become large enough to be detected in the clinic it is already too late to detect the cell of origin, meaning the cell that acquired the initial beneficial mutation that started the formation of a premalignant cell mass, which in turn would acquire additional mutations in an evolutionary manner and finally give rise to the tumor (Sukhdeo, Hambardzumyan et al. 2011). Despite the expression of common stem cell markers in glioma-initiating cells it is not known if the cell of origin for GBM is a stem or progenitor cell or a differentiated cell that acquired self-renewal capacity during transformation. The infiltrative nature of gliomas states a further problem for the identification of the cell and the region of origin.

Subventricular zone (SVZ) stem or progenitor cells as well as fully differentiated astrocytes have been discussed as cells of origin for malignant gliomas (Bachoo, Maher et al. 2002). However, in this *in vitro*-based study the authors could not rule out the possibility of a contamination with stem or progenitor cells in their astrocytic cultures. Further experiments demonstrated *in vivo* that tumor suppressor inactivation in neural stem/progenitor cells, but not in differentiated astrocytes, is necessary and sufficient to induce malignant gliomas, thus identifying neural stem/progenitor cells as the cells of origin (Alcantara Llaguno, Chen et al. 2009; Wang, Yang et al. 2009; Visvader 2011).

A recent study used a transgenic mosaic analysis cell-labeling system to track tumor growth in an inducible mouse model of gliomagenesis by sporadically inducing *Trp53/Nf1* mutations in neural stem cells. The authors detected significant aberrant growth prior to tumor formation only in oligodendrocyte precursor cells, but not in other-lineage precursor cells or neural stem cells (Liu, Sage et al. 2011).

Finally, using the RCAS/tv-a mouse glioma model, that is based on somatic cell viral gene delivery, Holland and colleagues found that when they induced aberrant *Kras* and *Akt* expression in *Nestin*-expressing cells (SVZ stem and progenitor cells) in wildtype mice, they could generate classical subtype GBM in 26% of the animals. In turn, no animals developed GBMs upon targeting *GFAP*-expressing cells (SVZ progenitor cells and mature astrocytes) (Holland, Celestino et al. 2000). In later studies using the same genetic lesions, they found that 44% of *Ink4a*$^{-/-}$ mice developed GBM when targeting *Nestin*-expressing cells, whereas only 5% of these mice developed GBM when targeting *GFAP*-expressing cells. In turn, when using *Arf*$^{-/-}$ animals, 83% of the animals developed GBM upon targeting *GFAP*-expressing

cells, but only 65% of mice upon targeting *Nestin*-expressing cells (Uhrbom, Kastemar et al. 2005). When overexpressing human *PDGFb* to generate proneural GBM they could not find any difference in tumor incidence between *Nestin* or *GFAP*-expressing cells (Hambardzumyan, Amankulor et al. 2009).

This may point to the fact that different initial genetic lesions may function in different cell types to generate subtypes of GBM. Therefore, different subtypes of GBM may have different cells of origin.

1.2. Standard of care treatment for glioblastoma

Standard of care treatment for GBM comprises gross surgical tumor resection, chemotherapy and radiotherapy. However, even with full treatment there is currently no cure for GBM. Surgery helps to reduce the symptoms caused by the tumor mass, such as intra-cranial tension that causes nausea, headaches, and seizures, but is not suitable to cure GBM due to the invasive nature of these tumors. Nevertheless maximal safe surgical resection has been shown to prolong survival and is recommended as an initial therapeutic step (Wen and Kesari 2008; Weathers and Gilbert 2014; Wilson, Karajannis et al. 2014).

In addition to surgical resection radio- and chemotherapy are used. Usually 60 Gy of ionizing radiation are administered to the surgical resection cavity and a margin of surrounding brain tissue. Ionizing radiation induces DNA damage in proliferating cells. It has been shown that the combined treatment of radiotherapy and administration of temozolomide, a DNA-alkylating cytotoxic agent, significantly prolongs overall survival of GBM patients (Figure 4) (Stupp, Mason et al. 2005). O-6-methylguanine-DNA methyltransferase (encoded by the *MGMT* gene) is a DNA repair enzyme that reverses the damage caused by alkylating agents (such as temozolomide) and has been implicated as a major mechanism of resistance to these drugs. The expression of this gene is regulated by the methylation status of its promoter, therefore tumors with methylated *MGMT* promoters are more susceptible to temozolomide treatment (TheCancerGenomeAtlas 2008; Wen and Kesari 2008; Weathers and Gilbert 2014; Wilson, Karajannis et al. 2014).

Chemo- and radiotherapy primarily target rapidly dividing, dedifferentiated bulk cells in GBM. Increasing evidence suggests the existence of quiescent, stem-like glioma-initiating cells. These cells are thought to evade chemo- and radiotherapy due to their quiescent state, and the expression of DNA repair enzymes (Bao, Wu et al. 2006)

and ABC (ATP-binding cassette) transporters (Dean, Fojo et al. 2005; Bleau, Hambardzumyan et al. 2009), and to reestablish the recurring tumor (Chen, Li et al. 2012; Jones and Holland 2012).

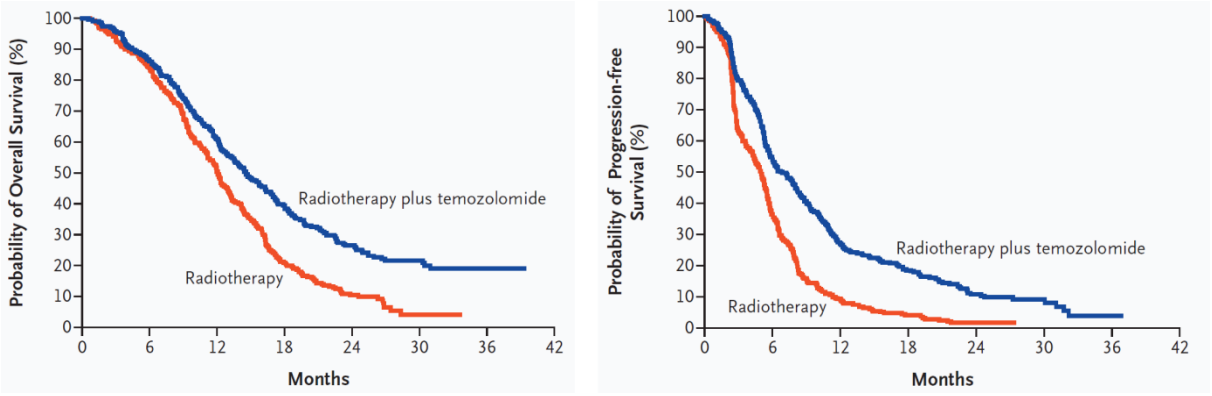

Figure 4 – The addition of temozolomide to standard of care therapy prolongs average survival of GBM patients.
Patients treated with temozolomide, in addition to surgery and radiotherapy exhibit an increased average overall survival (left panel) and progression-free survival (right panel). Image modified from (Stupp, Mason et al. 2005).

1.2.1. Molecularly targeted therapies

In addition to the standard of care therapy approaches several molecularly targeted therapies that target tumor-specific recurrent genetic alterations are currently under investigation. These therapeutic agents can be divided into small-molecule inhibitors, that can penetrate the cell wall and often target intracellular kinase domains or downstream effectors of receptor tyrosin kinases (such as EGFR and PDGFR; AKT and PI3K), and monoclonal antibodies that target and block soluble factors or extracellular domains of membrane proteins (such as bevacizumab which targets Vascular endothelial growth factor (VEGF)). These therapies aim to target either pathways in the tumor cells, such as aberrantly activated growth factor signaling pathways, or in the tumor stroma, for example angiogenic pathways. Unfortunately, clinical trials with these treatments have shown very limited effect (Raizer, Abrey et al. 2010; Yung, Vredenburgh et al. 2010; Kesavabhotla, Schlaff et al. 2012; Rahmathulla, Hovey et al. 2013; Chinot, Wick et al. 2014; Gilbert, Dignam et al. 2014). This might be due to limited penetrance of these agents in the tumor, redundancies of aberrant signaling pathways in the tumor cells, as well as the great heterogeneity of tumor cells within the tumor, which rely on different pathways.

1.2.2. Viral therapy

Another approach of a potential glioma therapy is viral therapy, meaning either the delivery of potential tumor-toxic genes to tumor cells, stimulation of the immune system by the expression of specific cytokines by the virus, or the direct lysis of tumor cells by genetically engineered viruses (Russell, Peng et al. 2012; Auffinger, Ahmed et al. 2013; Marsh, Goldfarb et al. 2013; Ning and Wakimoto 2014). Three phase I clinical studies on GBM patients showed that adenoviral-mediated delivery of *HSV-tk* to patients post-surgery resulted in a significantly increased overall survival time when compared to the control group that was treated with standard of care therapy, and that the procedure was generally well tolerated by the patients (Sandmair, Loimas et al. 2000; Immonen, Vapalahti et al. 2004; Chiocca, Aguilar et al. 2011). Factors that could hinder the anti-glioblastoma efficacy of viral approaches include the attenuated virulence of the viruses due to deletion or mutation of viral genes to improve safety, restricted viral spread within the tumor, and the inability of the viruses to infect diffusely infiltrating tumor cells at the margins of the tumor. One of the biggest obstacles of these approaches is the need of a specific receptor for the viruses to infect the tumor cells. Considering the heterogeneity and genetic instability of the tumor cells, it is likely that receptor-negative clones will emerge and render the tumor resistant to this kind of therapy.

1.2.3. Immunotherapy

The goal of immunologic therapies is to enhance recognition of glioma cells by the immune system and to increase the activity of tumor-infiltrating lymphocytes, either by stimulating the immune system via the administration of tumor-antigen specific antibodies or by autologous transfer of engineered immune cells, such as T or dendritic cells (Sampson, Heimberger et al. 2010; Marsh, Goldfarb et al. 2013). Clinical and animal studies investigating autologous transplantations of primed dendritic cells or antigen-specific T cells (specific against EGFRvIII or EPHA2) demonstrated safety and prolonged survival, but showed also therapy evasion of glioma cells that ultimately led to patient death (Yamanaka, Homma et al. 2005; De Vleeschouwer, Fieuws et al. 2008; Chang, Huang et al. 2011; Choi, Kuan et al. 2013; Chow, Naik et al. 2013; Chung, Shin et al. 2014; Schumacher, Bunse et al. 2014).

In conclusion, it must be said that therapies that are directed against one or multiple specific traits – a specific pathway or antigen – of the tumor cells may be suitable to

prolong survival of patients, but will fail to cure GBM. Even if a dominant subclone within a GBM tumor can be targeted, for example by pharmacological blocking of a pathway, antibody-based therapy, or T or dendritic cell-based immunotherapy against a tumor cell-specific antigen (Choi, Kuan et al. 2013; Chow, Naik et al. 2013; Marsh, Goldfarb et al. 2013), tumor cells that do not harbor or rely on this genetic trait can escape the therapy and lead to recurrence of a tumor that does not rely on this pathway. Hence, a systemic boost or activation of the immune system, which is not directed against a specific target may be more effective.

1.3. Tumor microenvironment

GBM are heterogeneous with regard to their cellular composition. Although the tissue and the margin around high grade glioma is usually devoid of neurons as these tumors release excitotoxic concentrations of glutamate (Ye and Sontheimer 1999; Takano, Lin et al. 2001; Sontheimer 2008), the tumor tissue also harbors a multitude of non-neoplastic stromal cells (Figure 5). Among these cells are entrapped naïve brain cells, such as astrocytes, pericytes, and oligodendrocytes, but also invading innate immune cells, such as brain-resident microglia, and peripheral macrophages, monocytes, dendritic cells, NK cells, and cells of the adaptive immune system (T and B cells). Although these cells are not of tumor-origin recent studies suggest that different type of cells can also have tumor-promoting functions.

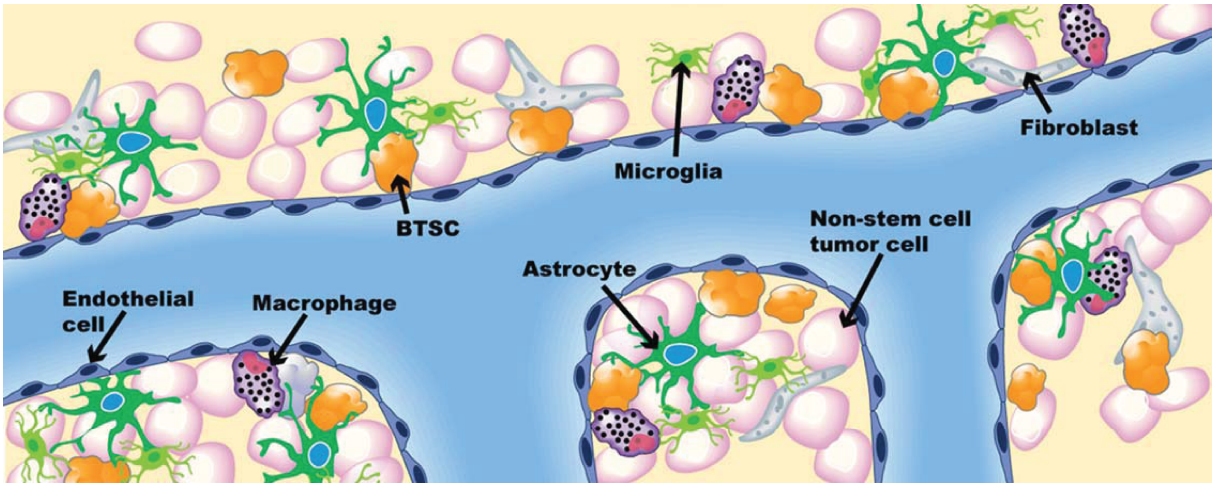

Figure 5 – The glioma microenvironment.
The glioma microenvironment consists of entrapped brain cells, such as astrocytes, cells that contribute to the vasculature (such as endothelial cells and fibroblasts), and invading immune cells (such as microglia, peripheral immune cells). Image taken from (Charles, Holland et al. 2011).

The tumor vasculature, formed by the interplay of endothelial cells, astrocytes, and pericytes, has different functions in the tumor. First it connects the tumor to the blood systems and supplies it with nutrients and oxygen. Tumors often display high microvascular proliferation and abnormal angiogenesis, and multiple angiogenic pathways are upregulated in tumor cells, but also in stromal cells (Wen and Kesari 2008). Second, the vasculature also constitutes a specialized niche for the glioma-initiating stem-like cells, the so-called perivascular niche (Charles, Holland et al. 2011).

Astrocytes are found within and around tumors and have been shown to play important roles for the tumor microenvironment. In the healthy brain astrocytes have different functions: structural support, nutrition of neurons, neurotransmitter uptake, as well as a role in the formation of the blood brain barrier. Astrocytic end-feet processes ensheath endothelial cells lining blood vessels and thereby contribute to the blood-brain barrier. Using gap junctions, multiple astrocytes can couple to larger networks and transport molecules, such as nutrients from blood vessels to neurons. Upon damage or in disease (such as GBM), astrocytes become reactive which is associated with breakdown of the blood brain barrier and increased vascular permeability. Reactive astrocytes can proliferate and secrete different factors that are also thought to promote glioma growth. Reactive astrocytes in glioma also produce stromal-derived factor 1 (SDF1), which can cause increased glioma cell proliferation and have been found to mediate glioma cell invasion by the activation of matrix metalloproteinase (MMP) 9 (Bajetto, Bonavia et al. 1999; Bajetto, Bonavia et al. 1999; Liu, Wu et al. 2010). A microarray screen of glioma-associated astrocytes revealed that these cells express potential pro-tumorigenic genes such as *Spp1*, *Ctgf*, and *Vgf* (Katz, Amankulor et al. 2012).

Invading immune cells play a double-edged role in glioma. Results from glioma animal models have shown that $CD11b^+$ microglia/macrophages support tumor growth and the depletion of $CD11b^+$ cells from a glioma mouse model resulted in prolonged survival of mice (Markovic, Vinnakota et al. 2009; Gabrusiewicz, Ellert-Miklaszewska et al. 2011). In contrast, increased invasion of $CD8^+$ effector T cells into the tumor tissue has been correlated with prolonged survival in patients (Lohr, Ratliff et al. 2011). However, several studies have shown that numbers of $CD4^+$ and $CD8^+$ T cells are decreased in high-grade glioma, and that these cells show abnormal and decreased functionality (Roszman and Brooks 1980; Morford, Elliott et

al. 1997; Fecci, Mitchell et al. 2006). In turn, studies have shown that glioma grade positively correlates with the numbers of infiltrating regulatory T cells (Tregs) and that depletion of $CD8^-/CD4^+/FoxP3^+$ Tregs from experimental gliomas resulted in increased survival of mice (El Andaloussi, Han et al. 2006; Jacobs, Idema et al. 2010; Wainwright, Chang et al. 2014). These cells have been implicated in participating in the establishment of an immunosuppressive milieu and preventing correct activation of immune cells, such as macrophages/monocytes and $CD4^+$ or $CD8^+$ T cells (Lowther and Hafler 2012).

1.4. Microglia in the CNS

Microglia are the professional phagocytes of the healthy brain and serve as the first line of defense against pathogens. In the healthy brain, microglia are distributed throughout the brain parenchyma, constantly scanning the surrounding tissue with their highly motile processes (Davalos, Grutzendler et al. 2005; Nimmerjahn, Kirchhoff et al. 2005). The disturbance of tissue homeostasis, e.g. the presence of a lesion, apoptotic cells, or microbial factors, leads to activation of the microglia. Activated microglia acquire an “amoeboid” morphology and can migrate to the site of the lesion, proliferate, release cytokines, and phagocytose (Hanisch and Kettenmann 2007; Kettenmann, Hanisch et al. 2011). Microglia are also involved in processes of the developing brain, such as removal of apoptotic neurons and synaptic pruning (Wake, Moorhouse et al. 2009; Paolicelli, Bolasco et al. 2011), as well as in homeostatic and regenerative processes in the adult brain, for example removal of dysfunctional, damaged cells or apoptotic cells and the uptake of molecules, such as debris and metabolites (Kettenmann, Hanisch et al. 2011). Upon damage of the blood brain barrier – e.g. caused by radiation or during different CNS diseases which involve a pronounced inflammation, such as glioma, multiple sclerosis or stroke – infiltration of peripheral immune cells occurs, among others also blood-borne monocytes and macrophages (Kerber, Reiss et al. 2008; Amantea, Nappi et al. 2009; Ransohoff 2011).

1.4.1. Activation/polarization states of microglia/macrophages

Microglia/macrophages can be polarized towards different activation states *in vitro*. When exposed to microbial products (e.g. lipopolysaccharide (LPS)) alone, or with additional co-stimulation by interferon-γ (IFN-γ) (produced by Th1 cells *in vivo*),

microglia/macrophages acquire a so-called classically-activated, pro-inflammatory phenotype (also termed M1 phenotype). The M1 phenotype is characterized by a high antigen-presentation capacity, production of the cytokines interleukin-1β (IL-1β), IL-6, IL-12, IFN-γ, and tumor necrosis factor alpha (TNF)-α, as well as high levels of nitric oxide (NO) and reactive oxygen species (ROS) (Mantovani, Sica et al. 2004; Kigerl, Gensel et al. 2009; Li and Graeber 2012). In contrast, when stimulated *in vitro* with the anti-inflammatory cytokines IL-4, IL-10 or IL-13 (major cytokines of Th2 cells) microglia/macrophages acquire an alternatively-activated phenotype, the so-called M2 phenotype. Alternative activation can be further divided into M2a (Th2 responses, type II inflammation, killing of pathogens, allergy), M2b (Th2 activation, immunoregulation), and M2c (immunoregulation, matrix deposition, tissue remodeling) activation (Mantovani, Sica et al. 2004). Generally speaking, M2-activated microglia/macrophages are thought to promote angiogenesis and tissue remodeling, which is mediated by the release of matrix-metalloproteinases and enhanced phagocytosis, e.g. of apoptotic cells or extracellular matrix (ECM) components. The enhancement of phagocytosis might be mediated at least partially by the increased production of scavenger receptors (Gratchev, Kzhyshkowska et al. 2005; Kigerl, Gensel et al. 2009). Furthermore, M2-activated microglia/macrophages downregulate inflammation via the production of anti-inflammatory molecules (e.g. transforming growth factor-β (TGF-β), IL-10, IL-1RA, arginase-1 (ARG1)) and possess a lower antigen-presenting capacity than M1-activated cells (Mantovani, Sica et al. 2004; Sica, Schioppa et al. 2006; Kigerl, Gensel et al. 2009).

The M1 and M2 phenotypes represent very useful tools for studying myeloid cell activation in acute inflammation, however, it is becoming increasingly clear that these "extreme" *in vitro* activation states only show a very incomplete picture of the dynamic activation properties of microglia/macrophages and the complex interplay of thousands of signaling molecules present *in vivo*, for example in chronic inflammation or cancer (Mosser and Edwards 2008; Lawrence and Natoli 2011; Xue, Schmidt et al. 2014). Recent findings demonstrate that macrophages acquire activation states independent from the bipolar M1/M2 axis when activated by free fatty acids, high-density lipoprotein (HDL), or combinations of stimuli associated with chronic inflammation (Xue, Schmidt et al. 2014). This highlights that macrophage activation is much more complex and diverse than previously recognized.

1.4.2. Microglia/macrophages in malignant glioma

Among other immune cells, brain-resident microglia and peripheral macrophages and monocytes are attracted toward glioma in large numbers and can amount up to 30% of the cells in the tumor tissue (Badie and Schartner 2001; Strik, Stoll et al. 2004; Watters, Schartner et al. 2005; Kerber, Reiss et al. 2008; Charles, Holland et al. 2011). Their abundance positively correlates with malignancy, invasiveness and grading of gliomas (Rodero, Marie et al. 2008). Experimental findings show that an anti-tumor activity of the glioma-associated microglia/macrophages (GAMs) is prevented by the tumor cells and the tumor microenvironment. In contrast, GAMs actively support tumor growth. They enhance glioma cell invasion by the degradation of the ECM, support tumor angiogenesis, and mediate an immunosuppressive milieu (Kerber, Reiss et al. 2008; Markovic, Vinnakota et al. 2009; Charles, Holland et al. 2011; Li and Graeber 2012).

Current anti-glioma therapies, such as surgery, chemo-, and radiotherapy, directly target the tumor cells, however fail due to different reasons, such as the highly invasive growth, radio- and chemo-resistance of glioma-initiating cells, and the cellular and genetic inter- and intra-tumor heterogeneity (Bao, Wu et al. 2006; Phillips, Kharbanda et al. 2006; Brennan, Momota et al. 2009; Sottoriva, Spiteri et al. 2013; Patel, Tirosh et al. 2014). In this light, GAMs might serve as attractive targets for potential future anti-glioma therapies. Recent studies have investigated GAMs as therapeutic targets and have shown that targeting these cells can delay tumor growth (Markovic, Vinnakota et al. 2009; Markovic, Vinnakota et al. 2011; Kees, Lohr et al. 2012; Pyonteck, Akkari et al. 2013; Mok, Koya et al. 2014; Sarkar, Doring et al. 2014).

Several studies investigated the expression of selected genes in GAMs *in vitro* and *in vivo* (Umemura, Saio et al. 2008; Zhang, Alizadeh et al. 2009; Gabrusiewicz, Ellert-Miklaszewska et al. 2011; Kees, Lohr et al. 2012). Similar to solid tumors in other organs, GAMs produce factors associated with an alternative macrophage activation, such as increased production of anti-inflammatory molecules (e.g. TGF-β1, ARG1, and IL-10), and molecules supporting tissue remodeling and angiogenesis (e.g. VEGF, MMP2, MMP9, and MMP14). However, GAMs also produce pro-inflammatory molecules (e.g. TNFα, IL1β, and CXCL10) (Figure 6) (Sica, Schioppa et al. 2006; Umemura, Saio et al. 2008; Markovic, Vinnakota et al. 2009; Gabrusiewicz, Ellert-Miklaszewska et al. 2011; Li and Graeber 2012; Ye, Xu et al. 2012).

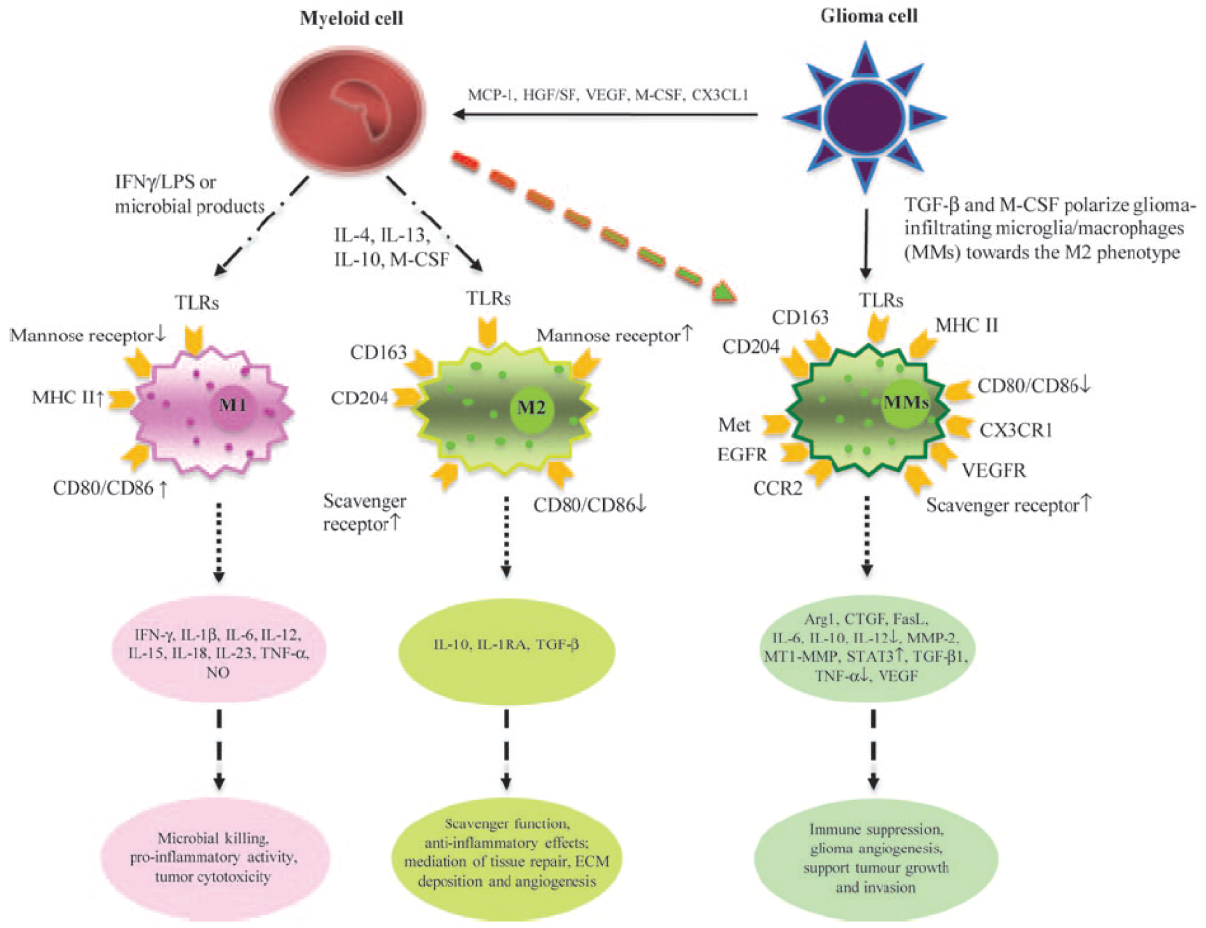

Figure 6 – Microglia/macrophages under the influence of glioma.
Several markers and secreted factors have been identified in GAMs. Studies have shown that GAMs express M1, as well as M2-associated genes. Image taken from (Li and Graeber 2012).

The exact mechanisms of glioma-microglia/macrophage interaction still remain unresolved. Possible factors that are released by the tumor cells and aid in the attraction of microglia/macrophage into the tumor tissue include colony-stimulating factor 1 (CSF-1), monocyte chemoattractant protein (MCP)-1, MCP-3, and glial cell-derived neurotrophic factor (GDNF) (Alterman and Stanley 1994; Papavasiliou, Mehler et al. 1997; Platten, Kretz et al. 2003; Okada, Saio et al. 2009; Ku, Wolf et al. 2013). However, reports about tumor-derived molecules polarizing GAMs are sparse. Postulated molecules include CSF-1, IL-4, and IL-10, but recent reports also suggest a TLR-mediated interaction (Pollard 2004; Sica, Schioppa et al. 2006; Markovic, Vinnakota et al. 2009; Vinnakota, Hu et al. 2013).

In conclusion, it can be said that the large number of these cells in the tumor microenvironment and their unique functionality makes them an attractive target for possible therapeutic approaches. It is crucial to further elucidate the role of these

cells in glioma progression and to identify new targets for stromal cell-directed anti-glioma therapy.

1.5. Fractalkine-fractalkine receptor signaling

There are many signals that keep microglia in homeostasis. It has been hypothesized that manipulating such signal cascades in favor of microglia anti-tumor activation could support new therapeutic approaches. One such effector/target pair is fractalkine and the fractalkine receptor.

The fractalkine receptor (also termed CX3CR1) is almost exclusively expressed by microglia in the naïve brain, and is also expressed in peripheral blood-borne circulating monocytes at lower levels (Harrison, Jiang et al. 1998; Biber, Neumann et al. 2007; Hu, Liou et al. 2014). The ligand fractalkine (also termed CX3CL1) is the most abundantly expressed chemokine in the CNS and is primarily expressed in neurons, but has also been shown to be expressed in activated endothelial and dendritic cells (Bazan, Bacon et al. 1997; Pan, Lloyd et al. 1997; Nishiyori, Minami et al. 1998; Kanazawa, Nakamura et al. 1999; Papadopoulos, Sassetti et al. 1999). Receptor and ligand have a mutually exclusive relationship and the ligand can either occur as a secreted or as a membrane-bound form (Garton, Gough et al. 2001). *Cx3cr1*-deficient mice exhibit higher microglial activation in combination with increased neuronal death in Alzheimer's and Parkinson's disease, suggesting a role of suppression of neurotoxic activity of microglia by the CX3CR1-CX3CL1 axis (Cardona, Pioro et al. 2006). In contrast, *Cx3cr1*-deficiency has also been reported to lead to decreased neuroinflammation and neuronal loss in a model of ischemia (Denes, Ferenczi et al. 2008). This might be explained by the different nature of CNS diseases. In diseases where brain-resident microglia are the predominant CNS effector cells, deficient CX3CR1 signaling is thought to be detrimental due to enhanced microglia activation. In turn, in diseases with prominent infiltration of peripheral macrophages and monocytes, deficient CX3CR1 signaling is thought to limit recruitment of these peripheral cells (Donnelly, Longbrake et al. 2011).

2. Aim of the thesis

Brain resident microglia and peripheral macrophages/monocytes invade the tissue of malignant glioma, become part of and modulate the tumor microenvironment, and have been shown to be reprogrammed by the tumor cells to support tumor growth. We and others have previously shown that GAMs support tumor growth by the production of molecules that support an immunosuppressive milieu (such as TGF-β1 and ARG1), tumor vascularization (VEGF), and tumor cell infiltration (MMP9, MMP14). However, to date no detailed study has been performed to investigate whole-genome expression changes to identify new effector functions and genes expressed by GAMs. In the second part of my study I investigated specifically the effect of *Cx3cr1*-deficiency in microglia on glioma-growth using a monocyte-free organotypic brain slice culture model.

Specific questions were:

Project 1: Genome-wide gene expression analysis of GAMs:

- What genes are upregulated or downregulated in GAMs?
- What is the difference in the regulation of these genes between resident microglia and peripheral macrophages/monocytes?
- What is the polarization state of GAMs in comparison to M1/M2 macrophages?
- Are these changes specific for one glioma model?
- Are they reflected in human glioma patient samples?
- Can we identify new target genes that might affect glioma growth?
- Do these genes have an effect on glioma growth in human patients?

Project 2: Effect of Cx3cr1-loss on GAMs in an organotypic brain slice model:

- What is the effect of microglial *Cx3cr1*-deficiency on glioma growth in a monocyte-free *in situ* model?
- What is the effect of *Cx3cr1*-deficiency on glioma-directed microglia migration in an *in situ* model?

3. Materials and Methods

11.0. Materials

11.0.1. Buffers and Media

ACK lysis buffer
pH 7,2 - 7,4
8.29 g/l NH_4Cl
1 g/l $KHCO_3$
37.2 mg/l Na_2-EDTA

Myelin gradient buffer
0,78 g/l $NaH_2PO_4 \cdot H_2O$
3,56 g/l $Na_2HPO_4 \cdot 2H_2O$
8 g/l NaCl
0,4 g/l KCl
2 g/l Glucose

22% Percoll solution
1x Myelin gradient buffer
22% Percoll (GE Healthcare, Little Chalfont, UK)
36 mM NaCl

Terrific Broth Medium (in dH_2O)
Tryptone 12 g/l
Yeast Extract 24 g/l
Glycerol 0.4%
Phosphate buffer solution 1x

Phosphate buffer solution (for Terrific Broth Medium, 10x)
0.17 M KH_2PO_4
0.72 M K_2HPO_4

11.0.2. Primer

Table 1 – Primers used for the validation of genes in mouse and human samples.

	Fwd	Rev
qRT-PCR Mouse Primers		
Actb	CGTGGGCCGCCCTAGGCACCA	CTTAGGGTTCAGGGGGGC
Cd200r4	GTTCATCTTCTCTGACACAAGTT	GAAGGCAGGTGTCTGTGT
Cd300lf	GCTGGCATTTACTGGTGTGG	GGTGGTGGTGGAGGTGATG
Clec7a	AGGCATCCCAAACTACAGGAG	GGAGCAGTGTCTCTTACTTCCAT
Creb5	CATGCAAGGTCCAAACCTCA	AGCCTTCAGTCTCATTTTGGC
Cxcl13	AGATCGGATTCAAGTTACGCC	GTAACCATTTGGCACGAGGAT
Cxcr4	GGCTGTAGAGCGAGTGTTGC	AGATGGTGGGCAGGAAGATCC
Gpnmb	AGAAATGGAGCTTTGTCTACGTC	CTTCGAGATGGGAATGTATGCC
Hpse	GGCCGGATGGATTACTTTCCA	TGCGGGGAGAGGTTTTTCTG
Il1rn	CAGAAAGGGCGGGAGATTTT	GGTTCATGGTGGACAACACT
Isg20	CGAGGGAGAGATCACGGACT	ACCACCAGCTTGCCTTTCAG
Ms4a4a	AAGGCTGTCACATGACCTTGTC	ACACATCACCCTGCATCCAAA
Ms4a4c	GCAAATCTATCTTCTGAACCACTC	GACAATGAACATTATTGGTCCCC
Sepx1	CTTCGGAGGCGAGGTTTTCC	GTGCGTACTTCGAGTGACTGG
Sh2d1b1	AGAGCTGAATGTTTATGAGAACAC	GCTTGCTTTGTCCAATGTCC
Spp1	AGCAAGAAACTCTTCCAAGCAA	GTGAGATTCGTCAGATTCATCCG
Tgfbi	CAGCACGGCCCCAATGTAT	GGGACCTTTTCATATCCAGGACA
Trem1	TTGTCTCAGAAGTCAAAGCTGC	TTCCCGTCTGGTAGTCTCTG
Uck2	CAGATCCCCGTGTACGACTTT	TCGGACCTCCTGGGAATAGAA

Nested-PCR Mouse Primers		
Actb N	CGAGCACAGCTTCTTTGCAG	TCCGGAGTCCATCACAATGC
Cd200r4 N	CCAGGGGGCTACGAATTGTG	AGTAGGTTACCTCAGGGGGC
Cd300lf N	GCCGATATACCTCAGGCTGG	CCTCACCATCCTCCAAGCAA
Clec7a N	GGAATCCTGTGCTTTGTGGT	CATGGCCCTTCACTCTGATT
Creb5 N	TCCATCTCCACAACAGACAGAG	GTTGTATTGTCTGGGTTGGCTG
Cxcl13 N	TAAAGGTTGAACTCCACCTCCAG	ACAAGGATGTGGGTTGGGTATG
Cxcr4 N	GTGCAGCAGGTAGCAGTGAA	CGCTGCTGTAGAGGTTGACA
Gpnmb N	CTCTGGTGGGTTCCAATATCACT	AGGAAATGGCAGAGTCGTTGA
Hpse N	CTCCGTTGTTCAGGAAACCAG	GCAAAGGGCTAAGCGTCATT
Il1rn N	TGCATGCACATGCTATGTATTGG	CTGGTGTTTGACCTGGGAGTA
Isg20 N	CGAGGGAGAGATCACGGACT	TGTAGCAGGCGCTTACACAG

Ms4a4a N	AATCCTTGGGATTGTGCAGATTG	TTCTGGTGGCATCAATCCACTT
Ms4a4c N	TGCAAGGACAGGAACAGACC	TGCCATCACAGTCACAGCAG
Sepx1 N	TTAGGGTTTTACCCGGACCTG	AGGATCCAAGAGTTCCCGGT
Sh2d1b1 N	TTACTACCATGGCTGCCTGAC	GCTTTGGAGCCTCTTGAGGAA
Spp1 N	CTGGCAGCTCAGAGGAGAAG	GGACTCCTTAGACTCACCGC
Tgfbi N	GCTCTGGCACTGTCTGTGG	AAGACCAGGCCTCATTGCTA
Trem1 N	TGGAGCTGAGCTTGAAGGATG	CTTGGGTAGGGATCGGGTTG
Uck2 N	GGCAGAATGAGGTGGATTACCA	AGGAATGATCACATCGGCGT

qRT-PCR Human Primers		
ACTB	GAGCTACGAGCTGCCTGAC	GACTCCATGCCCAGGAAGG
CD200R1L	GGAGGGCCACAAGTCTACTG	GACAACGCTGGAGATCCTGA
CD300LF	GAGCAGGAGGTGAAGAGGGA	ACCAGTAAGTGTCAGCATCAGTTT
CLEC7A	AGGGGCTCTCAAGAACAATGG	TCTGAAACAACAGCTATCCTGGT
CREB5	CAGGATCTTCCGCCGTCTTG	GCACAGGGGTTGCTGAGATT
CXCL13	GCTCAGTCTTTATCCCTAGACGC	CCATTCAGCTTGAGGGTCCAC
CXCR4	ACGCCACCAACAGTCAGAG	AGTCGGGAATAGTCAGCAGGA
GPNMB	TGCGGTGAACCTGATATTCCC	GTCCTCTGACCATGCTGTCC
HPSE	AGCGTGCAAGGTTCAAAGAG	AAGGATAGGGTAACCGCAAGT
IL1RN	GGAGGGAAGATGTGCCTGTC	CTGTTCTCGCTCAGGTCAGT
ISG20	AGGCTGTTGTGGCGTGAG	ATCGTTGCCCTCGCATCTTC
MS4A4A	AGTAACCCTATTTCCGTGTATATCG	GCCTTTTGTAGTTCTAATTCCTGC
SEPX1	GGCGAGGTTTTCCAGAATCACT	GTGAATGGTCTCGGTGAACGC
SH2D1B1	GAGACAGCGAGTCGATACCA	CCCGTGTTTCTCTCTGAAGATT
SPP1	GCCGAGGTGATAGTGTGGTT	AACGGGGATGGCCTTGTATG
TGFBI	ATGACCCTCACCTCTATGTACC	CACAGTTCACAGTTACAATCCCA
TREM1	CTGCTGTGGATGCTCTTTGTC	GTCTGCCCCTCTTTCAGTTCA
UCK2	TGCCAACAAAGAAGTATGCTGA	TAGCCGTTGAGACAGCCATT

Nested-PCR Human Primers		
ACTB N	GGCTACAGCTTCACCACCAC	ACATCTGCTGGAAGGTGGAC
CLEC7A N	GCCCACATGATTTGACTCAG	TTGTGTGGGTTGACTGTGGT
CXCR4 N	CCGTGGCAAACTGGTACTTT	TGGAGTGTGACAGCTTGGAG
GPNMB N	GGCAATGAAAGACCTTCTGC	AACATCGTCCCAATTTCTGG
IL1RN N	GGAGGGAAGATGTGCCTGTC	GGCAGTACTACTCGTCCTCC
ISG20 N	TGAGGGAGAGATCACCGATT	AAGCCGAAAGCCTCTAGTCC
SPP1 N	ACAGCCAGGACTCCATTGAC	GTGGGTTTCAGCACTCTGGT
TGFBI N	AGCAGCCCTACCACTCTCAA	GCTGGATGTTGTTGGTGATG

11.1. Methods

11.1.1. Animals

All *in vivo* work with the GL261 glioma model was done in C57BL/6 wild-type mice (Charles River Laboratories, Wilmington, MA, USA). Age matched naïve C57BL/6 wild-type mice were used as controls.

For the production of RCAS-*PDGFb*/RCAS-*PDGFb-RFP* tumors *Ntv-a*/*Ink4a/Arf*$^{-/-}$ *and Ntv-a*/*Ink4a-Arf*$^{-/-}$/*Pten*$^{flox/flox}$ mice were used, respectively. The genetic backgrounds of tv-a mice are FVB/N, C57BL/6, BALB/C, and tv-a. Primary RCAS-*PDGFb* tumors were re-implanted into *Cx3cr1*$^{GFP/wt}$ *Ccr2*$^{RFP/wt}$ mice (kind gift of Richard Ransohoff, (Saederup, Cardona et al. 2010)).

Cx3cr1$^{wt/wt}$, *Cx3cr1*$^{GFP/wt}$ and *Cx3cr1*$^{GFP/GFP}$ mice were used for organotypic brain slice experiments.

Mice were handled according to the rules and recommendations of the local authorities' (Germany: LaGeSo, animal protocol numbers: G O 268-10, G O 343-10, G 0438-12, Cleveland, OH, USA: CCF IACUC #2013-1029).

11.1.2. Glioma models

The first model I used was the GL261 glioma model. GL261 glioma cells originate from C3H mice that were treated with 20-methylcholanthrene in 1939 by Seligman and Shear (Seligman and Shear 1939; Ausman, Shapiro et al. 1970). Pieces of the original tumor were kept as frozen stocks and subsequently passaged subcutaneously in C57BL/6 mice for several generations. Later, Akbasak *et al*. established a monolayer culture from cryo-preserved tumor pieces (Akbasak, Oldfield et al. 1991). Upon intracranial injection of GL261 cells into C57BL/6 mice, these mice rapidly develop brain tumors that resemble human glioma and die within 20-25 days post-injection (Szatmari, Lumniczky et al. 2006).

In addition, I employed another murine glioma model based on somatic-cell gene transfer. Tumor formation is initiated by the overexpression of human *PDGFb* in *Nestin*-expressing cells *in vivo*. For this I used *Ntv-a*/*Ink4a-Arf*$^{-/-}$ mice that develop proneural high-grade gliomas 6 to 8 weeks following intracranial injection of RCAS-*PDGFb*-producing DF-1 chicken fibroblast cells at 4.5 to 10 weeks of age (Hambardzumyan, Amankulor et al. 2009). This tumor model histologically resembles primary human GBM more closely than the GL261 and displays several hallmarks of human GBM, such as a more invasive growth pattern, necrotic and pseudopalisading

areas, and multiple growth foci. Most importantly, these tumors are generated *in vivo* by viral targeting of a small population of stem and progenitor cells and subsequently acquire further genetic changes during tumor progression, similar to human GBM.

For isolation of glioma-associated microglia and macrophages/monocytes from RCAS-*PDGFb* tumors, primary tumors were intracranially re-transplanted into *Cx3cr1*$^{GFP/wt}$ *Ccr2*$^{RFP/wt}$ mice to distinguish between microglia and peripheral monocytes that invaded the brain. Naïve age-matched *Cx3cr1*$^{GFP/wt}$ *Ccr2*$^{RFP/wt}$ mice were used as controls. 5 to 7 weeks after intracranial injection of RCAS tumor cells into *Cx3cr1*$^{GFP/wt}$ *Ccr2*$^{RFP/wt}$ mice these mice develop tumors that are histologically identical to the original tumors in *Ntv-a*/*Ink4a-Arf-/-* mice.

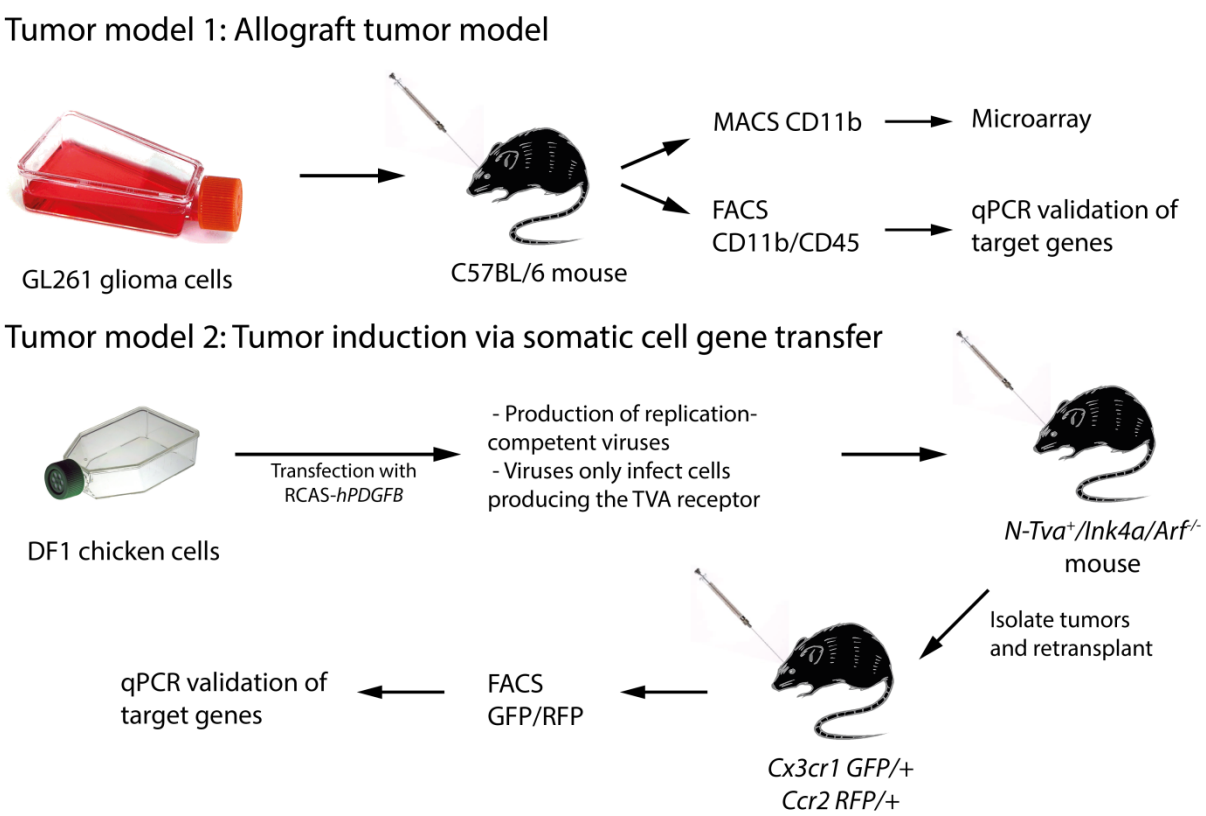

Figure 7 – Glioma models used in this study.
We used two different mouse glioma models in this study, the GL261 model (for the microarray and the qRT-PCR validation) and the RCAS-*PDGFb* model (for qRT-PCR validation).

11.1.3. Intracranial injections

Injections were performed using a stereotactic frame (Stoelting, Wood Dale, IL, USA). Mice used for these experiments were 8 to 10-weeks-old (C57BL/6 mice for GL261 injection), 4.5 to 10-weeks-old (*Ntv-a*/*Ink4a-Arf*$^{-/-}$ mice for DF-1 RCAS-*PDGFb*/RCAS-*PDGFb-RFP* injection), or 6 to 10-weeks-old (*Cx3cr1*$^{GFP/wt}$ *Ccr2*$^{RFP/wt}$ mice for RCAS-*PDGFb* tumor cell re-implantation). Mice were anesthetized with intraperitoneal injections of ketamine (0.1 mg/g, Pharmazeutischen Handelsgesellschaft, Garbsen, Germany) and xylazine (0.02 mg/g, Bayer, Leverkusen, Germany), fixated in a stereotactic micromanipulator (Kopf, Tujunga, CA, USA), and a small incision was made in the skin using a scalpel. One microliter cell suspension ($2x10^4$ GL261 cells, $4×10^4$ transfected DF-1 cells, or $5x10^4$ RCAS-*PDGFb* tumor cells) was delivered using a 30-gauge needle attached to a Hamilton syringe (Hamilton, Reno, NV, USA). Coordinates for GL261 injections into C57BL/6 mice were bregma 1 mm anterior, Lat (lateral) -2 mm (right of midline), and a depth -3 mm from the dural surface. Coordinates for injections of DF-1 cells, and RCAS-*PDGFb* tumor cells into *Ntv-a*/*Ink4a-Arf*$^{-/-}$ mice, and *Cx3cr1*$^{GFP/wt}$ *Ccr2*$^{RFP/wt}$ mice, respectively were bregma 1.5 mm anterior, Lat -0.5 mm, and a depth 2.0 mm. Post-surgery, the incision was closed with surgical suture and mice were carefully monitored.

11.1.4. Cultivation of cell lines

Cells of the murine GL261 glioma cell line (National Cancer Institute, MD, USA) and HEK293T cells were grown in Dulbecco's modified Eagle's medium (DMEM; Sigma-Aldrich, St. Louis, MO, USA) with 10% fetal calf serum (FCS), 200 mM glutamine, 100 U/mL penicillin, and 100 mg/ml streptomycin (all from Invitrogen, Carlsbad, CA, USA). DF-1 cells were purchased from ATCC (Manassas, VA, USA). Cells were grown at 39°C according to ATCC instructions. Transfections with RCAS-*PDGFb* were performed using Fugene 6 transfection kit (no. 11814443001; Roche, Mannheim, Germany) according to manufacturer's protocol.

11.1.5. Cultivation of primary RCAS-*PDGFb* tumor cells

RCAS-*PDGFb* and RCAS-*PDGFb-RFP* tumors were excised from tumor brains using a scalpel, minced, and incubated with Accutase (eBioscience, San Diego, CA, USA) for 15 minutes at 37°C. Tissue pieces were mechanically dissociated using a 1 ml pipette and washed in DMEM. Cells were passed through a 70 µm cell strainer and seeded into a T25 cell culture flask. Cells were grown in GIC medium containing DMEM-F12 GlutaMAX (GIBCO-Invitrogen, Carlsbad, CA, USA), 1% penicillin G/streptomycin sulfate (Sigma-Aldrich), B-27 without vitamin A (1:50; GIBCO-Invitrogen), HEPES (0.2 mM, Sigma-Aldrich), insulin (20 ng/ml, Sigma-Aldrich), supplemented with fibroblast growth factor 2 (FGF2, 20 ng/ml, Cell Systems, Kirkland, WA, USA) and epidermal growth factor (EGF, 20 ng/ml, Cell Systems).

11.1.6. Generation of mCherry$^+$ GL261 cells

The *eGFP* coding sequence was cut out of the lentiviral expression plasmid pRRL.PPT.MP.eGFP.pre using BamHI and SalI (both New England Biolabs (NEB), Ipswich, MA, USA). The mCherry coding sequence was cut out of another non-lentiviral expression plasmid, using EcoRI and BglII (both NEB). Both fragments were blunted using the Klenow fragment (NEB), purified via gel electrophoresis, ligated to generate pRRL.PPT.MP.mCherry, and transformed into JM109 competent *E. coli* (Promega, Fitchburg, WI, USA). A suitable clone was grown overnight in Terrific Broth growth medium (see 11.0.1) and larger quantities of plasmid DNA extracted using the EndoFree Plasmid Maxi Kit (Qiagen).

HEK293T cells were transfected with the lentiviral expression plasmid, and two helper plasmids (containing the *gag* and *pol*, as well as the VSV-G *env* gene) to produce replication-incompetent lentiviral particles. In brief, HEK293T cells were grown to 70-80% confluence in T175 flasks, washed with PBS and 11 ml of fresh medium (growth medium see 11.1.4, without FCS) was added. For the transfection of one T175 flask, 310 µl of 5% glucose solution (in PBS) were mixed with 70 µl PEI (polyethylenimine, Cat.no. 408727 Sigma-Aldrich) and vortexed for 1 min. Separately, 12.22 µg of the VSV-G *env* plasmid, 22.68 µg of the *gag*/*pol* plasmid, and 34.88 µg of the expression plasmid were mixed with 310 µl 5% glucose solution (in PBS) and vortexed for 1 min. After 10 min of incubation the two solutions were mixed, vortexed for 1 min, incubated for 10 min, medium (growth medium without FCS) was added to a final volume of 3 ml, and all 3 ml of the DNA solution were

added to the cells. After 6 h of incubation, 1.6 ml of FCS were added to the cells. 20-24 h after transfection the medium was exchanged with fresh growth medium. 24 h later, the viral supernatant was harvested, filtered using a 0.45 µm Millex Syringe-driven Filter Unit (Millipore, Billerica, MA, USA) and filled into an ultra centrifugal tube. 4.5 ml of 20% sucrose solution were carefully underlayed. Tubes were placed in a SW28-bucket (Beckman Coulter, Pasadena, CA, USA) and centrifuged at 28,000 rpm, 4 °C for 3h using an ultra centrifuge. The supernatant was discarded and the viral particles carefully resuspended in 100 µl PBS.

GL261 cells were grown to 60-70% confluence, growth medium, containing 4 µg/ml Polybrene (Sigma-Aldrich), and 5 µl of concentrated viral supernatant were added to the cells. After 24 h of incubation, the medium was exchanged with normal growth medium. Cells were sorted using FACS according to mCherry intensity.

11.1.7. Organotypic brain slices

P14-P16 *Cx3cr1*$^{GFP/GFP}$, *Cx3cr1*$^{GFP/wt}$, and *Cx3cr1*$^{wt/wt}$ littermate mice were decapitated and brains were removed and placed in ice-cold phosphate-buffered saline (PBS) under sterile conditions. The forebrain was dissected from the brainstem and glued (using cyanoacrylate glue) onto a metal block and cut in the coronal plane into 250 µm sections with a vibratome (Microm HM 650 V, Thermo Scientific, Waltham, MA, USA). The brain slices were transferred onto the 0.4 µm polycarbonate membrane in the upper chamber of a transwell tissue insert (Falcon model 3090, Becton Dickinson), which was inserted into a 6-well-plate (Falcon model 3502, BectonDickinson). Thereafter, the brain slices were incubated in 1 ml of culture medium per well containing DMEM supplemented with 10% heat-inactivated fetal bovine serum (Atlanta Biological), 0.2 mM glutamine, 100 U/ml penicillin, and 100 mg/ml streptomycin (medium-1). After overnight equilibration of the brain slices in medium-1, this was exchanged for cultivation medium (medium-2). Medium-2 contained 25% heat-inactivated horse serum, 50 mM sodium bicarbonate, 2% glutamine, 25% Hank's balanced salt solution, 1 mg/ml insulin (all from Gibco), 2.46 mg/ml glucose (Braun Melsungen, Germany), 0.8 mg/ml vitamin C (Sigma Aldrich), 100 U/ml penicillin, 100 mg/ml streptomycin (Sigma Aldrich), and 5 mM Tris in DMEM (Gibco).

11.1.8. Tumor cell injections into cultured brain slices

One day after cutting the slices, 5,000 cultured mCherry-GL261 cells or RCAS-*PDGFb-RFP* tumor cells in a volume of 0.1 µl were injected into the slices using a syringe (Hamilton, Reno, NV, USA) mounted to a micromanipulator (Kopf, Tujunga, CA, USA). An injection canal was formed that reached 150 µm deep into the 250 µm-thick slice. The needle was then retracted by 50 µm, leaving an injection cavity of approximately 50 µm. The cell suspension was slowly injected over 30 seconds and subsequently the syringe was slowly pulled out in 10 µm incremental steps over 60 seconds. To ensure identical experimental conditions, gliomas were always inoculated into the same area, 1 mm anterior of the ventricle. Tumor sizes were determined 6 and 12 days post-injection by fluorescence microscopy (Axiovert 135, Carl Zeiss, Jena, Germany) using a 5x objective and the fluorescent area was evaluated using Fiji ImageJ. Statistical significances were calculated applying a One-Way-ANOVA using GraphPad Prism 5.

11.1.9. Re-cutting of cultured slices

For analysis of microglia invasion into tumor areas, slices were fixed 4 days post-injection of tumor cells with 4% PFA for 1 hour and subsequently stored in 30% sucrose until further use. Fixed slices were mounted on plain-cut blocks of Tissue-Tek O.C.T. (Sakura, Tokyo, Japan), covered with more Tissue-Tek O.C.T. and subsequently cut into 10 µm section using a Leica CM1950 Cryostat (Leica Microsystems, Wetzlar, Germany). Recut sections were transferred to glass slides (Superfrost, Thermo Scientific) and embedded in Aqua-Poly/Mount (Polysciences, Eppenheim). Confocal pictures were prepared using a Leica TCS SPE confocal microscope (Leica Microsystems) using a 40x objective and evaluated using Adobe Photoshop and Fiji ImageJ. Statistical significances were calculated applying a One-Way-ANOVA using GraphPad Prism 5.

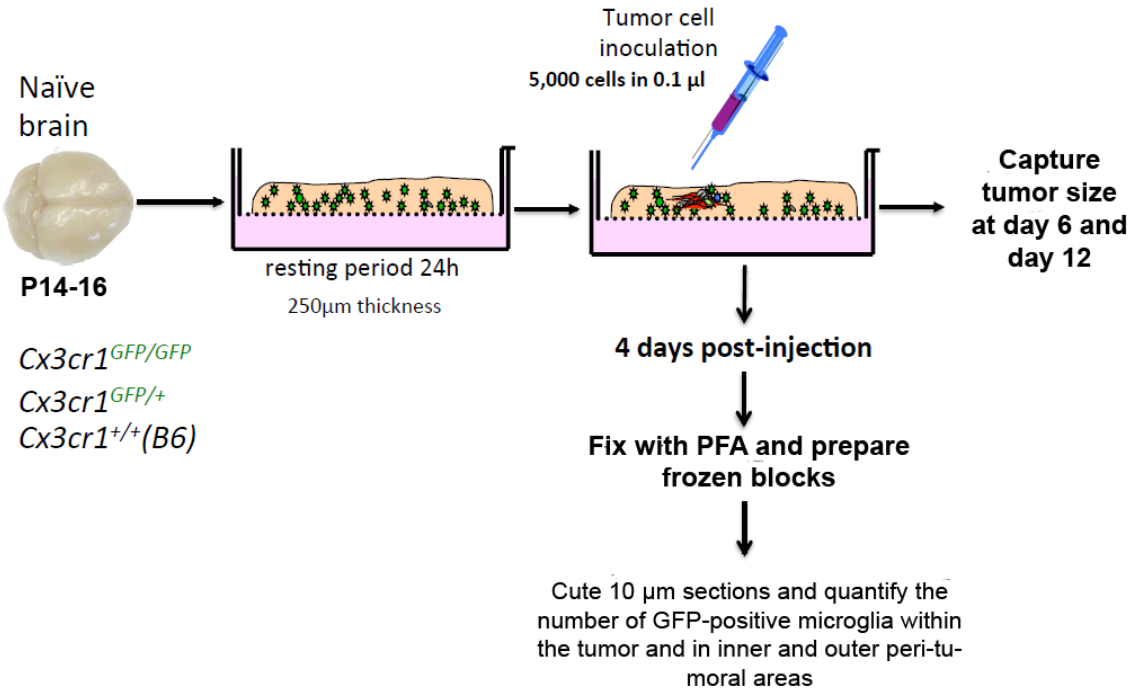

Figure 8 – Graphical scheme for the experiments with *Cx3cr1* wt/mutant organotypic slice cultures.

11.1.10. Human tissue

Resected tissues were provided by the Department for Neurosurgery Charité University Hospital (Berlin, Germany). Analysis of resected human brain tumor and control tissue was performed according to the rules by the Ethical Committee and with patient's consents (Charité University Hospital, EA4/098/11). Briefly, tumor and control tissue was taken during surgery while patients were under a general anesthetic, and was placed immediately in culture medium for transportation. Cells were isolated from the tissue as described below no later than 2 hours after resection. Cell sorting was performed via magnetic-activated cell sorting (MACS), using anti-CD11b microbeads (described below).

11.1.11. Cell isolation

GL261-implanted mice were sacrificed 20 days post-injection, RCAS-*PDGFb*-implanted mice were sacrificed 4-5 weeks post-injection. Tumor-bearing and control mice were euthanized by i.p. injection of 200 µl pentobarbital-sodium (Narcoren, Pharmazeutischen Handelsgesellschaft) and perfused using a 0.9% NaCl solution. The brain and spleen were extracted and stored in ice-cold HBSS (Gibco-Invitrogen). For naïve mouse brains, the olfactory bulbs and the cerebellum were cut away using a scalpel and discarded. The rest of the tissue was used for dissociation. In tumor-bearing mouse brains, only the visible tumor area around the injection site was used.
Human and mouse tissue was dissociated with the Neural Tissue Dissociation Kit (Miltenyi Biotec, Bergisch-Gladbach, Germany) according to the manufacturer's instructions. To remove the myelin I followed a protocol published elsewhere (Olah, Raj et al. 2012). In brief, the brain cell suspension was mixed with a total of 25 ml of a 22% Percoll (Th.Geyer, Renningen, Germany) solution and a layer of 5 ml cold PBS (Gibco-Invitrogen) was added on top. Centrifugation at 950 g with slow acceleration and without breaks created a gradient that separated the cell pellet on the bottom of the tube from the myelin which was carefully aspirated. The cell pellet was resuspended in sorting buffer for subsequent magnetic-activated cell sorting (MACS) or fluorescence-activated cell sorting (FACS) isolation (see below).
Spleens were processed through a 70 µm cell strainer with a syringe plunger and the mesh rinsed with 10 ml of PBS per spleen. The cells were centrifuged and the pellet subjected to erythrocyte lysis by adding 5 ml of 1x RBC lysis buffer (Cat# 420301, Biolegend, San Diego, CA, USA). The lysis was carried out by shaking the tube mildly for 5 min at RT and subsequently stopped with 20 ml of PBS. The pellet was washed once with PBS and resuspended in PBS, containing 0.5% FCS and 2mM EDTA (FACS buffer) for subsequent FACS isolation.
For RCAS-*PDGFb* tumors blood monocytes were used as peripheral controls (instead of monocytes isolated from spleens). To obtain blood monocytes, 200 µl of blood was mixed with 500 µl of PBS, containing 2.5 mM EDTA, centrifuged, the clear phase aspirated and the remaining phase mixed with 1 ml 1x RBC lysis buffer and incubated for 3 min on ice. The reaction was stopped by adding PBS, cells were centrifuged, washed once in 1x RBC lysis buffer and resuspended in FACS buffer.

11.1.12. Magnetic-activated cell sorting

The $CD11b^+$ samples for the microarray were generated using MACS. Following Percoll gradient centrifugation, tumor and control cell pellets were resuspended in PBS, containing 0.5% FCS and 2 mM EDTA and labeled with anti-CD11b microbeads™ (Miltenyi Biotec, 130-093-634). The MACS isolation was carried out according to the manufacturer's instructions and cells were subsequently used for RNA isolation.

11.1.13. Fluorescence-activated cell sorting

Samples for qRT-PCR validation of target genes that were generated from GL261-bearing and corresponding naïve control mice were FACS sorted using CD11b, CD45, Ly6C, and Ly6G to distinguish between resident microglia ($CD11b^+/CD45^{low}$) and invading macrophages/monocytes ($CD11b^+/CD45^{high}/Ly6G^-/Ly6C^{high}$). The gating strategy is displayed in Figure 9. Following Percoll gradient centrifugation, cell pellets were resuspended in FACS buffer (containing 2% FCS) and stained with 2 µl of dye-coupled antibodies per $1*10^7$ cells. The staining was done with CD45-e450 (48-0451-82), Ly6G-PE (12-5931-82), Ly6C-PerCpCy5.5 (45-5932-82) and CD11b-APC (17-0112-82) (all eBioscience, San Diego, CA, USA) for 30 min at 4 °C. Thereafter, the cells were washed and resuspended in 500 µl FACS buffer per $5*10^6$ cells for sorting at a BD FACSAria™ (BD Bioscience). Compensation was calculated with single-stained beads (552844, BD Bioscience, Franklin Lakes, NJ, USA) and unstained cells. Generation of flow-sorted samples from GL261 for qRT-PCR analysis was done by me and by my student Andreas Pelz (under my supervision).

Samples generated from RCAS-*PDGFb* tumors were isolated without antibody staining. Instead, tumor cells were re-implanted into $Cx3cr1^{GFP/wt}$ $Ccr2^{RFP/wt}$ mice which contain RFP^+/GFP^{low} macrophages/monocytes and RFP^-/GFP^+ microglia. Accordingly, fluorescence-activated cell sorting was based on RFP and GFP positivity, in order to distinguish between resident microglia and invading macrophages/monocytes. RFP^+/GFP^{low} peripheral macrophages/monocytes resemble the $CD11b^+/CD45^{high}/Ly6G^-/Ly6C^{high}$ population. The RFP^-/GFP^+ microglia resemble the $CD11b^+/CD45^{low}$ population (unpublished observation). Generation of flow-sorted samples from re-implanted RCAS-*PDGFb* for qRT-PCR analysis was done in the lab of Prof. Dolores Hambardzumyan at Cleveland Clinic (Cleveland, Ohio, USA) by Dr. Xi Feng and by me.

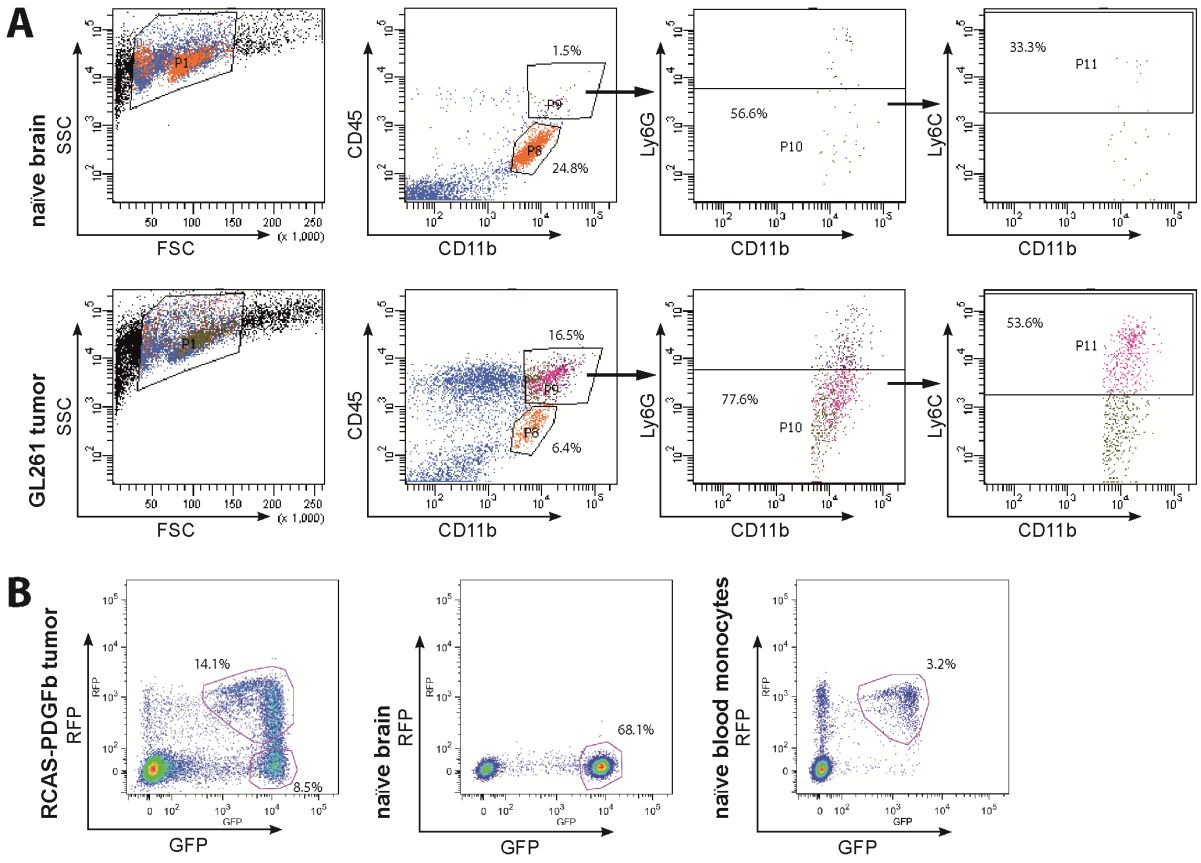

Figure 9 – Flow cytometry isolation strategies for generation of mouse qRT-PCR samples.

A) Plots depicting the strategy for isolation of microglia and macrophages from naïve brains and GL161 glioma-bearing brains using antibody staining for CD11b, CD45, Ly6C, and Ly6G. CD45 staining was used to distinguish between $CD11b^{+}/CD45^{low}$ resident microglia (gate P9) and $CD11b^{+}/CD45^{high}/Ly6G^{-}/Ly6C^{high}$ invading macrophages/monocytes (gates P8, P10, and P11), which were mostly absent in naïve brain samples. B) GAMs from RCAS-*PDGFb* tumors were isolated relying on an antibody-independent approach. Primary tumors from *Ntv-a/Ink4a-Arf*$^{-/-}$ mice were re-implanted into *Cx3cr1*$^{GFP/wt}$ *Ccr2*$^{RFP/wt}$ mice and GAMS were sorted according to GFP and RFP expression. In naïve *Cx3cr1*$^{GFP/wt}$ *Ccr2*$^{RFP/wt}$ mice only GFP^{+} cells were present in the brain. In tumor-bearing mice, resident microglia were GFP^{+}, whereas invading macrophages/monocytes were RFP^{+}/GFP^{low} or GFP^{+}/RFP^{+}. RFP^{+}/GFP^{low} naïve blood monocytes were used as peripheral controls. Generation of flow-sorted samples from GL261 for qRT-PCR analysis was done by me and by my student Andreas Pelz (under my supervision). Generation of flow-sorted samples from re-implanted RCAS-*PDGFb* for qRT-PCR analysis was done in the lab of Prof. Dolores Hambardzumyan at Cleveland Clinic (Cleveland, Ohio, USA) by Dr. Xi Feng and by me.

11.1.14. RNA protocols

Total RNA from MACS or FACS-sorted cells was isolated using the RNeasy Plus Mini Kit (Qiagen, Hilden, Germany). On-column DNase 1 (Qiagen) digestion was performed and total RNA was eluted in RNase-free water. RNA yield was measured using a Nanodrop 1000 (Nanodrop, Wilmington, DE, USA) spectrophotometer and quality was assessed using an Agilent 2100 Bioanalyzer (Agilent, Santa Clara, CA, USA). Samples were stored at -80 °C until further use. For qRT-PCR, first strand cDNA synthesis of RNA was done using the Superscript II (Invitrogen) reverse transcriptase according to the manufacturer's instructions. For mRNA transcription oligo-dT primers (Invitrogen) were used. cDNA was stored at -20 °C until further processing.

11.1.15. Microarray

For the microarray MACS-isolated $CD11b^+$ cells from GL261 gliomas (injected into 6-8-week-old C57BL/6 mice; 3 samples; one tumor sample per RNA sample), and age-matched naïve control mice (3 samples; three control brains were pooled per sample). Yields of 500ng to 1 µg of total RNA of good quality (Agilent RNA Integrity Number, RIN=8.2-10.0) were obtained.

Sample preparation for microarray hybridization was carried out as described in the Ambion WT Expression Kit Protocol (Life Technologies, Carlsbad, CA, USA) and the Affymetrix WT Terminal Labeling and Hybridization User Manual (Affymetrix, Inc., Santa Clara, CA, USA). In brief, 300 ng of total RNA were used to generate double-stranded cDNA. 12 µg of subsequently synthesized cRNA was purified and reverse transcribed into sense-strand (ss) cDNA, whereat unnatural dUTP residues were incorporated. Purified ss cDNA was fragmented using a combination of uracil DNA glycosylase (UDG) and apurinic/apyrimidinic endonuclease 1 (APE 1) followed by a terminal labeling with biotin. 3.8 µg fragmented and labeled ss cDNA were hybridized to Affymetrix Mouse Gene 1.0 ST arrays for 16 h at 45 °C in a rotating chamber. Hybridized arrays were washed and stained in an Affymetrix Fluidics Station FS450, and the fluorescent signals were measured with an Affymetrix GeneChip Scanner 3000 7G.

Sample processing was performed at an Affymetrix Service Provider and Core Facility, "KFB - Center of Excellence for Fluorescent Bioanalytics" (Regensburg, Germany; www.kfb-regensburg.de).

11.1.16. Bioinformatic analysis of microarray data

Two additional data sets consisting of three samples each that were generated from $CD11b^+$ MACS-isolated peritoneal myeloid cells were downloaded from http://www.ebi.ac.uk/arrayexpress (Young, Eksmond et al. 2012) - E-MEXP-3623; (Keller, Mazuch et al. 2009) - E-GEOD-25585) and used as controls for peripheral macrophages.

Two independent approaches were used for bioinformatic data analysis. For the first method the Affymetrix Expression Console Software Version 1.0 was used to create summarized expression values (CHP-files) from the expression array feature intensities (CEL-files). The Robust Multichip Analysis (RMA) algorithm was applied (Irizarry, Bolstad et al. 2003). Integrative analysis of genome-wide expression activities from DNA-microarray data sets was performed with the Gene Expression Dynamics Inspector (GEDI), a Matlab (Mathworks, Natick, MA) freeware program which uses self-organizing maps (SOMs) to translate high-dimensional data into a 2D mosaic (Eichler, Huang et al. 2003). Each tile of the mosaic represents an individual SOM cluster and is color-coded to represent high or low expression of the cluster's genes, thus identifying the underlying pattern. The GEDI analysis was performed by Prof. Thomas Langmann at the University of Cologne, Cologne, Germany.

For the second approach, basal expression values (from CEL-files) were processed in R using Bioconductor package Affy (Gautier, Cope et al. 2004). The Affy-scale-value-expression-set-function was set to 500 and data was normalized with expresso-function, set to quantile normalization, and pmonly correcte.method and medianpolish summary method. Gene annotation was done with mogene10sttranscriptcluster (Li 2013), and only annotated probes were included in the analysis. Subsequently, collapseRows, was used to obtain a single representative probe for each gene, resulting in 13,943 genes taken into the analysis (Miller, Cai et al. 2011). Signed network analysis was done with Weighted Gene Coexpression Network Analysis (WGCNA (Langfelder and Horvath 2007)). An adjacency network was made using a softpower (β) value of 20, based upon the scale free criteria, and low connected genes were filtered out of the analysis, resulting in 10,875 genes. Dendrogram formation and module determination was done by average linkage clustering and an arbitrary cut-off, determined by WGCNA. From each module, the Module Eigengene (ME) was calculated, which is the first principal component and functions as a representative of the expression profile of the

module. Next, as a measure for intramodular connectivity, the ME was correlated to the expression profile of all intramodular genes, resulting in a kME-table, to determine which genes are most important, e.g. hub-genes. These module membership values were multiple testing corrected using the R package Stats. Genes significantly associated to these modules (FDR p value <0.01) were used for further analysis. Heat maps were generated using heatmap.2 function of Bioconductor Package Gplots (Warnes, Bolker et al. 2013).
The WGCNA analysis was performed by Inge R. Holtman in the lab of Prof. H.W.G.M. Boddeke at the University of Groningen, Groningen, The Netherlands.

11.1.17. Quantitative RT-PCR

Quantitative RT-PCR (qRT-PCR) reactions were performed using the SYBR Select Mastermix (Applied Biosystems, Foster City, CA, USA) according to the manufacturer's instructions on a 7500 Fast Real-Time PCR System (Applied Biosystems).
Primers for target genes were designed to recognize all validated mRNA splice variants of the gene, relying on the RefSeq sequences of the UCSC genome browser (http://genome.ucsc.edu/). The primer sequences were generated using the Primer-Blast tool (http://www.ncbi.nlm.nih.gov/tools/primer-blast/). Amplification of unintended targets was excluded by BLAST search (http://blast.ncbi.nlm.nih.gov/Blast.cgi). Calculation of unfavorable secondary structures and primer-dimer amplification was done with the IDT oligo analyzer (http://eu.idtdna.com/analyzer/applications/oligoanalyzer/).
For absolute quantification of target genes, nested primers flanking the original primers were designed. Nested amplicons were purified from agarose gels, and serial dilutions were used to generate standard curves for each gene. Molar masses of nested amplicons were calculated using http://www.basic.northwestern.edu/biotools/OligoCalc.html. Primer sequences can be found in Table 1.
QRT-PCRs of murine pro-tumorigenic genes (*Spp1*, *Gpnmb*, *Il1rn*, *Cd200r4*, *Cd300lf*, *Sh2d1b1*, *Uck2*, *Creb5*, *Trem1*, *Cxcl13*, *Hpse*, *Sepx1*) were performed by my student Andreas Pelz under my supervision. Primer design of qRT-PCR primers for human and mouse was done by me.

11.1.18. Semi-quantitative RT-PCR

Semi-quantitative RT-PCR reactions were performed using the GoTaq Green PCR Kit (Promega). The PCR reaction was carried out with a T3000 thermocycler (Biometra, Göttingen, Germany). The following cycle numbers were used for the amplification of human cDNA: *ACTB* 24 cycles, *SPP1* and *GPNMB* 26 cycles, all other genes 31 cycles. DNA product separation was carried out using gels containing 3% agarose (Peglab, Erlangen, Germany). DNA bands were visualized using a Gel documentation G-Box (Syngene, Cambridge, United Kingdom). The pUC19 DNA/MspI (HpaII) marker was used for amplicon size determination.

11.1.19. Survival outcome analysis

Cbioportal (http://www.cbioportal.org/public-portal/) was used to access patient information survival information and tumor gene expression data of these patients (Study: Glioblastoma multiforme, TCGA Provisional, mRNA Expression z-Scores (microarray), accessed in August 2014) (Cerami, Gao et al. 2012; Gao, Aksoy et al. 2013). Subtype information was retrieved from (Brennan, Verhaak et al. 2013). The Rembrandt database (http://caintegrator.nci.nih.gov/rembrandt/home.do) was used for additional survival analysis.

11.1.20. Statistical analysis

Statistical analysis were performed using GraphPad Prism 5, Microsoft Excel 2007, and R (R Development Core Team 2010).

Statistical analysis of mouse and human qRT-PCR data was done with students t test. Error bars indicate the Standard Error of the Mean (SEM).

For analysis of TCGA patient survival data the standard deviation of the gene expression values of all patients was calculated. Patients with a gene expression lower than the negative standard deviation were clustered into the low expression group, whereas patients with a gene expression higher than the positive standard deviation were clustered into the high expression group. Statistical significances between high and low expression groups were calculated using the Log Rank (Mantel-Cox) test. Survival plots were generated and Kaplan-Meier curves were produced.

Functional annotation and transcription factor binding site enrichment analysis of the gene modules was done using Webgestalt (Zhang, Kirov et al. 2005; Wang, Duncan

et al. 2013). Statistical tests under hypergeometric distribution were conducted with Bonferroni multi test correction.

To determine the significance of the overlap between the GAMs and the M1/M2a,b,c data sets the WGCNA UserlistEnrichment method was employed using a Hypergeometric test (Miller, Cai et al. 2011).

To determine significances in tumor sizes and numbers of invading GFP^+ microglia between *Cx3cr1*$^{wt/wt}$, *Cx3cr1*$^{GFP/wt}$, and *Cx3cr1*$^{GFP/GFP}$ slices I used a non-parametric One-Way ANOVA with a Bonferroni post-hoc test.

Indicators for all significant results: *, $p<0.05$; **, $p<0.01$; ***, $p<0.001$

4. Results

11.1. **Project 1:** Genome-wide gene expression analysis of glioma-associated microglia/macrophages

11.1.1. Microarray

11.1.1.1. Comparison of GAMs to naïve microglia

To identify glioma-regulated transcripts in glioma-associated microglia/macrophages (GAMs), I isolated microglia/macrophages from GL261 glioma-bearing brains (3 samples; one tumor sample per RNA sample) using MACS with anti-CD11b antibodies. As controls I isolated microglia from age-matched healthy mouse brain (3 samples; three control brains were pooled per sample). I extracted total RNA from these samples and performed Affymetrix GeneChip Mouse Gene 1.0ST microarrays. Comparing the global gene expression profiles – 28,351 genes were taken into comparison – of these two sample groups I saw that around 1,500 genes were >2-fold significantly upregulated and around 1,400 genes >2-fold significantly downregulated in GAMs. Lists of the 25 highest up- and downregulated genes in GAMs when compared to naïve control microglia can be found in Table 2.

11.1.1.2. Comparison of GAMs to naïve microglia and peritoneal macrophages

As GAMs consist of brain-resident microglia and invading peripheral macrophages/monocytes I also downloaded two published data sets from Affymetrix GeneChip Mouse Gene 1.0ST microarrays that were generated from peritoneal myeloid cells as peripheral controls and included these sets into our analysis. These data sets were downloaded from http://www.ebi.ac.uk/arrayexpress ((Young, Eksmond et al. 2012) - E-MEXP-3623; (Keller, Mazuch et al. 2009) - E-GEOD-25585). The two additional data sets consisted of three samples each, generated from either $CD11b^+$ MACS-sorted (Keller, Mazuch et al. 2009) or $CD11b^+MHC\text{-}II^{hi}B220^-Gr1^-$ flow-sorted cells (Young, Eksmond et al. 2012).

Table 2 – The 25 highest up- and downregulated genes in GAMs when compared to naïve microglia in our screen.

Upregulated in GAMs vs. naïve microglia					Downregulated in GAMs vs. naïve microglia				
Gene	p value	log2 expression GAMs	logs2 expression naïve MG	Fold change	Gene	p value	log2 expression GAMs	logs2 expression naïve MG	Fold change
Gpnmb	0.00000	12.97	6.52	87.36	**Gpr165**	0.00000	6.86	12.39	-46.32
Ifi205	0.00001	12.44	6.27	71.73	**Ttr**	0.00309	8.01	13.14	-34.83
Cxcl13	0.00099	12.17	6.04	69.84	**Csmd3**	0.00004	5.37	9.76	-21.00
Arg1	0.00034	11.87	6.04	56.99	**Lgi1**	0.00112	6.38	10.70	-20.00
Dnase1l3	0.00000	11.64	5.89	54	**Slc6a11**	0.00119	8.63	12.48	-14.44
Ly6i	0.00010	12.1	6.41	51.36	**Cd209a**	0.00365	7.33	11.17	-14.30
Cxcl9	0.00001	13.28	7.6	51.1	**Cldn10**	0.00149	7.28	11.11	-14.24
Cfb	0.00000	12.55	6.89	50.75	**Gm2897**	0.00018	6.98	10.53	-11.75
Adamdec 1	0.00011	11.64	6.06	47.68	**Luzp2**	0.00201	7.84	11.37	-11.49
BC023105	0.00000	9.16	3.83	40.22	**Gm3002**	0.00024	7.57	11.09	-11.48
Acp5	0.00000	12.9	7.8	34.29	**Ntsr2**	0.00041	8.24	11.74	-11.33
AA467197	0.00001	11.58	6.52	33.34	**Gp9**	0.00005	7.93	11.43	-11.27
Saa3	0.01383	10.8	5.76	32.85	**Grm3**	0.00141	7.73	11.21	-11.20
Mmp13	0.00042	11.88	6.9	31.55	**Gm3696**	0.00022	7.62	11.04	-10.75
Atp6v0d2	0.00184	10.28	5.31	31.34	**Gpr37l1**	0.00110	8.90	12.29	-10.50
Ms4a4c	0.00000	12.63	7.71	30.36	**Slc4a4**	0.00258	7.81	11.17	-10.23
Dpep2	0.00002	11.72	6.81	30.13	**Gm10790**	0.00016	8.47	11.81	-10.19
Car6	0.00075	10.42	5.56	29.1	**Gabrb1**	0.00156	6.58	9.91	-10.06
Gpr171	0.00001	11.54	6.68	29.03	**Gpr34**	0.00062	7.95	11.28	-10.05
Serpina3f	0.00006	10.55	5.71	28.52	**Nrsn1**	0.00119	8.46	11.78	-10.00
Cyp4f18	0.00000	12.79	7.98	28.21	**Gm10406**	0.00021	7.32	10.64	-9.99
Iigp1	0.00002	11.01	6.21	27.82	**Slc6a1**	0.00108	8.71	12.02	-9.95
E030037K 03Rik	0.00001	11.38	6.6	27.51	**Gpm6a**	0.00487	8.81	12.10	-9.83
Moxd1	0.00040	11.41	6.65	26.97	**Gm1973**	0.00038	7.23	10.52	-9.82
Hpse	0.00000	11.88	7.20	25.54	**Hpgd**	0.00012	9.53	12.80	-9.69

11.1.1.3. Graphical representation of gene expression patterns using GEDI

Next, we applied the Gene Expression Dynamics Inspector (GEDI) to the four data sets to visualize the global gene expression patterns in GAMs versus naive microglia and peritoneal macrophages. GEDI uses self-organizing maps to capture genome-wide transcriptome activity via 'gestalt' recognition (Eichler, Huang et al. 2003) and is used to visualize global gene expression changes in the different sample groups. Each mosaic tile in the GEDI map represents a gene cluster that is expressed at similar levels (and each mosaic tile contains the same set of genes in each of the four representations). The four GEDI maps, with blue colour indicating low and red colour high mRNA expression levels, show that the gene expression patterns of GAMs and naive microglia are more similar to each other than the two macrophage data sets. Closer inspection of the GAMs and naive microglia GEDI patterns then revealed a central cluster of highly expressed genes in GAMs that is different from naive microglia or peripheral myeloid cells (white circle) (Figure 10).

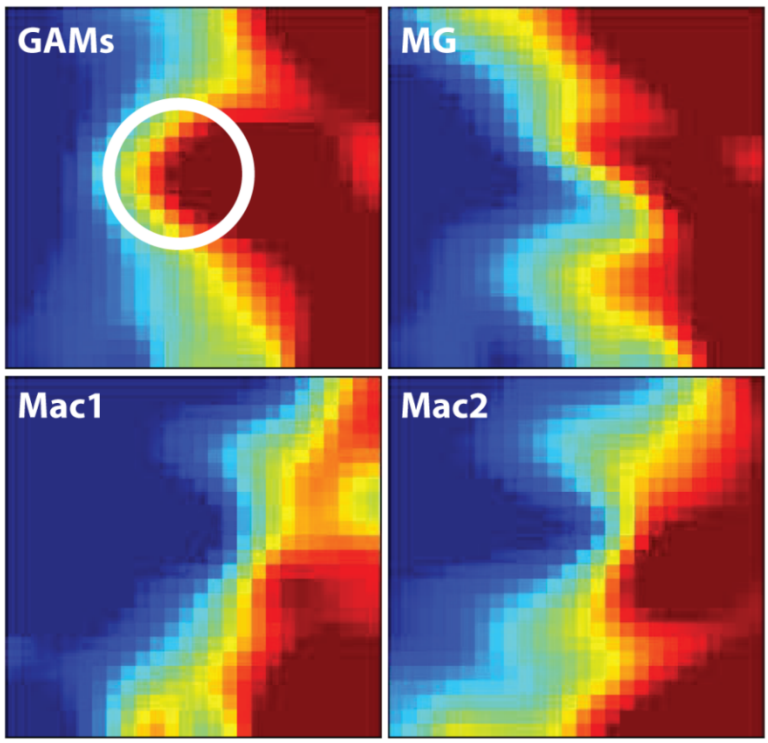

Figure 10 – Graphical representation of gene expression patterns in the four data sets. The four GEDI maps show that the gene expression patterns of GAMs and naive microglia are more similar to each other than both macrophage data sets (blue colour indicating low and red colour high mRNA expression levels). The white circle highlights a central cluster of highly expressed genes in GAMs that is different from naive microglia. GAMs: glioma-associated microglia/macrophage microarray data; MG: naive microglia microarray data; Mac1: external data set from Keller, Mazuch et al. 2009; Mac2: external data set from Young, Eksmond et al. 2012. The GEDI analysis was performed by Prof. Thomas Langmann at the University of Cologne, Cologne, Germany.

11.1.1.4. Weighted Gene Coexpression Network Analysis of the data sets

When comparing the GAMs data set to the three naïve control data sets (10,875 genes were considered), 783 genes were significantly upregulated >2-fold and 198 genes downregulated at least 2-fold in GAMs. Using Weighted Gene Coexpression Network Analysis (WGCNA), we clustered genes into different modules according to their co-expression pattern within the four sample groups (Figure 11). Within each module genes were ranked according to how closely they correlated to the Eigengene expression of this module (termed Module Membership). The Module Eigengene is the first principal component, representing the gene expression patterns of all genes clustered into this module (Langfelder and Horvath 2007). Two modules contained genes that were upregulated in the GAMs samples compared to the three control data sets (labeled red and brown in Figure 11). A list of the 25 highest upregulated genes in comparison to the three control groups can be found in Table 3.

In addition, the gene clustering revealed genes that were specific for either microglia or macrophages. The orange module contains genes that were highly expressed in GAMs and already showed high expression in naïve microglia, but low expression in naïve macrophages (Figure 11). Genes that showed high expression in GAMs and naïve macrophages, but low expression in naïve microglia were clustered into the green module. Two studies used RNA sequencing and microarray analysis to investigate the expression of either microglia or macrophage-specific genes (Hickman, Kingery et al. 2013; Pong, Walker et al. 2013). Genes that were found to be microglia-specific in these reports predominantly clustered into our orange module, whereas macrophage-specific genes are enriched in our green module.

Table 3 – The 25 highest upregulated genes in GAMs (in comparison to the three control data sets) in our microarray.

			Log2 Expression				
Gene Symbol	Module	P Value	GAMs	Naïve Microglia	Control Mϕ1	Control Mϕ2	Fold Change
Gpnmb	red	2.06E-07	12.63	7.26	7.60	7.51	36.02
Cxcl9	red	1.69E-08	12.83	7.63	7.14	8.67	32.27
Spp1	red	7.59E-06	12.31	7.92	7.84	6.88	27.24
Ly6i	red	6.84E-09	11.55	6.94	6.79	7.07	24.48
Gjc3	red	1.41E-08	11.62	7.74	6.97	7.13	20.32
Il1r2	red	1.86E-06	11.64	8.22	7.03	6.99	18.70
Cd72	red	1.63E-06	12.13	8.81	7.63	7.42	18.04
Ms4a4c	red	2.36E-07	12.11	7.72	8.00	8.15	17.76
Mmp13	red	2.34E-07	11.08	7.11	6.77	6.91	17.73
Serpina3n	red	3.08E-08	11.71	8.18	7.17	7.39	17.45
Ptgs2	orange	0.001883	12.61	11.09	7.167	7.23	17.28
Gpr171	red	1.02E-07	11.23	7.20	7.21	7.24	16.12
Igfbp7	orange	0.00065	12.52	10.53	7.59	7.49	15.83
Il1b	orange	0.001877	12.71	11.25	7.42	7.58	15.54
Ccl5	red	1.58E-10	12.46	9.02	8.00	8.64	15.03
Adamdec1	red	2.47E-07	10.69	6.75	6.81	6.84	14.78
Il1rn	red	1.99E-10	11.63	8.03	7.46	7.77	14.76
Ifi44	red	3.59E-07	11.42	7.53	7.27	7.95	14.32
Spon1	red	4.10E-07	11.77	8.72	7.52	7.55	14.30
Acp5	brown	0.000145	12.38	7.74	9.24	8.88	13.58
Moxd1	red	4.40E-08	10.83	7.21	7.15	7.11	12.77
Trem1	red	7.96E-07	11.43	8.10	7.65	7.57	12.62
Gm6377	red	2.25E-06	11.14	8.45	7.05	7.02	12.40
Vcam1	orange	0.000315	11.76	9.95	7.19	7.36	12.12
Dnase1l3	brown	0.000265	10.98	6.91	7.68	7.66	11.84

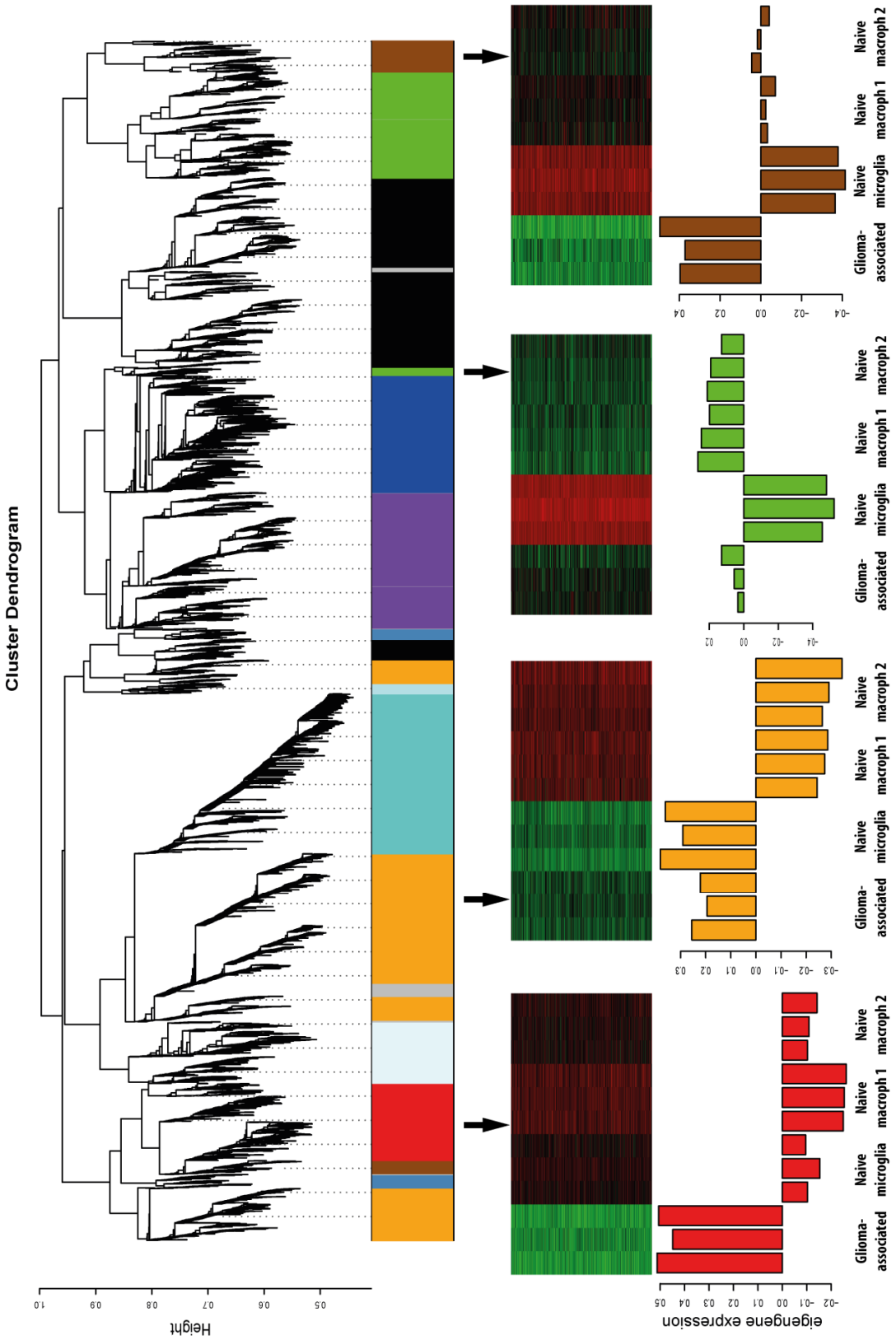

Figure 11 – WGCNA gene clustering reveals glioma-regulated gene modules.
Each color represents a different module and each module contains genes with similar expression patterns over all four sample sets. The glioma-regulated modules (labeled as red and brown) were further analyzed, as they contained genes that were upregulated in the glioma-associated set when compared to all three control sets. The WGCNA analysis was performed by Inge R. Holtman in the lab of Prof. H.W.G.M. Boddeke at the University of Groningen, Groningen, The Netherlands.

11.1.1.5. Gene ontology (GO) enrichment and transcription factor binding site analysis

I used Webgestalt to perform gene ontology (GO) enrichment analysis on all >2-fold upregulated genes that clustered into the glioma-regulated (red and brown) modules (438 genes in total) to identify overrepresented GO terms (Table 4). Several GO terms were overrepresented in the GAMs data set that can be grouped into three main groups: regulation of immune response/activation, programmed cell death, and response to other organism/virus. Next, I used Webgestalt to identify transcription factor binding sites that are enriched in the same set of genes (Table 5). This analysis revealed that enriched binding sites included known sites for IRF1, IRF2, IRF7, IRF8, IRF9/STAT1/STAT2, STAT5A, STAT5B, and NFAT. Both *Stat1* and *Stat2* clustered into the glioma-regulated brown module and were around 2.5-fold upregulated. In contrast, *Stat5a* and *Stat5b* were not significantly regulated on transcriptional level. *Irf7* and *Irf9* were 6.9-fold and 1.4-fold upregulated and clustered into the brown and red module, respectively.

Table 4 – Overrepresented GO terms in >2-fold upregulated genes in the glioma-regulated (red and brown) modules.
Statistical tests under hypergeometric distribution were conducted with Bonferroni multi test correction.

Biological process	Number of genes	Adjacent p value
Immune system process	102 genes	adjP=1.21e-30
Immune response	72 genes	adjP=9.65e-30
Defense response	68 genes	adjP=6.25e-23
Innate immune response	44 genes	adjP=6.25e-23
Response to biotic stimulus	53 genes	adjP=3.70e-22
Response to other organism	51 genes	adjP=5.91e-22
Immune effector process	45 genes	adjP=1.47e-18
Response to stress	106 genes	adjP=7.91e-18
Response to cytokine stimulus	40 genes	adjP=1.23e-17
Regulation of immune system process	57 genes	adjP=1.40e-17
Multi-organism process	55 genes	adjP=2.53e-16
Response to virus	25 genes	adjP=1.19e-13
Leucocyte activation	39 genes	adjP=2.52e-10
Cell activation	41 genes	adjP=7.62e-10
Programmed cell death	67 genes	adjP=1.24e-09
Cell death	69 genes	adjP=2.22e-09

Table 5 – Enriched transcription factor binding sites in >2-fold upregulated genes in the glioma-regulated (red and brown) modules.
Statistical tests under hypergeometric distribution were conducted with Bonferroni multi test correction.

Enriched transcription factor targets	Genes	Statistics
mmu_STTTCRNTTT_V$IRF_Q6	*Bst2, Ddr2, Dhx58, Dtx3l, Epsti1, Hgf, Ifi44, Ifit2, Ifit3, Il18bp, Isg15, Lgals3bp, Nampt, Tap1, Tnfsf13b, Usp18, Xaf1, Zbp1*	adjP=2.16e-05
mmu_V$ISRE_01	*Ammecr1, Bst2, Cxcr4, Dhx58, Dtx3l, Epsti1, Gpr65, Ifi44, Ifih1, Ifit2, Ifit3, Isg15, Kynu, Met, Mmp25, Pgk1, Tnfsf13b, Usp18, Xaf1, Zbp1*	adjP=2.84e-05
mmu_V$ICSBP_Q6	*Adam8, Bst2, Cxcr4, Dtx3l, Emp1, Ifi44, Ifih1, Ifit3, Il18bp, Isg15, Kynu, Parp12, Tap1, Tfec, Tnfsf13b, Usp18, Zbp1, Zmynd15*	adjP=0.0004
mmu_V$IRF7_01	*Bst2, Cxcr4, Dll4, Dtx3l, Epsti1, Ifit2, Il18bp, Isg15, Lgals3bp, Nr4a2, Nr4a3, Parp12, Pdgfc, Tap1, Usp18, Xaf1, Zmynd15*	adjP=0.0012
mmu_V$IRF_Q6	*Bst2, Cd80, Cxcr4, Dhx58, Dnase1l3, Dtx3l, Fcgr2b, Ifi44, Ifit2, Il18bp, Isg15, Kynu, Parp12, Tnfsf13b, Ube2l6, Zbp1*	adjP=0.0026
mmu_V$IRF1_01	*Bst2, Ccl5, Dnase1l3, Dtx3l, Isg15, Kynu, Neto1, Pdgfc, Slamf8, Tap1, Tfec, Tgfb3, Tnfsf13b, Usp18, Xaf1*	adjP=0.0083
mmu_TTCYNRGAA_V$STAT5B_01	*Ccl5, Cish, Crem, Dll4, Gzmb, Il18bp, Nfil3, Nkg7, Nr4a3, Pcolce, Plagl1, Plscr1, Serping1, Socs2, Stc1, Tnfrsf9, Trim25*	adjP=0.0213
mmu_TGGAAA_V$NFAT_Q4_01	*Adam9, Adamtsl4, Adm, Aig1, Arrdc4, Bhlhe40, Ccl5, Cd72, Cdkn1a, Chl1, Cish, Creb5, Crem, Ctgf, Ctla4, Dab2, Ddr2, Dll4, Emp1, Erbb3, Gsn, Has2, Hgf, Hif1a, Htr7, Htra4, Ifng, Igfbp3, Il1rn, Impa2, Inhba, Irs2, Isg15, Kynu, Lgals1, Mcam, Mdfic, Mmp14, N4bp1, Nfil3, Nr4a2, Nr4a3, Pde4b, Pdk3, Pgam1, Plod2, Prr11, Prrx1, Sema6a, Socs2, Spp1, Stc1, Tgfb3, Tmem97, Tnfsf10, Trim25, Vegfa*	adjP=0.0221
mmu_V$STAT5B_01	*Ccl5, Cish, Crem, Dll4, Nfil3, Nr4a2, Nr4a3, Pcolce, Plagl1, Plscr1, Serping1, Socs2, Stc1, Trim25*	adjP=0.0221
mmu_V$STAT5A_01	*Ccl5, Cish, Crem, Dll4, Nfil3, Nr4a2, Nr4a3, Pcolce, Plagl1, Plscr1, Serping1, Socs2, Stc1, Tnfrsf9*	adjP=0.0249
mmu_TGANTCA_V$AP1_C	*Adm, Aig1, Ass1, Atp6v0d2, Ccr7, Cd109, Cdkn1a, Creb5, Cst7, Emp1, Furin, Gpnmb, Gpr141, Gzmb, Hspb6, Il10, Il1rn, Isg20, Itgax, Krt8, Lgals1, Mmp12, Mmp13, Mmp19, N4bp1, Osmr, Plp2, Procr, Prrg4, Stat1, Stc1, Tm4sf19, Tnfrsf9, Trim25, Vat1, Vdr, Vegfa*	adjP=0.0460
mmu_V$STAT_01	*Cish, Crem, Gzmb, Il18bp, Nfil3, Nkg7, Nr4a3, Pcolce, Plscr1, Runx3, Serping1, Socs2, Trim25*	adjP=0.0460
mmu_V$IRF2_01	*Bst2, Dnase1l3, Dtx3l, Pdgfc, Tap1, Tgfb3, Tnfsf13b, Usp18, Xaf1*	adjP=0.0460

11.1.2. Comparison to M1/M2 macrophages

11.1.2.1. Expression of known M1/M2 and TAM markers in glioma-associated microglia/macrophages

In general, GAMs are usually considered to be polarized toward a glioma-promoting M2-like phenotype. Previous studies have investigated the expression of selected M1 (such as *Ifng*, *Tnfa*, *Il1b*, and *Nos2*) and M2 (e.g. *Arg1*/*2*, *Tgfb*, and *Il6*) markers in GAMs – either isolated from *in vivo* mouse glioma models or after stimulation of cultured microglia with glioma-conditioned medium – via qRT-PCR (Umemura, Saio et al. 2008; Gabrusiewicz, Ellert-Miklaszewska et al. 2011; Li and Graeber 2012). However, to date no detailed genome-wide expression analysis was performed that investigated the expression profile on a larger scale.

I compared our GAMs expression profile with known markers for M1 and M2 polarization, as well as to known marker genes for tumor-associated macrophages (TAMs) in peripheral tumors (Table 6). I observed that several M1, as well as M2 marker genes are upregulated and expressed at relatively high levels in GAMs. This indicates that GAMs possess a mixed phenotype. However, not all of the considered marker genes were expressed in GAMs at high levels.

Furthermore, most of the selected known TAM marker genes were also highly expressed in GAMs and upregulated in comparison to naïve control cells. This indicates that despite a different tumor-type and location, there are similarities in the gene regulation of tumor-associated macrophages in peripheral tumors and GAMs.

Table 6 – Expression of known M1, M2, and TAM marker genes in our GAMs data set. Marker genes were taken from literature reviews (Mantovani, Sica et al. 2004; Hao, Lu et al. 2012; Li and Graeber 2012).

	M1	Log2 Expression	Regulation	M2	Log2 Expression	Regulation	TAMs	Log2 Expression	Regulation
Receptors and intracellular	*Stat1*	11.56	2.27	*Tgm2*	12.28	6.94	*Cd204*	11.87	13.55
	Tlr2	11.29	2.51	*Cd206*	12.15	1.54	*Stat3*	11.67	1.42
	Cd80	11.20	2.38	*Cd204*	11.87	13.55	*Vegfr2*	9.34	2.13
	Cd86	11.13	2.03	*Il1rll*	11.63	1.72	*Met*	8.08	2.60
	Tlr4	9.72	-1.33	*Tlr8*	11.00	3.21	*Egfr*	7.20	-1.52
	Il1rl	7.67	1.49	*Tlr1*	10.72	2.00	*Cd163*	7.10	-4.40
				Cd163	7.10	-4.40			
Secreted facrots and cytoskines	*Il1b*	12.71	15.54	*Il1rn*	11.63	14.76	*Arg1*	11.48	3.91
	Tnfa	11.03	2.89	*Tgfb3*	10.28	7.85	*Mmp14*	11.36	9.91
	Nos2	10.14	7.24	*Il10*	8.96	3.76	*VegfA*	11.34	8.35
	Il18	9.33	1.71	*Il6*	8.32	1.90	*Mmp13*	11.08	17.73
	Ifng	8.56	2.57				*Tnfa*	11.03	2.89
	Il15	8.47	-1.36				*Ctgf*	10.53	5.35
	Il23a	7.28	1.41				*Arg2*	10.43	11.37
	Indol1	6.93	1.02				*Mmp2*	10.43	4.07
	Il12a	6.61	1.18				*Tgfb3*	10.28	7.85
							Hgf	10.12	4.13
							Il10	8.96	3.76
							Mmp9	8.08	-2.22
							Il12a	6.61	1.18
Chemokines	*Ccl3*	13.21	7.93	*Ccl17*	8.84	2.47	*Cxcl10*	12.83	10.60
	Cxcl9	12.82	32.27	*Ccl24*	8.05	-5.04	*Ccl5*	12.46	15.03
	Ccl5	12.46	15.03	*Ccl22*	7.98	1.61	*Cxcl16*	12.18	5.94
	Ccl2	11.15	4.86	*Ccl1*	6.86	1.22	*Ccl17*	8.84	2.47
	Ccl9	11.03	-1.47				*Ccl22*	7.98	1.61
	Ccl4	10.43	2.68				*Cxcl12*	7.01	-1.77
	Ccl8	10.25	10.52				*Ccl18*	6.20	1.02
	Ccl11	8.54	2.00						

11.1.2.2. GAMs transcriptome only partially resembles an M1 or M2 polarization

Furthermore, I compared our data set with data sets of macrophages that were polarized *in vitro* into an M1 or M2a,b,c phenotype. I used published data sets (Data set: E-GEOD-32690; (Riquelme, Tomiuk et al. 2013)) that contained data of macrophages stimulated *in vitro* for 24 h with LPS and IFN-γ (M1 polarization), IL4 (M2a polarization), IFN-γ and complexed Ig (M2b polarization), and Dexamethasone (M2c polarization) – in comparison to unstimulated M0 macrophages.

For this analysis I considered genes in our GAMs data set that were glioma-regulated (genes that clustered into the red and brown module) and were >2-fold upregulated and compared them with genes that were >2-fold up- or downregulated in the four M1/M2a,b,c data sets (in comparison to the M0 state). GAMs: 438 upregulated genes; M1: 1243 genes up-, 1704 genes downregulated; M2a: 227 genes up-, 322 genes downregulated; M2b: 501 genes up-, 483 genes downregulated; M2c: 381 genes up-, 358 genes downregulated. When comparing genes that were upregulated in the four macrophage sets, our data set showed the highest correlation with M1 (138 out of 438 upregulated genes in GAMs were also upregulated in M1 macrophages, 31.5%, Bonferroni p value: 2.01e-60) and M2b-polarized macrophages (80 out of 438 upregulated genes in GAMs were also upregulated in M2b macrophages, 18.3%, p value: 5.29e-43). The correlation with M2c- (34 out of 381 genes, 7.8%, p value: 1.62e-11) and M2a (23 out of 438 genes, 5.3%, p value: 6.88e-09) was not as strong (Figure 12 A and B). Table 7 lists all genes that overlap between our GAMs data set and are specific for either M1, M2a, M2b, or M2c polarization. However, 59.6% of the genes that were upregulated in GAMs (261 out of 438 genes) were not upregulated in any of the four macrophage phenotypes (Figure 12C). This indicates that the GAM phenotype is distinct from the classical M1 or M2 macrophage phenotype.

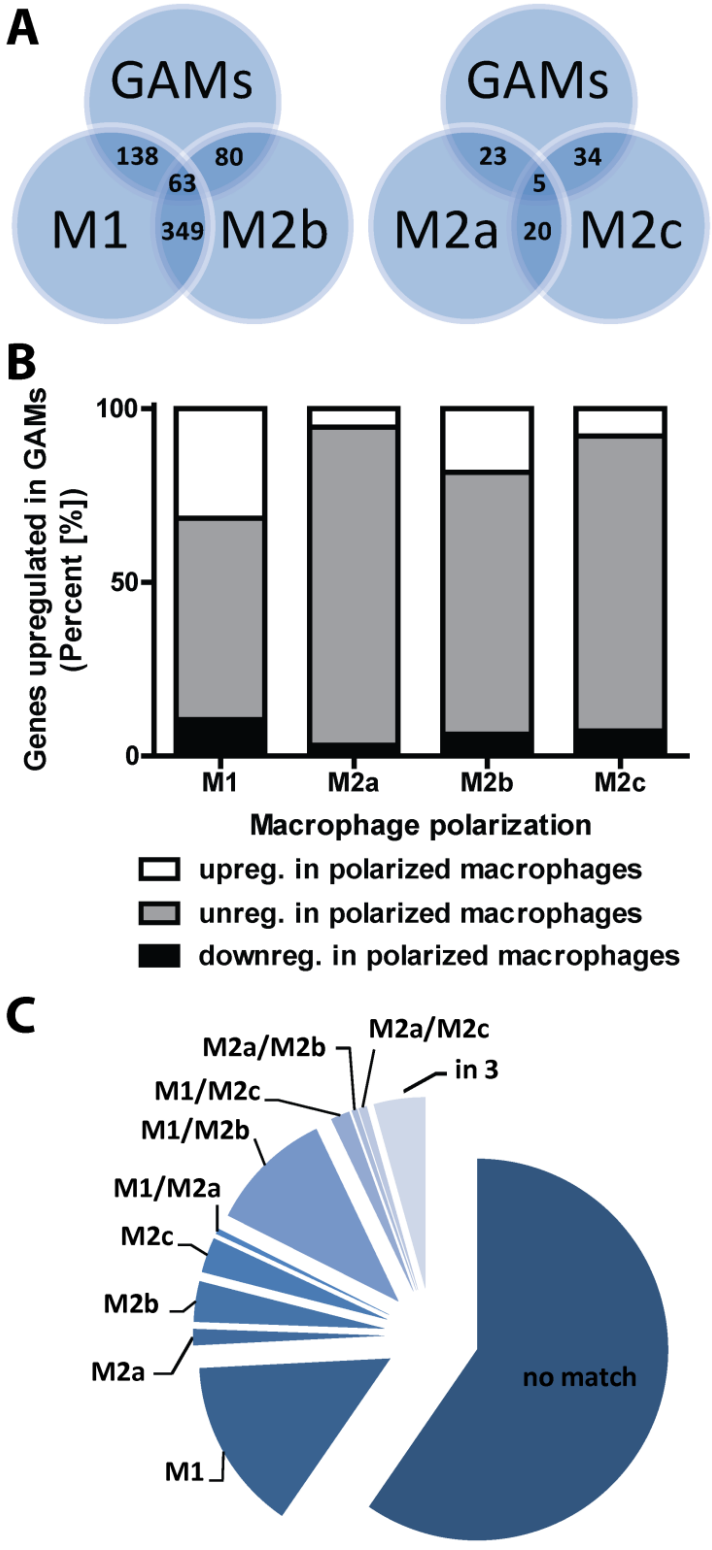

Figure 12 – Comparison of GAMs with data sets of M1/M2-polarized macrophages.
A: A graphical representation of the overlap of >2-fold upregulated genes in GAMs (red and brown modules) and the four macrophage data sets. The GAMs gene expression profile shows the greatest number of overlaps with M1 and M2b polarized macrophages. B: I determined how genes that were upregulated in GAMs were regulated in M1, M2a, M2b, and M2c-polarized macrophages. GAMs have the highest overlap to the M1 and M2b phenotype. C: Only a minority of genes upregulated in GAMs were also induced in the M1 to M2c phenotype, 59.5% of the genes that were upregulated in GAMs were not regulated in any of the four macrophage phenotypes.

Table 7 – M1/M2a,b,c-specific genes that are >2-fold upregulated in our GAMs data set.

	Genes
M1-specific	*1500012F01Rik, 1600014C10Rik, Ahr, Arrdc4, BC023105, Best1, Bst2, C2, Car13, Ccr7, Cd200, Cd52, Clec4n, Clic4, Cpd, Crem, D16Ertd472e, Ell2, Epsti1, Ero1l, Fmnl2, Gpr132, Gpr31c, Hmox1, Htra4, Ifi204, Ifih1, Il1rn, Inhba, Irf7, Isg20, Itga5, Kynu, Malt1, Mefv, Met, Mmp14, Mmp25, Mxd1, Nos2, Nr1h3, Nr4a2, Oas3, Oasl2, Parp12, Plagl1, Ppa1, Procr, Pvr, Rab11fip1, Rasgrp1, Rnf213, Runx3, Slamf7, Slfn5, Srxn1, Stat2, Timp1, Tiparp, Tnfaip2, Treml4, Trim25, Ube2l6, Zmynd15*
M2a-specific	*Atp6v0d2, Clec7a, Itgax, Mmp13, Tnfrsf26, Vwf*
M2b-specific	*AI504432, Casp12, Gpr171, Ifitm1, Il12rb2, Impa2, Itga1, Pdgfc, Plac8, Rspo1, Tgfb3, Tgfbi, Tmem171, Tnfsf13b, Vdr*
M2c-specific	*Adamtsl4, Amica1, Arhgap19, Ctla2a, Cxcr4, Cyp4f18, Fbxo32, Gpr35, Gpx3, Il1r2, Ldlrad3, Mmp19, Wbp5*

11.1.2.3. Validation of M1 and M2a,b,c marker gene expression in glioma-associated microglia/macrophages

I selected five genes that were upregulated in GAMs, clustered into the glioma-regulated (red and brown) modules, and were specifically upregulated in either M1, M2a, M2b, or M2c-polarized macrophages and validated the expression of these genes by qRT-PCR in FACS-sorted samples. I selected *Il1rn*, *Isg20* (both specific for M1-polarized macrophages), *Clec7a* (M2a), *Tgfbi* (M2b), and *Cxcr4* (M2c).

We FACS-isolated GAMs from GL261 tumors and RCAS-*PDGFb* tumors and measured the expression by qRT-PCR in comparison to microglia and peripheral macrophages isolated from control animals. For GAMs isolated from the GL261 mouse model, we distinguished between resident microglia ($CD11b^{+}/CD45^{low}$) and invading macrophages/monocytes ($CD11b^{+}/CD45^{high}/Ly6G^{-}/Ly6C^{high}$) by FACS sorting (Figure 9a; (Dunay, Damatta et al. 2008)). In addition to microglia derived from naïve animals, we also used spleen-derived macrophages/monocytes as additional controls.

As a further validation I used the RCAS-*PDGFb* tumor model, which produces proneural high-grade glioma, as a second glioma model system (Hambardzumyan, Amankulor et al. 2009). For this tumor model we re-transplanted primary RCAS-*PDGFb* tumors into $Cx3cr1^{GFP/wt}$ $Ccr2^{RFP/wt}$ mice, which allowed us to FACS-isolate RFP^{-}/GFP^{+} microglia and RFP^{+}/GFP^{low} macrophages/monocytes from tumors, as well as RFP^{-}/GFP^{+} microglia from control brains and RFP^{+}/GFP^{low} monocytes from peripheral blood without further antibody staining (Figure 9b; (Saederup, Cardona et al. 2010)).

In the GL261 model I was able to confirm a significantly higher expression of all selected genes in glioma-associated macrophages/monocytes and for *Il1rn*, *Clec7a*, and *Cxcr4* in glioma-associated microglia, compared to the respective control cells. (Figure 13). In the RCAS model I saw a significantly higher expression of all selected genes when comparing glioma-associated microglia to naïve microglia. When comparing glioma-associated macrophages/monocytes to naïve monocytes, only the expression of *Il1rn*, *Tgfbi*, and *Cxcr4* was significantly higher. For *Isg20* a lower expression in glioma-associated macrophages/monocytes could be detected when compared to naïve monocytes. Furthermore, the expression of *Clec7a* was unchanged in glioma-associated macrophages/monocytes when compared to naïve monocytes. All investigated genes were expressed at higher levels in naïve monocytes when compared to naïve microglia. In part the expression was as high as in glioma-associated microglia (Figure 13).

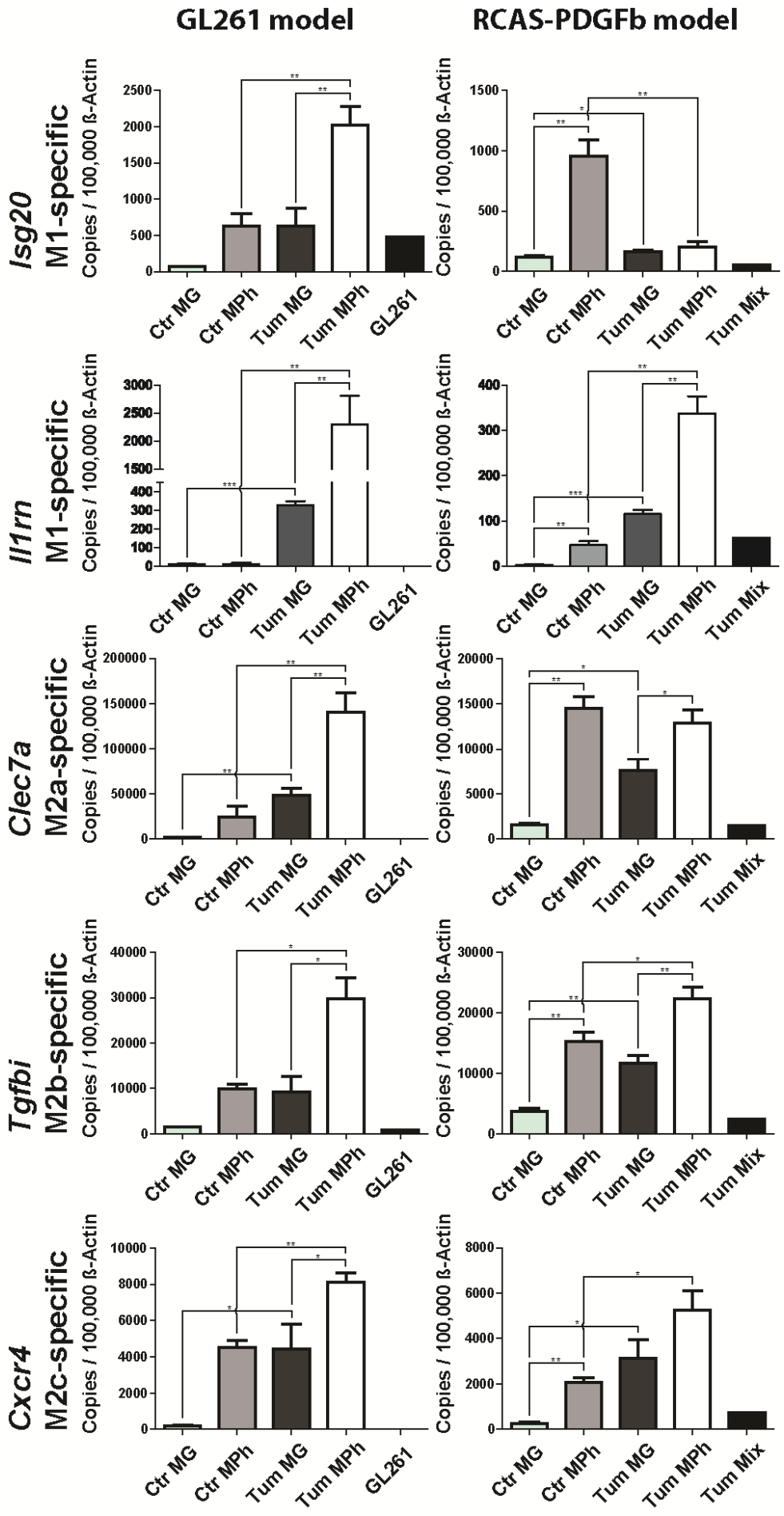
GL261 model
RCAS-PDGFb model
Isg20
M1-specific
Il1rn
M1-specific
Clec7a
M2a-specific
Tgfbi
M2b-specific
Cxcr4
M2c-specific
Copies / 100,000 ß-Actin
Ctr MG
Ctr MPh
Tum MG
Tum MPh
GL261
Tum Mix

Figure 13 – qRT-PCR validation of selected M1 and M2a,b,c-specific genes in murine GAMs.
We selected 5 genes that were upregulated in GAMs and specific for either M1 (*Il1rn* and *Isg20*), M2a (*Clec7a*), M2b (*Tgfbi*), or M2c polarization (*Cxcr4*) and investigated the expression of these using qRT-PCR. For this we isolated GAMs from GL261 and RCAS-*PDGFb* tumors using flow cytometry, in order to distinguish between resident microglia and invading macrophages/monocytes and used microglia, and spleen-derived macrophages/monocytes from naïve mice as controls. CTR MG: naïve microglia, CTR Mph: naïve monocytes, Tum MG: glioma-associated microglia, Tum Mph: glioma-associated macrophages/monocytes, GL261: cultured GL261 cells, Tum Mix: cultured RCAS-*PDGFb* tumor cells. Bar graphs illustrate the absolute number of transcripts normalized to 100,000 transcripts of *Actb* (n=4). Statistical analysis was done by students t test. Error bars indicate the Standard Error of the Mean (SEM). *, $p<0.05$; **, $p<0.01$; ***, $p<0.001$

Since up to date there is no reliable method to distinguish between invading monocytes/macrophages and microglia in human glioma samples, the only method I could use was the MACS isolation using CD11b only. I collected human GBM samples and isolated $CD11b^+$ microglia/macrophages via MACS. I analyzed the gene expression of GAMs ($CD11b^+$ sorted cells) in GBM samples, the flow through of these tumor samples (the CD11b-negative fraction after MACS-isolation), control microglia samples (taken from brain resections of hippocampus, epilepsy, and trauma patients), and blood monocytes (Figure 14).

I detected high expression of all genes in $CD11b^+$ GAMs isolated from GBM samples, however only the gene expression of *IL1RN*, *ISG20* (both M1-specific), and *TGFBI* (M2b-specific) was significantly higher in $CD11b^+$ cells isolated from GBM samples, when compared to $CD11b^+$ cells isolated from control brain samples. The expression of *CXCR4* was not significantly higher, whereas the expression of *CLEC7A* was significantly lower in $CD11b^+$ cells isolated from GBM samples. This might be in part due to the fact that the control brain specimen were not taken from healthy patients, but patients suffering from epilepsy (3 samples) and trauma injury (1 sample). In these conditions the microglia might have already been polarized toward an M2-like phenotype.

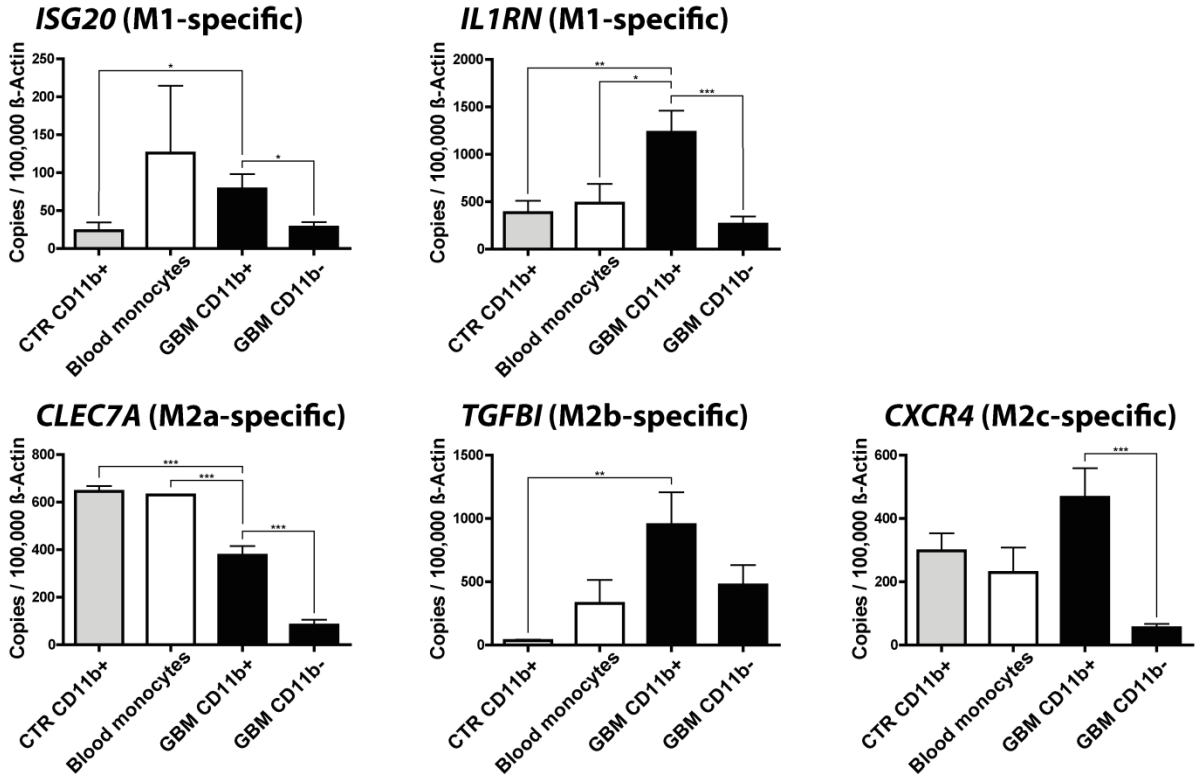

Figure 14 – qRT-PCR validation of selected M1 and M2a,b,c-specific genes in human GAMs.

I determined the expression of the M1 (*IL1RN* and *ISG20*), M2a (*CLEC7A*), M2b (*TGFBI*), and M2c-specific (*CXCR4*) genes in $CD11b^+$ and $CD11b^-$ cells isolated from human GBM ($CD11b^+$ n=13, $CD11b^-$ n=5), control brain ($CD11b^+$ n=5, $CD11b^-$ n=2) and blood monocyte samples (n=2). Bar graphs illustrate the absolute number of transcripts normalized to 100,000 transcripts of *ACTB*. Statistical analysis was done by students t test. Error bars indicate the SEM. *, $p<0.05$; **, $p<0.01$; ***, $p<0.001$

11.1.3. Screen for potential pro-tumorigenic genes in glioma-associated microglia/macrophages

11.1.3.1. Resident microglia and invading peripheral macrophages/monocytes have different gene expression profiles in glioma

To identify novel glioma-associated genes expressed by microglia/macrophages, I analyzed the data sets for genes that were upregulated in GAMs and might support glioma progression. I pre-selected genes that fulfilled multiple criteria: First, they had to be highly expressed in GAMs and at least 2-fold upregulated when compared to the three control data sets. These criteria comprised mostly genes that highly correlated with the glioma-regulated (red and brown) modules. Second, I also considered genes that were upregulated in GAMs compared to the naïve microglia control data set and were already highly expressed in peripheral macrophages (green module, Figure 11). I excluded genes that have already been reported in the GAMs context.

Two features of high grade glioma are the aggressive invasion into the brain parenchyma and the immune-suppressive environment which prevents tumor rejection. Therefore, I narrowed down the list of our selected genes by focusing on targets that had been implicated in supporting tumor cell invasion in peripheral tumors (*Spp1*, *Hpse*), myeloid cell activation (*Gpnmb*, *Trem1*, *Cd200r4*, *Cd300lf*, *Creb5*), or suppression of adaptive immunity (*Gpnmb*, *Sh2d1b1*, *Cxcl13*, *Il1rn*).

To investigate the expression of these genes in GAMs via qRT-PCR in FACS-sorted samples from GL261 and RCAS-*PDGFb* tumors in comparison to naïve control cells, we used the same samples as described above for the validation of the M1 and M2a,b,c-specific genes (chapter 11.1.2.3).

We were able to validate the expression of all selected genes from the microarray using qRT-PCRs. Furthermore, the regulation of the genes was very similar in both brain tumor models – GL261, as well as RCAS-*PDGFb* tumors. This shows that the upregulation of these genes was not specific for one tumor model, but was observed in two different independent models. In addition, the expression of most genes was higher in GAMs when compared to the tumor cells, indicating that GAMs may be the primary source, which is especially interesting for secreted proteins. We grouped the genes according to their expression pattern in glioma-associated resident microglia and invading macrophages/monocytes. The genes *Spp1*, *Cd200r4*, and *Cxcl13* (Figure 15) were upregulated in both cell types, but were higher expressed in

resident microglia than invading macrophages/monocytes. The genes *Gpnmb*, *Il1rn*, *Cd300lf*, *Trem1*, *Creb5*, and *Uck2* (Figure 16) were also upregulated in both cell types but were higher expressed in invading macrophages/monocytes than in resident microglia. The genes *Hpse*, *Sh2d1b1*, and *Sepx1* were glioma-dependent upregulated in microglia, but not in macrophages/monocytes, as already naïve control macrophages/monocytes expressed these genes at similarly high levels (Figure 17).

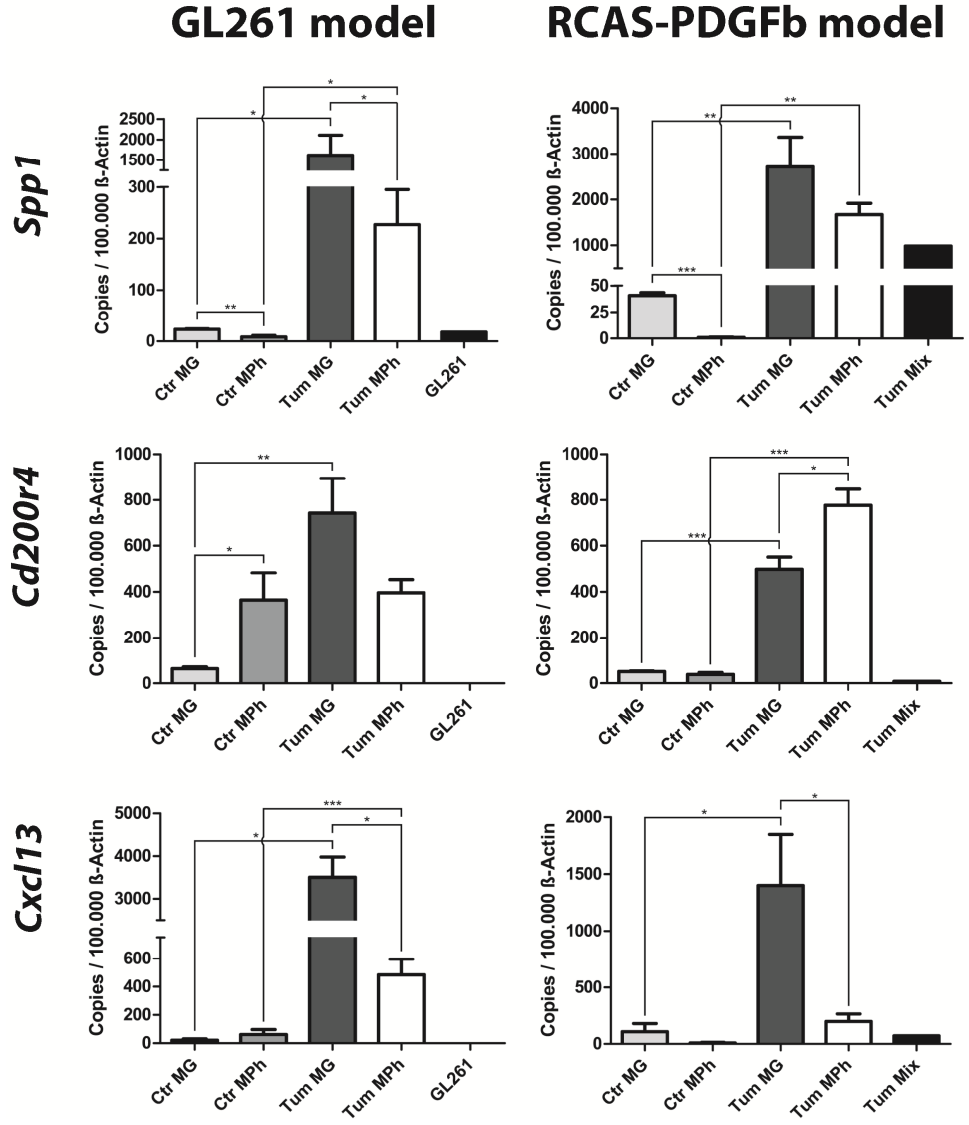

Figure 15 – Genes that were predominantly expressed by mouse glioma-associated brain-resident microglia as assessed by qRT-PCR.
We isolated GAMs from GL261 and RCAS-*PDGFb* tumors using flow cytometry, in order to distinguish between resident microglia (Tum MG) and invading macrophages/monocytes (Tum MPh) and used microglia (CTR MG), and spleen-derived macrophages/monocytes (CTR MPh) from naïve mice as controls. Bar graphs illustrate the absolute number of transcripts normalized to 100,000 transcripts of *Actb* (n=4). Statistical analysis was done by students t test. Error bars indicate the SEM. *, $p<0.05$; **, $p<0.01$; ***, $p<0.001$. QRT-PCRs were performed by my student Andreas Pelz under my supervision.

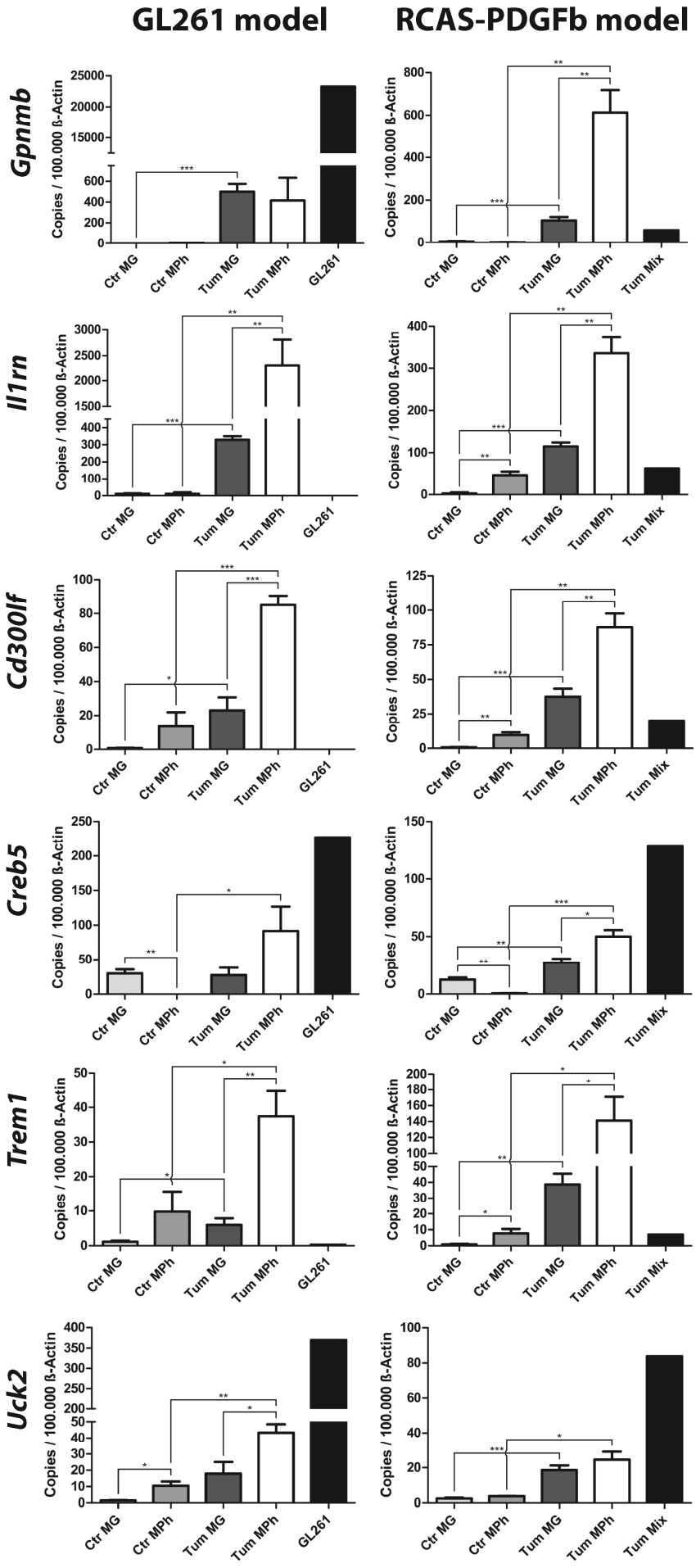
GL261 model
RCAS-PDGFb model
Gpnmb
Il1rn
Cd300lf
Creb5
Trem1
Uck2
Copies / 100.000 ß-Actin
Ctr MG
Ctr MPh
Tum MG
Tum MPh
GL261
Tum Mix

Figure 16 – Genes that were predominantly expressed by mouse glioma-associated invading macrophages/monocytes as assessed by qRT-PCR.
We isolated GAMs from GL261 and RCAS-*PDGFb* tumors using flow cytometry, in order to distinguish between resident microglia (Tum MG) and invading macrophages/monocytes (Tum MPh) and used microglia (CTR MG), and spleen-derived macrophages/monocytes (CTR MPh) from naïve mice as controls. Bar graphs illustrate the absolute number of transcripts normalized to 100,000 transcripts of *Actb* (n=4). Statistical analysis was done by students t test. Error bars indicate the SEM. *, p<0.05; **, p<0.01; ***, p<0.001. QRT-PCRs were performed by my student Andreas Pelz under my supervision.

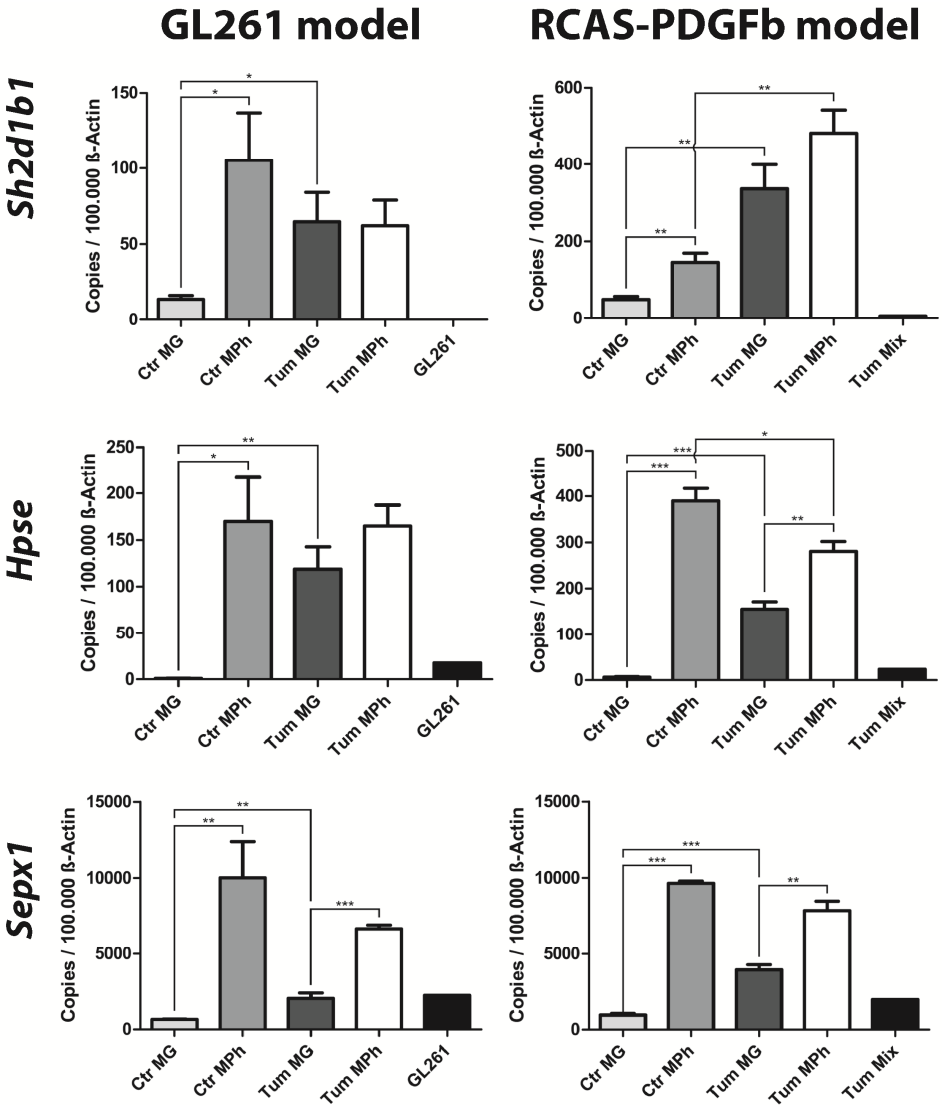

Figure 17 – Genes that were upregulated in glioma-associated microglia, but not in glioma-associated macrophages/monocytes as assessed by qRT-PCR.
We isolated GAMs from GL261 and RCAS-*PDGFb* tumors using flow cytometry, in order to distinguish between resident microglia (Tum MG) and invading macrophages/monocytes (Tum MPh) and used microglia (CTR MG), and spleen-derived macrophages/monocytes (CTR MPh) from naïve mice as controls. Bar graphs illustrate the absolute number of transcripts normalized to 100,000 transcripts of *Actb* (n=4). Statistical analysis was done by students t test. Error bars indicate the SEM. *, p<0.05; **, p<0.01; ***, p<0.001. QRT-PCRs were performed by my student Andreas Pelz under my supervision.

11.1.3.2. Expression of *GPNMB*, *SPP1*, *IL1RN*, and *HPSE* is upregulated in human GBM-associated microglia/macrophages

As described above, I collected human samples and isolated $CD11b^+$ microglia/macrophages via MACS to use qRT-PCR to determine the expression of the selected target genes in these samples. In addition to $CD11b^+$ and $CD11b^-$ cells isolated from GBM samples and naïve brain tissue, I also investigated meningioma and anaplastic astrocytoma (grade III glioma) samples.

Prior to performing qRT-PCRs with all samples I determined the expression of all genes in a small subset of samples using gel-based sqRT-PCR. I used GAMs isolated from GBM samples (3 samples), grade III anaplastic astrocytoma (1 sample), meningioma (1 sample), intracranial metastase (1 sample), and $CD11b^+$ cells isolated from non-neoplastic control samples (3 samples). I could detect gene expression for all genes (Figure 18) except *SH2D1B*, *CXCL13*, and *CD200R1L* (no visible bands were present, images not shown). Already using sqRT-PCR it could be seen that GPNMB was highly expressed in GAMs when compared to microglia isolated from control samples. In contrast, the expression of *CREB5*, *SEPX1*, and *UCK2* was higher in control cells than in GAMs.

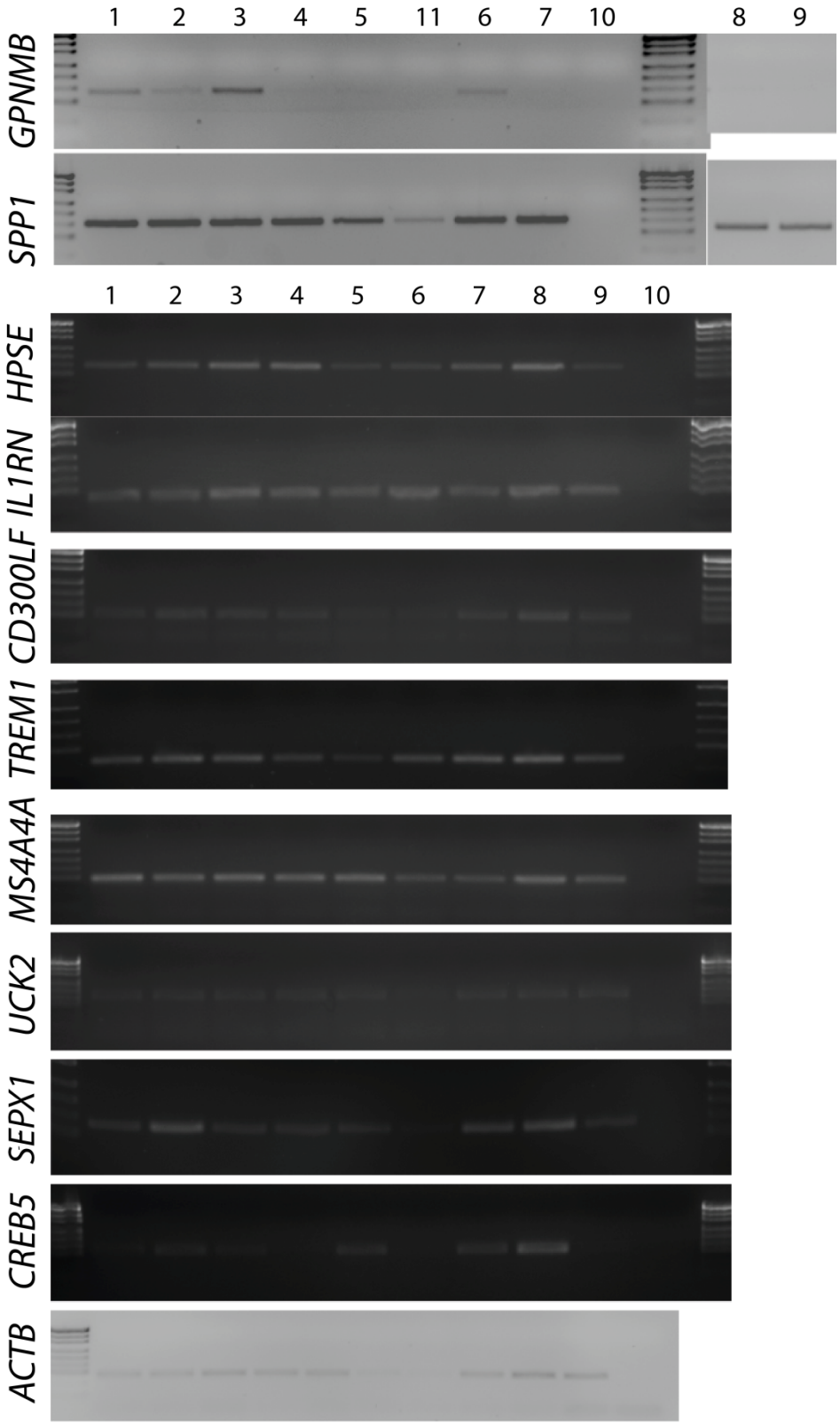

Figure 18 – Results of the first mini screen with a small set of CD11b$^+$ cells isolated from human samples.
I tested the expression of the human target genes with fewer samples by sqRT-PCR to select the most promising genes for qRT-PCR validation. Legend: GAMs isolated from GBM samples (1-3), from anaplastic astrocytoma (4), from CD11b$^+$ cells from meningioma sample (5,11), from an intracranial metastasis (6), CD11b$^+$ cells isolated from non-neoplastic brain tissue (7-9), and negative control (10).

Based on the results of the first screen, I decided to investigate the expression of *GPNMB*, *SPP1*, *HPSE*, *IL1RN*, *CD300LF*, and *TREM1* in a larger set of human samples by qRT-PCR. I found that the expression of *GPNMB*, *SPP1*, *IL1RN*, and *HPSE* was significantly higher in human GAMs isolated from GBM samples, when compared to non-tumor-associated control microglia and blood monocytes (Figure 19 A-D). The expression of these genes was significantly higher in GAMs than in the tumor flow through ($CD11b^-$ fraction), indicating that GAMs were the greatest source for these transcripts. The source and rate of expression of *GPNMB* seems to be dependent on the grade of malignancy of the tumor. In GBM GAMs were the main source for the expression, showing a five times higher expression than the GBM flow through, which comprises the tumor cells and other stromal cells. However, in microglia/macrophages isolated from meningioma, which is a benign tumor of the meninges, the expression of *GPNMB* was higher in the tumor flow through, compared to associated microglia/macrophages. The overall expression of *GPNMB* was higher in GBM than in meningioma and grade III astrocytoma samples. The expression of *SPP1* was also dependent on tumor grade. Similar to *GPNMB*, the expression of *SPP1* was higher in GAMs isolated from GBM specimen, compared to the GBM flow through. Whereas, in lower grade tumors the expression of *SPP1* was generally lower, which might indicate a possible role for *SPP1* in higher grade tumors. I performed absolute quantification for *SPP1* and *GPNMB*. The results for *HPSE* and *IL1RN* are similar, however, *HPSE* was even more strongly expressed in GAMs isolated from grade III anaplastic astrocytoma, when compared to GAMs isolated from GBM samples.

In contrast, the expression of *CD300LF* and *TREM1* in GAMs was different in human when compared to the murine tumors. Despite the upregulation of these genes in both murine tumor models tested, the expression of *CD300LF* was not upregulated in $CD11b^+$ microglia/macrophages isolated from GBM, meningioma, and anaplastic astrocytoma samples when compared to $CD11b^+$ cells isolated from control brain tissues. However, *CD300LF* was significantly higher expressed in $CD11b^+$ cells than $CD11b^-$ cells in GBM samples (Figure 19 E). In addition, the expression of *TREM1* was lower in human $CD11b^+$ cells isolated from GBM samples when compared to $CD11b^+$ cells isolated from control brain tissue (Figure 19 F). I tested the expression of *TREM1* only in $CD11b^+$ cells isolated from GBM samples and non-neoplastic control brain samples.

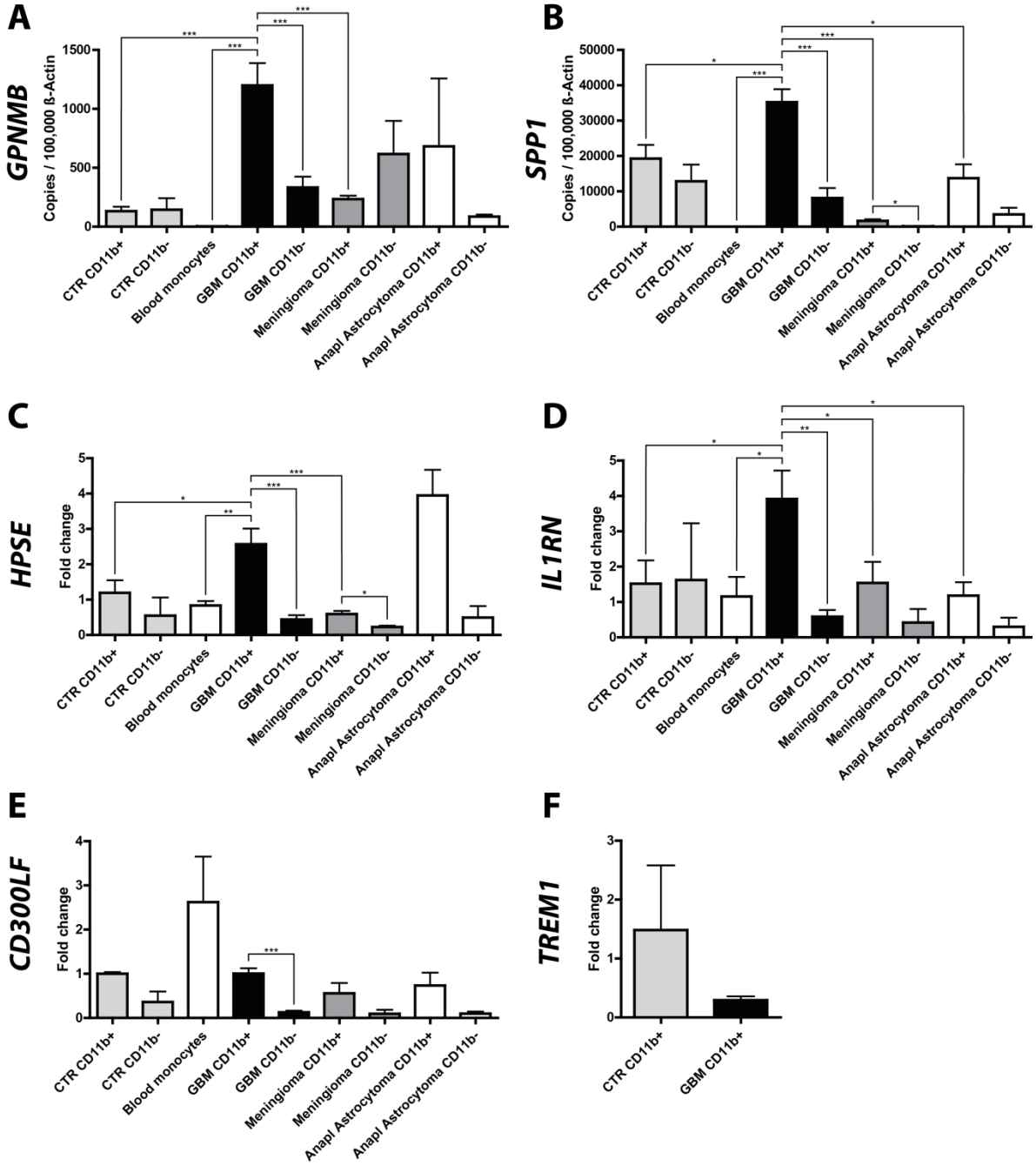

Figure 19 – The expression of the genes *GPNMB*, *SPP1*, *HPSE*, *IL1RN*, and *CD300LF* in CD11b$^+$ and CD11b$^-$ cells isolated from human samples.
GBM (CD11b$^+$ n=13, CD11b$^-$ n=5), meningioma (CD11b$^+$ n=5, CD11b$^-$ n=3), grade III anaplastic astrocytoma (CD11b$^+$ n=2, CD11b$^-$ n=2), control brain (CD11b$^+$ n=5, CD11b$^-$ n=2) and blood monocyte samples (n=2) were used. The expression of *GPNMB*, *IL1RN*, *HPSE*, and *SPP1* was significantly higher in CD11b$^+$ cells isolated from GBMs compared to CD11b$^+$ cells isolated from control brain, benign meningioma samples, blood monocytes, and CD11b$^-$ cells in GBM (A-D). However, in contrast to the results from the murine tumor models the expression of *CD300LF* was not upregulated in CD11b$^+$ microglia/macrophages isolated from human GBM samples compared to CD11b$^+$ microglia isolated control brain samples (E). The expression of *TREM1* was measured in CD11b$^+$ cells isolated from 4 GBM samples and from 2 non-neoplastic control samples. A-B: Bar graphs illustrate the absolute number of transcripts normalized to 100,000 transcripts of *ACTB*. C-F: Bar graphs illustrate the mean relative expression normalized to the mean "Control CD11b$^+$" expression. Statistical analysis was done by students t test. Error bars indicate the SEM. *, p<0.05; **, p<0.01; ***, p<0.001

11.1.3.3. High expression of *GPNMB, SPP1*, *CD300LF*, and *TREM1* in human GBM tissues is associated with a worsened survival outcome

I used the NCI Rembrandt database (https://caintegrator.nci.nih.gov/rembrandt/home.do), which provides gene expression data correlated with patient survival data. High expression of *GPNMB*, *SPP1*, *HPSE*, *IL1RN*, and *CD300LF* in human glioma is associated with a worse patient survival prognosis (Figure 20), whereas low expression is associated with a longer patient survival – compared to intermediate expression of these genes in glioma samples. High expression of *GPNMB* and *SPP1* has the most dramatic effect on patient prognosis (Figure 20A-B), whereas the effects of high expression of HPSE and IL1RN are more moderate (Figure 20C-D). Even though I was not able to detect a higher expression of *CD300LF* in the $CD11b^+$ fractions isolated from GBM and meningioma samples, when compared to $CD11b^+$ cells isolated from control samples, patients with high expression of *CD300LF* have a poor survival prognosis (Figure 20E). GAMs expressed *GPNMB, SPP1, IL1RN, HPSE,* and *CD300LF* in human tumor samples at a higher rate than other stromal and tumor cells ($CD11b^-$ fraction, Figure 19), indicating that GAMs may be the main source for the high gene expression measured in the Rembrandt data.

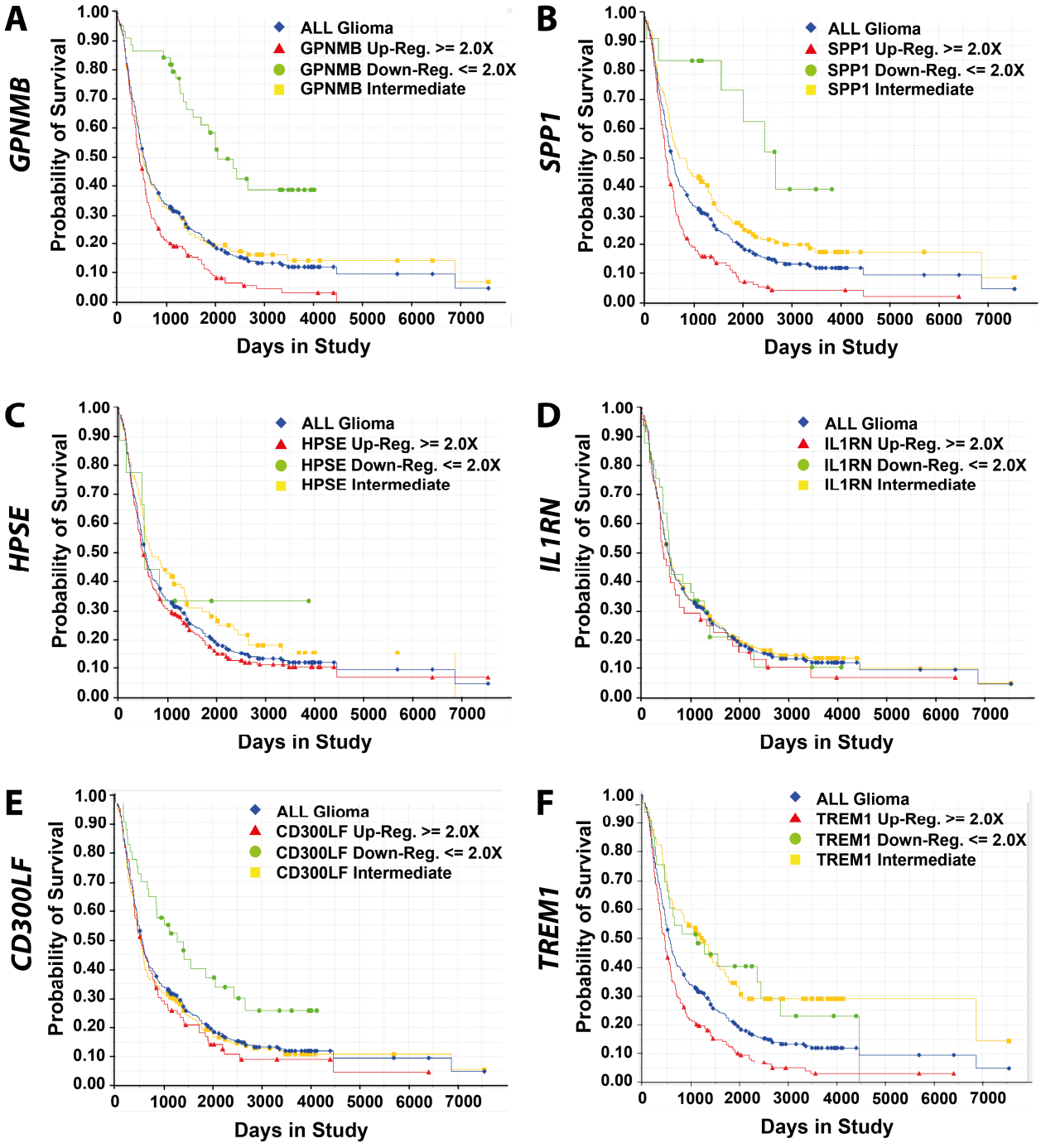

Figure 20 – Data taken from the Rembrandt database.
The data shows survival probability of glioma patients grouped according to high, intermediate, and low expression of our target genes *GPNMB*, *SPP1*, *HPSE*, *IL1RN*, *CD300LF*, and *TREM1*. High expression of all target genes has a negative effect on patient prognosis. The effect is most severe for high expression of the genes *GPNMB*, *SPP1*, and *TREM1*.

The Rembrandt database uses patient data without distinguishing between low- and high-grade glioma, therefore the data is not restricted to GBM samples. To assess the effect of the expression of our target genes on patient survival purely in GBM patients I also used the cBioPortal database (http://www.cbioportal.org/public-portal/) that uses data generated from The Cancer Genome Atlas (TCGA) project (Cerami, Gao et al. 2012; Gao, Aksoy et al. 2013).

High expression of both SPP1 and GPNMB has a negative effect on patient prognosis (Figure 21). In addition, I grouped patients into the four molecular subtypes (proneural, neural, mesenchymal, and classical) to investigate the effect of high *GPNMB* and *SPP1* expression in these subtypes. Low *GPNMB* expression is associated with the most positive effect on patient prognosis in the proneural subtype, but no significant effect in the other subtypes. Low *SPP1* expression is associated with the most beneficial effect on patient prognosis in the proneural and classical subtypes. Mesenchymal tumors have a higher probability of high *GPNMB* and *SPP1* expression, whereas classical tumors have a higher probability of low expression of both genes.

The data from the Rembrandt database showed that high *HPSE* and *IL1RN* expression had a small negative effect on patient survival (Figure 20). The TCGA data shows no correlation between HPSE or IL1RN expression and patient survival outcome (Figure 22). High expression of *CD300LF* correlates with a significantly worse prognosis of patients suffering from GBM of the classical subtype, but no significant effect can be observed for all GBM subtypes combined (Figure 23A). High *TREM1* expression is linked with shorter patient survival in GBM patients and with patients suffering from proneural subtype GBM (Figure 23B). Furthermore, all six genes are differently regulated within the four subtypes. Tumors of the mesenchymal subtypes express all six genes at the highest level.

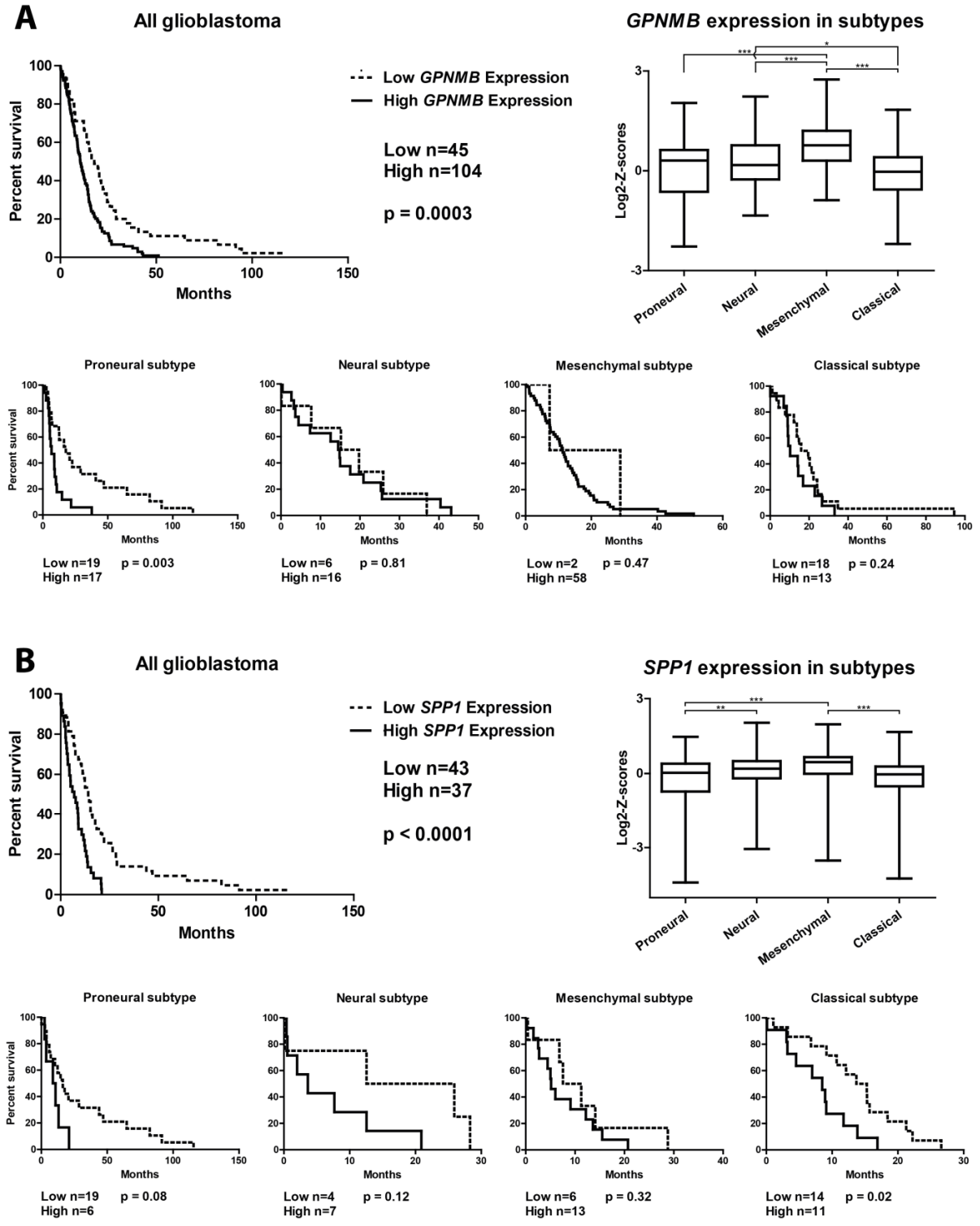

Figure 21 – High *GPNMB* and *SPP1* expression is associated with worsened survival prognosis in human GBM patients.
Data taken from the TCGA database, showing survival probability of glioma patients grouped according to high and low expression of our target genes *GPNMB* (A) and *SPP1* (B). High expression of both genes has a negative effect on patient prognosis. Patients were in addition grouped into the four molecular subtypes (proneural, neural, mesenchymal, and classical). Low *GPNMB* expression seems to have the most severe effect on patient prognosis in the proneural subtype, but not a significant effect in the other subtypes. Low *SPP1* expression seems to have the highest effect on patient prognosis in the proneural and classical subtypes. Furthermore, both genes are differently regulated in the four subtypes (box plots in A and B). Statistics were performed as described in 11.1.20.

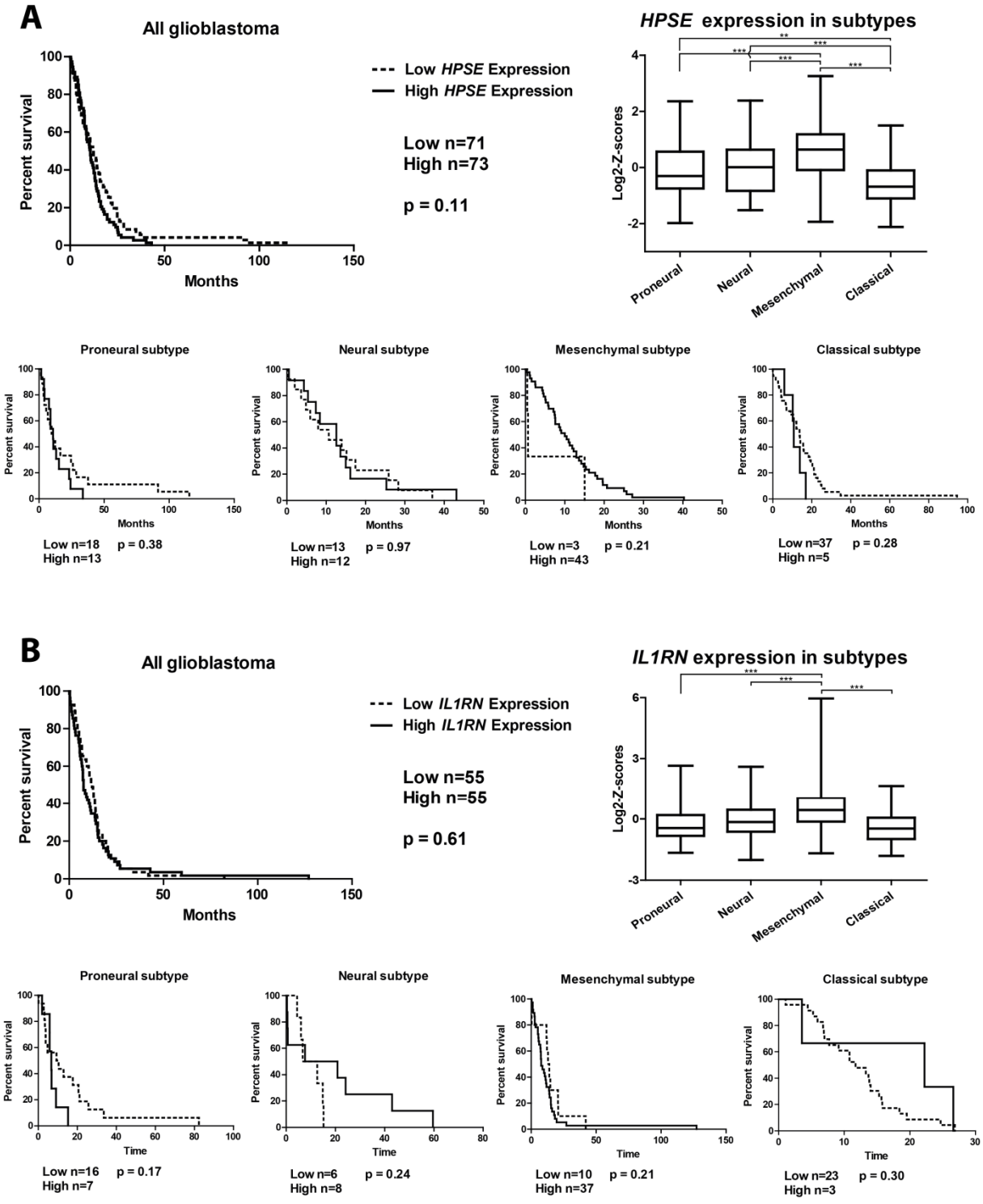

Figure 22 – Data taken from the TCGA database, showing survival probability of glioma patients grouped according to high and low expression of our target genes *HPSE* (A) and *IL1RN* (B).

No significant correlation between GBM patient survival and gene expression of *HPSE* or *IL1RN* can be found. Both genes are differently regulated in the four subtypes (box plots in A and B). Statistics were performed as described in 11.1.20.

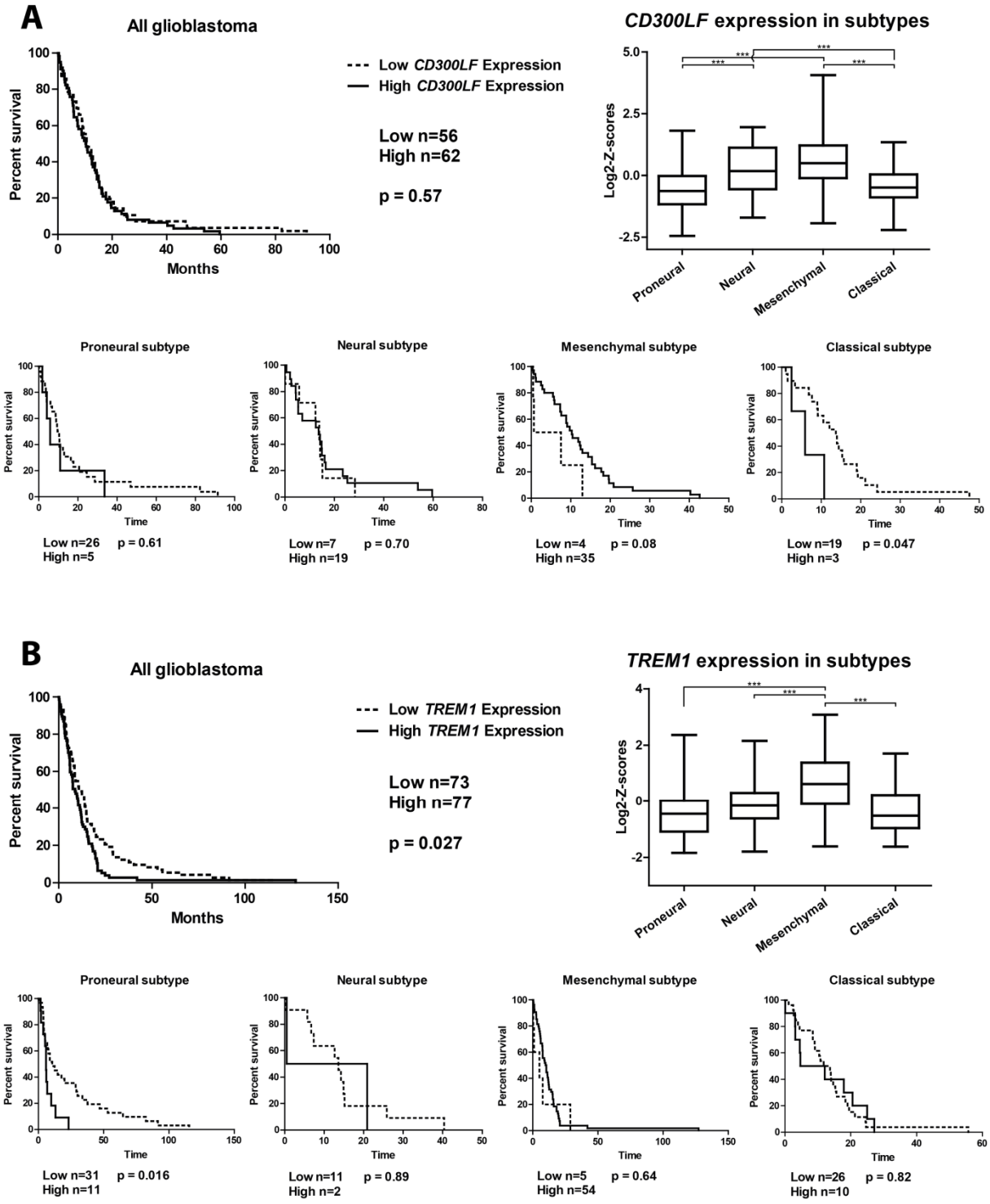

Figure 23 – Data taken from the TCGA database, showing survival probability of glioma patients grouped according to high and low expression of our target genes *CD300LF* (A) and *TREM1* (B).

High expression of *CD300LF* seems to be linked with a significantly worsened prognosis of patients suffering from GBM of the mesenchymal subtype (A). High *TREM1* expression is linked with shorter patient survival in GBM patients (B). Both genes are differently regulated in the four subtypes (box plots in A and B). Statistics were performed as described in 11.1.20.

11.2. **Project 2:** Effect of *Cx3cr1*-loss on GAMs in an organotypic brain slice model

Using *in vivo* mouse studies employing the RCAS-*PDGFb* glioma model and the *Cx3cr1-GFP* knock in mouse model, we found that homozygous *Cx3cr1* loss (*Cx3cr1*$^{GFP/GFP}$) leads to higher glioma incidence and shorter symptom-free survival time (defined by fixed criteria such as weight loss, hunch-back, seizures, immobility) of glioma-bearing mice. Further analysis showed greater accumulation of periphery-derived monocytes in tumor areas (Feng X., et al, manuscript submitted). In order to investigate if the higher incidence and aggressiveness of gliomas growing in *Cx3cr1*$^{GFP/GFP}$ mice is mainly facilitated by invading peripheral monocytes or also by brain-resident microglia I applied an *in situ* model for which I prepared and cultured brain slices from P14-P16 *Cx3cr1*$^{GFP/GFP}$, *Cx3cr1*$^{GFP/wt}$, and *Cx3cr1*$^{wt/wt}$ mice and implanted GL261 and RCAS-*PDGFb-RFP* tumors into these slices, in order to investigate the effect of *Cx3cr1* expression on tumor growth and microglia migration toward the tumor in a monocyte-free model (see chapter 11.1.7 and following chapters).

11.2.1. Loss of *Cx3cr1* enhances GL261 tumor growth *in situ*

5,000 mCherry^{+} GL261 cells were injected into brain slices from P14-P16 *Cx3cr1*$^{GFP/GFP}$, *Cx3cr1*$^{GFP/wt}$, and *Cx3cr1*$^{wt/wt}$ mice 1 day after cutting. The tumor size was measured according to the fluorescent area at day 6 and 12 post-injection. Tumors grew in all three genetic conditions and also still increased in size after 6 days of injection. There was no significant difference in tumor size 6 days post-injection, however, 12 days post-injection tumors growing in *Cx3cr1*$^{GFP/GFP}$ were significantly larger when compared to tumors growing in *Cx3cr1*$^{GFP/wt}$ and *Cx3cr1*$^{wt/wt}$ slices. There was no significant difference in tumor size between *Cx3cr1*$^{GFP/wt}$ and *Cx3cr1*$^{wt/wt}$ slices (Figure 24B). There was no obvious difference in growth pattern between GL261 tumors in all three conditions, as these tumors showed very confined borders in all three genetic conditions and grew minimally invasive. Furthermore, after 6 and 12 days the normal tissue in the tumor area was largely removed and displaced by tumor cells (Figure 24A).

Next I asked if the increase in tumor volume in the *Cx3cr1*$^{GFP/GFP}$ slices correlated with increased microglia migration toward the tumor in this genotype. To answer this question I cultured *Cx3cr1*$^{GFP/GFP}$ and *Cx3cr1*$^{GFP/wt}$ slices, fixed the slices 4 days after the injection of GL261 cells, and recut them to 10 µm section using a cryostat device.

It was necessary to fix the slices at a relatively early time point, as with longer culturing the slices get more degraded and unstable, which prevents proper recutting. Using confocal microscopy I investigated the migration of GFP^+ microglia cells towards the $mCherry^+$ GL261 tumor cells and quantified the number of microglia/area within the tumor itself, in the inner (0 to 85 µm from tumor border) and the outer (85 to 170 µm from tumor border) peritumoral area. In both genetic backgrounds I detected only a small number of microglia within the tumor area. This was most likely due to the fact that the GL261 tumors grew very densely, restricting the migration of stromal cells into the tumor. Larger numbers of microglia were detected in the peritumoral areas. I saw a non-significant trend towards higher numbers of microglia in the inner peritumoral area of tumor in *Cx3cr1*$^{GFP/GFP}$ slices when compared to the outer area and to tumors in *Cx3cr1*$^{GFP/wt}$ slices (Figure 25). This correlated with the increased size of GL261 tumors in *Cx3cr1*$^{GFP/GFP}$ slices.

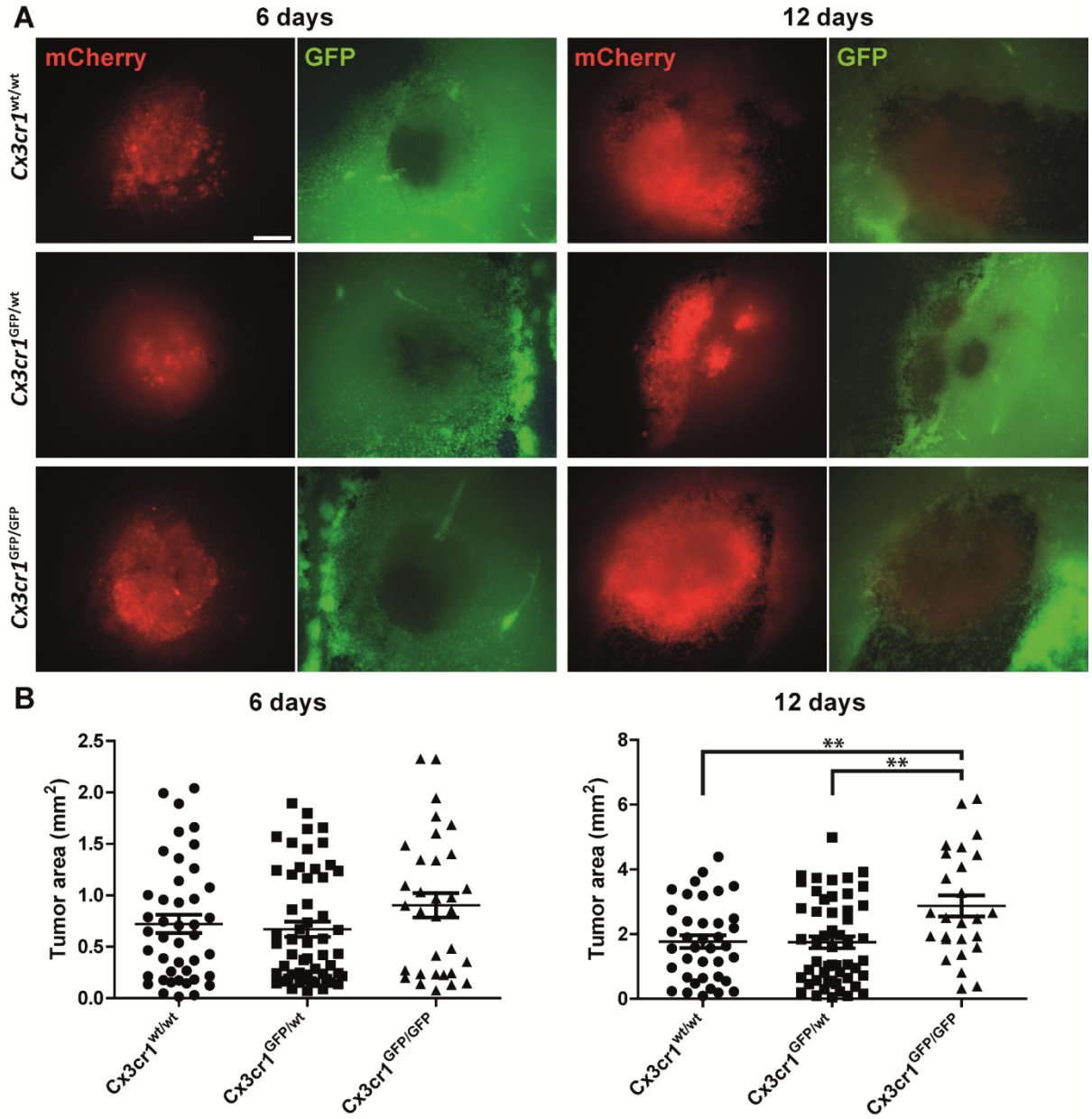

Figure 24 – mCherry^{+} GL261 glioma cells were injected into cultured organotypic brain slices of *Cx3cr1*$^{wt/wt}$, *Cx3cr1*$^{GFP/wt}$, and *Cx3cr1*$^{GFP/GFP}$ mice to investigate the role of *Cx3cr1* on tumor growth in a monocyte-free model.

A: Representative images of tumors (red fluorescence) in slices of all three genotypes at 6 and 12 days post-injection. Accumulation of GFP^{+} microglia can be observed in *Cx3cr1*$^{GFP/wt}$ and *Cx3cr1*$^{GFP/GFP}$ slices (green fluorescence). The slice tissue also shows strong auto fluorescence in the green channel and shows the degradation of the normal tissue in the tumor area. B: Tumors in *Cx3cr1*$^{GFP/GFP}$ slices were significantly bigger 12 days after injection. Statistical significances were calculated applying a One-Way-ANOVA. **, $p<0.01$ Scale bar: 400 µm.

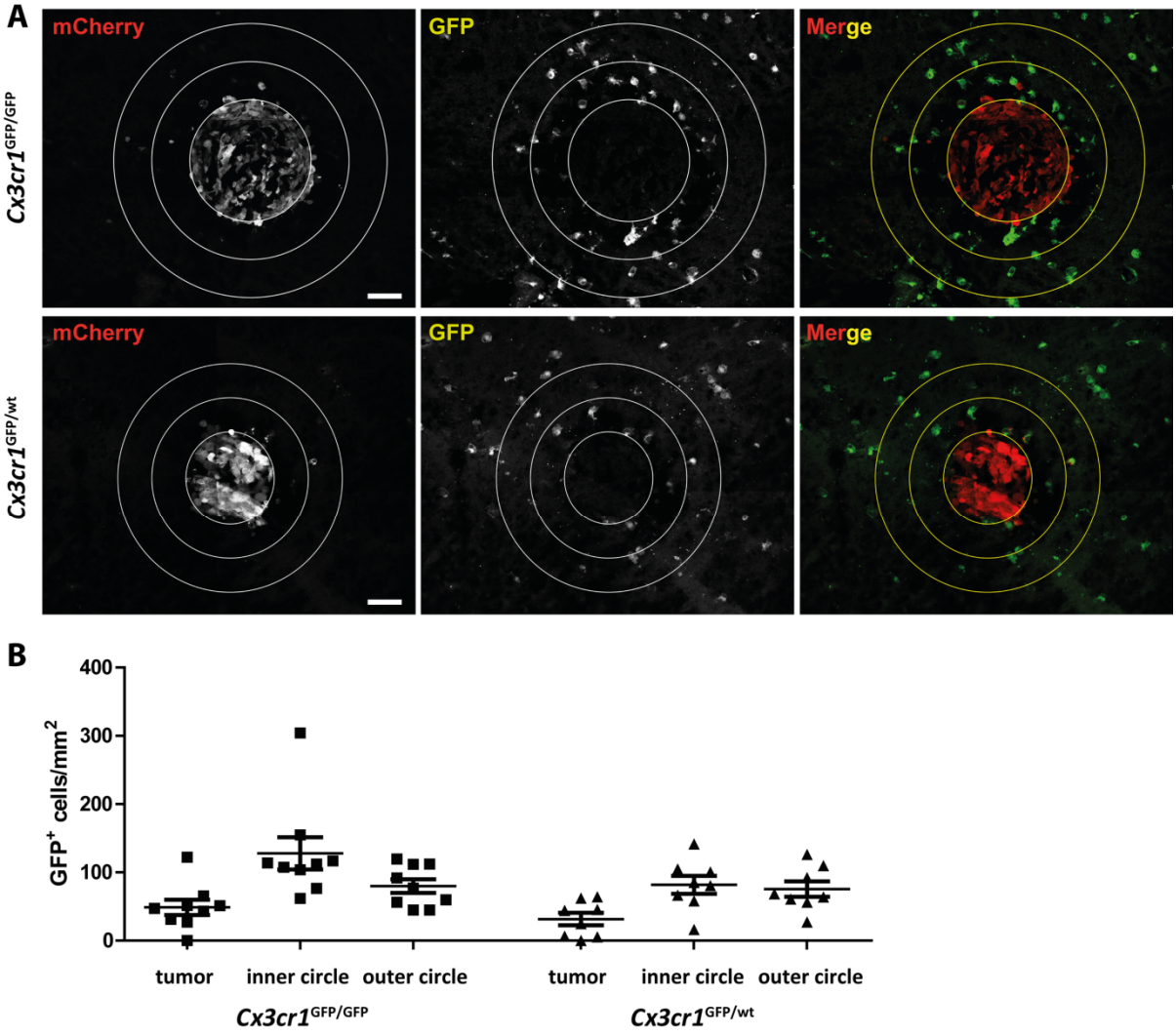

Figure 25 – GL261-implanted cultured organotypic brain slices from *Cx3cr1*$^{GFP/wt}$ and *Cx3cr1*$^{GFP/GFP}$ mice were fixed and cut into 10 µm cryosections 4 days after injection to investigate the migration of GFP$^+$ microglia toward the tumors.
A: Representative images from both genotypes. I counted cells in the tumor area and in the inner and outer peritumoral area (circles). B: No significant difference in attraction of GFP$^+$ microglia could be observed between both genotypes. Statistical significances were calculated applying a One-Way-ANOVA. Scale bar: 75 µm.

11.2.2. Loss of *Cx3cr1* has no significant effect on RCAS-*PDGFb* tumor growth *in situ*

I repeated these experiments with cultured RCAS-*PDGFb-RFP* tumor cells. For this, primary RCAS-*PDGFb-RFP* tumors – derived from *Ntv-a*/*Ink4a-Arf*$^{-/-}$/*Pten*$^{flox/flox}$ mice injected with RCAS-*PDGFb-RFP* and RCAS-*Cre*-producing DF1 cells (see chapter 11.1.1 and following chapters) – were cultured in stem-like cell-promoting medium, and FACS-sorted for RFP expression. Similar to GL261 experiments, 5,000 cells were injected into brain slices from P14-P16 *Cx3cr1*$^{GFP/GFP}$, *Cx3cr1*$^{GFP/wt}$, and *Cx3cr1*$^{wt/wt}$ mice 1 day after cutting. In contrast to GL261 tumors, I detected no significantly larger RCAS-*PDGFb* tumors in *Cx3cr1*$^{GFP/GFP}$ slices, when compared to *Cx3cr1*$^{GFP/wt}$ slices, however a trend can be observed (Figure 26B). In contrast to the GL261 tumors, these cells did not form a dense tumor mass. Instead, these cells infiltrated rather diffusely into the slice tissue. Furthermore, no further increase of the tumor size was detected between day 6 and 12 post-injection. Also, the fluorescence signal detected was much weaker, which was most likely owed to the less dense tumor tissue.

I also repeated the quantification of microglia migration toward the tumor in these tumors. Like with the GL261 tumors, I fixed *Cx3cr1*$^{GFP/GFP}$ and *Cx3cr1*$^{GFP/wt}$ slices 4 days post-injection, recut the slices into 10 µm sections and quantified microglia numbers in and around the tumors by confocal microscopy. It should be mentioned, that these tumors grew very invasive, several tumor cells could be observed in regions up to 200 µm away from the main tumor mass. RCAS-*PDGFb-RFP* tumors covered larger areas when compared to GL261 tumors, despite the fact that the overall fluorescence intensity was much lower for RCAS-*PDGFb-RFP* tumors when observed by conventional fluorescence imaging 6 and 12 days after injection. I observed large numbers of microglia in the tumor area, but also in the peritumoral areas. In accordance with the result that RCAS-*PDGFb-RFP* tumors were not significantly larger in *Cx3cr1*$^{GFP/GFP}$ slices, when compared to *Cx3cr1*$^{GFP/wt}$ slices, I also did not detect significantly more microglia in tumors growing in *Cx3cr1*$^{GFP/GFP}$ slices (Figure 27).

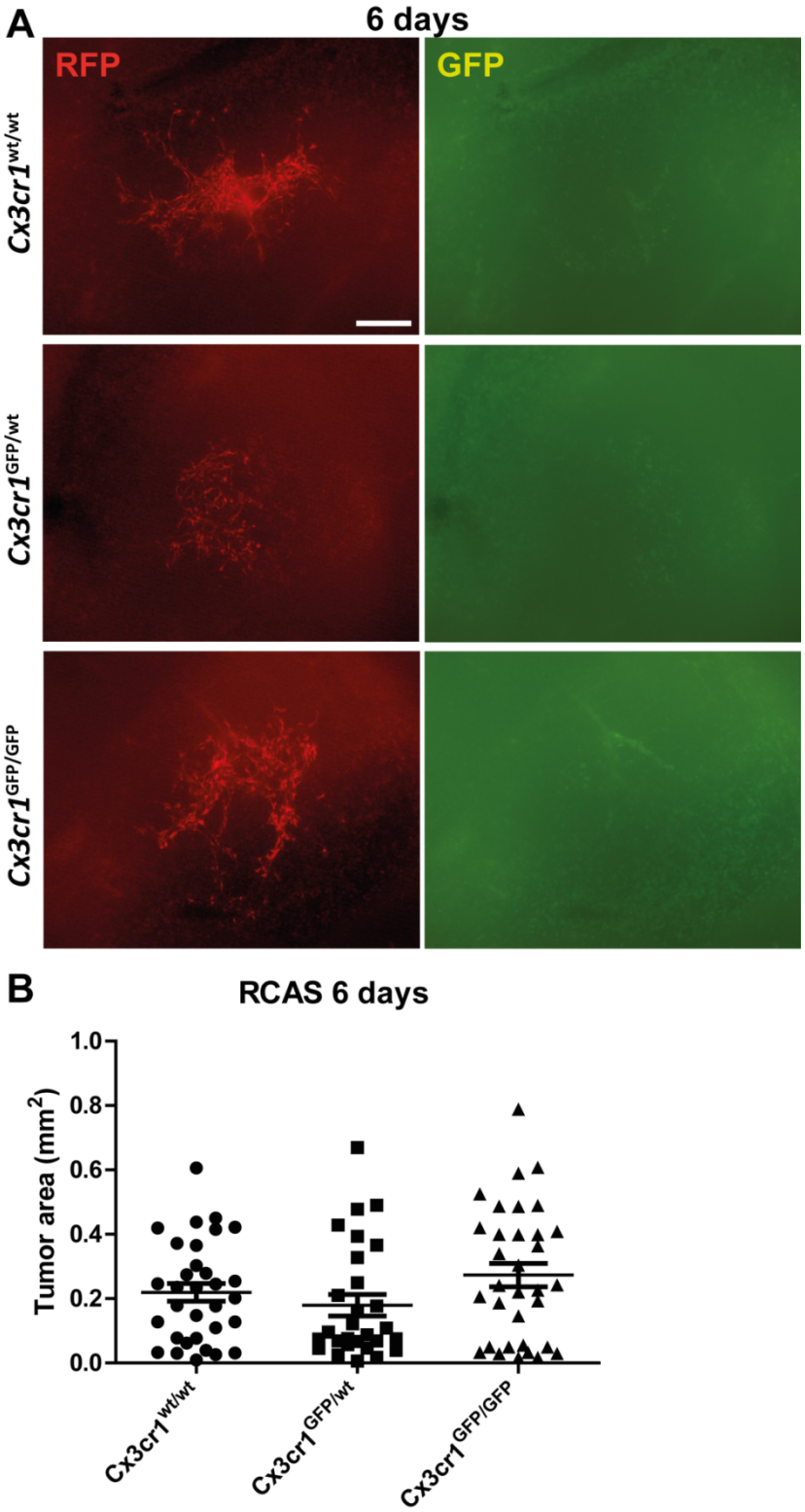

Figure 26 – Cultured RCAS-PDFGb-RFP glioma cells were injected into cultured organotypic brain slices of *Cx3cr1*$^{wt/wt}$, *Cx3cr1*$^{GFP/wt}$, and *Cx3cr1*$^{GFP/GFP}$ mice to investigate the role of *Cx3cr1* on tumor growth in a monocyte-free model.
A: Representative images of tumors (red fluorescence) in slices of all three genotypes at 6 days post-injection. Accumulation of GFP^{+} microglia can be observed in *Cx3cr1*$^{GFP/wt}$ and *Cx3cr1*$^{GFP/GFP}$ slices (green fluorescence). The slice tissue also shows strong auto fluorescence in the green channel (also in *Cx3cr1*$^{wt/wt}$ slices). B: No significant difference in tumor size could be observed between the different genotypes 6 days post-injection. Statistical significances were calculated applying a One-Way-ANOVA.Scale bar: 400 µm.

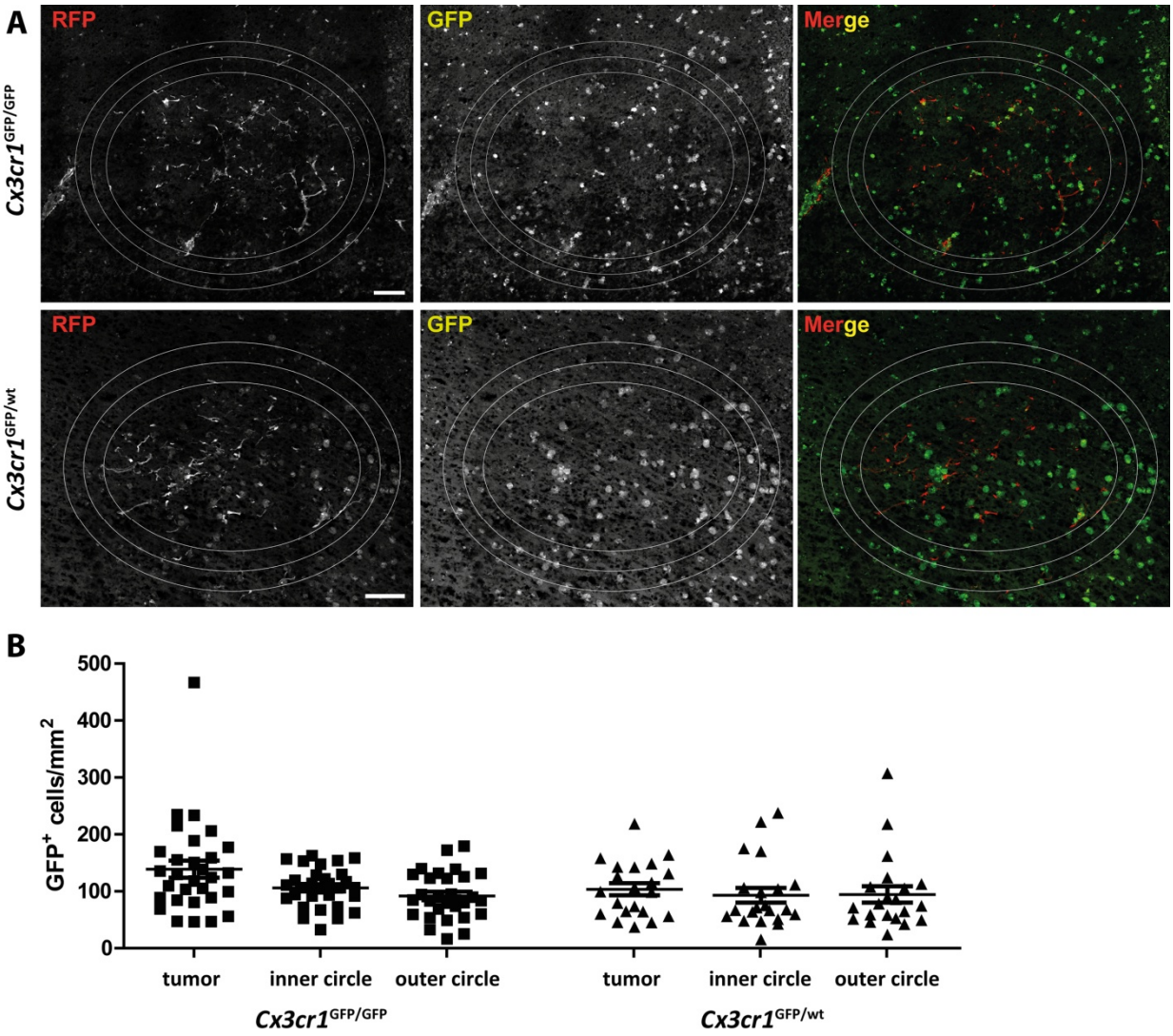

Figure 27 – RCAS-*PDGFb-RFP*-implanted cultured organotypic brain slices from *Cx3cr1*$^{GFP/wt}$ and *Cx3cr1*$^{GFP/GFP}$ mice were fixed and cut into 10 µm cryosections 4 days after injection to investigate the migration of GFP^{+} microglia toward the tumors.
A: Representative images from both genotypes. I counted cells in the tumor area and in the inner and outer peritumoral area (circles). B: No significant difference in attraction of GFP^{+} microglia could be observed between both genotypes. Statistical significances were calculated applying a One-Way-ANOVA. Scale bar: 150 µm.

5. Discussion

There is currently no successful treatment for GBM and despite the standard of care treatment, which includes gross total resection of the tumor tissue, radiotherapy, and chemotherapy, patients only have a median prognosis of 12-15 months after diagnosis. The lack of efficiency of novel treatment approaches in clinical trials makes it necessary to include the glioma microenvironment into the focus of research. Current treatments, such as viral-based therapies and molecularly targeted therapies (reviewed in 1.2.1 and 1.2.2), target different traits of the tumor cells. However, due to the high degree of heterogeneity among the tumor cells (Sottoriva, Spiteri et al. 2013; Francis, Zhang et al. 2014; Patel, Tirosh et al. 2014), therapies that target single traits are likely to fail, due to the emergence of tumor cell clones that are negative for (and independent from) this specific trait (Sampson, Heimberger et al. 2010). In turn, it could be promising to modulate and activate the immune system, to overcome the immunosuppressive glioma milieu.

GAMs constitute one of the biggest classes of stromal cells in the glioma microenvironment and on average represent around 15-30% of all cells in the tumor (Badie and Schartner 2001; Strik, Stoll et al. 2004; Watters, Schartner et al. 2005). Therefore these cells pose an attractive target for possible future anti-glioma therapies. GAMs have previously been shown to actively support glioma growth by the release of factors that stimulate angiogenesis, invasion, and suppression of immunity. The modulation of the GAMs has been shown to delay tumor growth in different mouse models *in vivo* (Rodriguez, Quiceno et al. 2004; Rodriguez, Quiceno et al. 2007; Du, Lu et al. 2008; Markovic, Vinnakota et al. 2009; Gabrusiewicz, Ellert-Miklaszewska et al. 2011; Li and Graeber 2012; Pyonteck, Akkari et al. 2013; Hu, Ku et al. 2014). However, until now only little is known about the actual polarization and phenotype of GAMs *in vivo*. Therefore, it is necessary and important to further investigate the features of GAMs and their role in glioma. In this thesis I present two independent projects that both investigate the properties and the role of GAMs.

5.1. Project 1: Genome-wide gene expression analysis of glioma-associated microglia/macrophages

In this work I performed a genome-wide expression analysis of acutely isolated GAMs from an experimental mouse glioma model. I compared the expression profile of our GAMs data set with M1, M2a, M2b, M2c-polarized macrophages and show that GAMs are polarized toward a phenotype that is distinct from any of these phenotypes. Furthermore, I identified potential pro-tumorigenic genes which are specifically regulated in glioma-associated microglia/macrophages when compared to naïve microglia or peripheral macrophages. I selected some of these genes – based on their expression level and reported protein functions in peripheral tumors – and validated the expression in two independent glioma mouse models as well as in human GBM, lower grade brain tumor and non-tumor control samples. In addition, I could show that the expression of these genes is different in microglia and macrophages/monocytes.

5.1.1. Polarization of glioma-associated microglia/macrophages

Previous studies reported that GAMs express both markers of the M1 and M2 macrophage phenotype, and to date the term “M2-like polarization” has often been used for describing the polarization of GAMs (Umemura, Saio et al. 2008; Gabrusiewicz, Ellert-Miklaszewska et al. 2011) – however, no extensive comparison of these phenotypes has been performed so far. By comparing our expression data to data generated from M1, M2a, M2b, and M2c-polarized macrophages, I show that the GAM phenotype shows only partial overlap with the M1, M2a, M2b, and M2c phenotypes and that GAMs do not fit into a classical M1 or M2 phenotype, but represent a specific phenotype. This is in line with results of a microarray study with TAMs isolated from human ovarian cancer. This study also found a mixed phenotype, unrelated to a clear M1/M2 polarization (Reinartz, Schumann et al. 2014). As an alternate explanation our findings might reflect heterogeneity among GAMs within one tumor. One might speculate that depending on the location in the tumor tissue, some GAMs are polarized toward an M1-like phenotype, whereas other GAMs possess a more M2-like phenotype and another population of GAMs is not polarized toward M1 or M2-like states.

When looking at the expression of the selected M1, M2a, M2b, and M2c-specific genes in FACS-sorted mouse glioma-associated microglia and

macrophages/monocytes it is apparent that all of the investigated genes are higher expressed in glioma-associated macrophages/monocytes when compared to glioma-associated microglia (Figure 13). This is probably owing to the fact that I used only data sets from *in vitro*-polarized macrophages, and thereby selected for macrophage-specific genes. Of course, the use of data sets from *in vitro* polarized macrophages creates a bias, and additional microglia-specific polarization data sets would have been useful to investigate differences in gene expression between polarized microglia and macrophages/monocytes. However, these data sets were not available online. In turn, all investigated M1, M2a,b,c-specific genes were also upregulated in glioma-associated microglia, underlining the similarities of gene expression changes between microglia and macrophages/monocytes in the glioma context.

The results of the qRT-PCR validation of these five selected M1, M2a,b,c-specfic genes show that the upregulation of *Il1rn*, *Clec7a*, *Tgfbi*, and *Cxcr4* is similar in both glioma models, however, the expression strength is usually lower in GAMs isolated from RCAS-*PDGFb* tumors. Solely the expression of *Isg20* is, in contrast to the GL261 model, not upregulated in GAMs isolated from RCAS-*PDGFb* tumors. Furthermore, the expression of *Isg20* in the results from the RCAS-*PDGFb* model, is highest in naïve blood monocytes. This is most likely owing to two facts. First, the expression was not highly induced in glioma-associated macrophages/monocytes in this model, and second, the peripheral control cells were isolated from blood, whereas in the GL261 model they were isolated from spleens.

There is only a slight chance that the difference of gene expression between the RCAS and the GL261 model is due to the different isolation procedures. I used *GFP/RFP* expression in *Cx3cr1*$^{GFP/wt}$ *Ccr2*$^{RFP/wt}$ mice for the RCAS model, as compared to antibody staining for CD11b/CD45/Ly6G/Ly6C in the GL261 model. Testing of the FACS antibodies on the *Cx3cr1*$^{GFP/wt}$ *Ccr2*$^{RFP/wt}$ cells did not reveal a difference between genetic labeling vs. staining; the impact of the different methods should be minor. However, differences in the tumor biology, different growth pattern and kinetics of both models might influence the expression of the selected genes. Mice injected with GL261 tumors were sacrificed 20 days post-injection, whereas mice implanted with RCAS tumors were sacrificed 4-5 weeks post-operation. Thus, GAMs in RCAS tumors were exposed to the tumor environment over longer times and the transcriptional program might have changed over the duration of the stimulus.

It is noteworthy that a higher expression in GAMs isolated from human GBM samples, when compared to microglia isolated from non-neoplastic samples, could not be validated for all of the five selected genes. This was in part in line, but also partly in contrast to the results from the mouse glioma models. The expression of all five selected genes could be detected in human GAMs, however the expression of *CLEC7A* was lower in human GAMs when compared to human non-neoplastic microglia and blood monocytes. Whereas in the GL261 model a higher expression could be detected in all GAMs, in the RCAS-*PDGFb* model glioma-associated macrophages/monocytes showed no higher expression of *Clec7a* when compared to naïve blood monocytes. Furthermore, a higher expression of *ISG20* could be detected in human blood monocytes when compared to GAMs, whereas GAMs showed a higher expression when compared to control microglia. This was again in line with the results from the RCAS-*PDGFb* model, where the highest expression was detected in naïve blood monocytes. Another factor is the origin of the human control samples. In contrast to the mouse samples for which I could use naïve brain samples, the human control samples came from patients who either underwent surgery due to epileptic seizures, or due to trauma with extensive bleeding. Cells isolated from these samples where most likely already activated.

In the light of the recent findings it is clear that the M1/M2 concept is just a small subset of the macrophage activation spectrum (Xue, Schmidt et al. 2014). The glioma milieu is by far more complex in the composition of effector molecules and polarizing stimuli than *in vitro* settings that mostly rely on stimulation with single substances. Xue *et al*. showed that macrophages acquire activation states independent from the bipolar M1/M2 axis when activated by free fatty acids, high-density lipoprotein (HDL), or combinations of stimuli associated with chronic inflammation. A future comparison of our data set with additional data sets from these studies will be interesting and helpful to define the activation characteristics of these cells.

5.1.2. Identification of pro-tumorigenic genes

The ability of GBM to evade current treatment is based on multiple properties of these tumors. Apart from the high degree of genetic heterogeneity of the tumor cells that renders these tumors virtually immune to targeted therapies, the highly invasive growth pattern and the immunosuppressive tumor milieu also contribute to the failure of treatment. GAMs have been reported to support tumor growth by supporting both features of GBM by secreting factors that assist the invasion of tumor cells (for example by the release of MMP9 and MMP14), and suppression of immunity, (for example by the release of Arginase 1 and 2 that inhibit effector T cell maturation) (Rodriguez, Quiceno et al. 2004; Rodriguez, Quiceno et al. 2007; Du, Lu et al. 2008; Markovic, Vinnakota et al. 2009; Gabrusiewicz, Ellert-Miklaszewska et al. 2011; Kees, Lohr et al. 2012; Pyonteck, Akkari et al. 2013; Hu, Ku et al. 2014). Therefore, these cells represent an attractive target for anti-glioma therapy, as modulation of their activation state might be useful to inhibit glioma progression (Markovic, Vinnakota et al. 2011; Sarkar, Doring et al. 2014).

Here I present several possible candidate genes that are upregulated in GAMs and might have a potential pro-tumorigenic function in GBM. The genes that I selected can be grouped according to the function and localization of the encoded protein. The suppression of immunity can be separated into two groups. First, the activation of the myeloid cells themselves, and second, the enhancement or repression of adaptive immunity, for example by the release of factors that prevent activation or maturation of effector T cells, or the recruitment of suppressive regulatory T cells. Accordingly, I also separated these genes into these two groups.

Genes that I investigated encode for proteins implicated in supporting tumor cell invasion in peripheral tumors (*Spp1*, *Hpse*), myeloid cell activation (*Gpnmb*, *Trem1*, *Cd200r4*, *Cd300lf*, *Creb5, Il1rn*), or suppression of adaptive immunity (*Gpnmb*, *Sh2d1b1*, *Cxcl13*, *Il1rn*). Four genes encode for proteins that are secreted (*Spp1, Hpse, Il1rn, Cxcl13*), three genes encode for proteins that are localized intracellularly (*Uck2, Sepx1, Creb5*), and five genes encode for proteins that are transmembrane proteins/receptors (*Gpnmb, Trem1, Cd200r4, Cd300lf, Sh2d1b1*). Based on the results of a screen with a small set of $CD11b^+$ samples isolated from human GBM and non-neoplastic, tissues I selected *GPNMB*, *SPP1*, *HPSE*, *IL1RN*, *CD300LF*, and *TREM1* for a further analysis in a larger set of human samples. I saw that *GPNMB*, *SPP1*, *HPSE*, and *IL1RN* were higher expressed in human $CD11b^+$ GAMs when

compared to CD11b$^+$ cells isolated from non-neoplastic control tissues and lower grade or benign tumors (except for *HPSE* that was also highly expressed in GAMs isolated from grade III gliomas), thus validating our findings from the mouse models. In contrast, *CD300LF* was higher expressed in CD11b$^+$ cells isolated from GBM, lower grade tumors or non-neoplastic tissues, when compared to the flow through. However, the expression level was not higher in GAMs when compared to CD11b$^+$ cells isolated from non-neoplastic tissues and lower grade tumors. The expression of *TREM1* was downregulated in GAMs when compared to CD11b$^+$ cells isolated from non-neoplastic samples.

Two of the most promising candidate genes are *GPNMB* and *SPP1*. I propose these genes as possible new targets and show that these genes are highly expressed in GAMs in different glioma mouse models and in human GBM. High expression of these genes correlates with shorter glioma-patient survival. The expression of neither of these genes was previously linked to GAMs.

The expression of *GPNMB* has been reported in tumor cells for different cancers (Zhou, Liu et al. 2012). The data from our GL261 glioma model suggests that GL261 cells express *GPNMB* at a very high level. However, GAMs were the predominant source for *GPNMB* expression in the RCAS-*PDGFb* glioma mouse model and in human GBM samples. GPNMB (also called Osteoactivin) is a transmembrane protein that might have different functions in GAMs and in the tumor. Ripoll *et al.*, have shown that GPNMB acts as a negative regulator of pro-inflammatory macrophage activation in RAW264.7 cells (Ripoll, Irvine et al. 2007). Thus, high *GPNMB* expression in GAMs could participate in the modulation of the pro-tumorigenic phenotype of GAMs. Furthermore, GPNMB has been shown to inhibit T cell activation via direct cell-cell interaction of antigen-presenting cells and T cells, and could thus contribute to the immunosuppressive milieu in gliomas (Chung, Dougherty et al. 2007; Chung, Sato et al. 2007; Chung, Bonkobara et al. 2009). Finally, anti-GPNMB antibodies conjugated with a cytotoxic agent are under investigation for the treatment of malignant glioma, breast cancer, and cutaneous melanoma (Tse, Jeffers et al. 2006; Naumovski and Junutula 2010; Kuan, Wakiya et al. 2011).

I found that GAMs highly express *SPP1*. SPP1 (also called Osteopontin) is a secreted protein that has been postulated to increase tumor cell invasion *in vivo* and migration *in vitro*, and was found to be highly expressed in different types of cancers, such as lung cancer, ovarian cancer, and also glioma (Brown, Papadopoulos-Sergiou

et al. 1994; Fong, Liu et al. 2009; Jan, Lee et al. 2010; Sreekanthreddy, Srinivasan et al. 2010; Engler, Robinson et al. 2012; Lu, Yeh et al. 2012). Another study showed that SPP1 binds and activates CD44, which is in turn expressed by stem-like cells in GBM. Pietras *et al*. could show that activation of CD44 by SPP1 leads to a higher stemness of these cells, and an increased size of a cell population that is believed to contain stem-like cells in GBM (Pietras, Katz et al. 2014). Here I show that GAMs and not glioma cells are the most predominant source for *SPP1* expression.

HPSE and *IL1RN* were also expressed in GAMs at higher levels when compared to $CD11b^+$ cells isolated from non-neoplastic and lower grade tumor samples, as well as in the $CD11b^-$ fraction in GBM samples. Although the effect of high expression of these two genes was less severe when compared to *GPNMB* and *SPP1*, both genes might still contribute to the beneficial role of GAMs on tumor progression.

HPSE encodes for the Heparanase protein. Heparanase is a secreted enzyme that is associated with enhanced invasion, metastatic potential and angiogenesis. It can act on two levels: the first one is mediated by its function of cleaving heparin sulfate (HS) proteoglycans in the ECM or on the surface of other cells, thereby facilitating tumor invasion. Heparanase-mediated cleavage of HS releases ECM-bound molecules such as VEGF for angiogenesis and other growth factors (Meirovitz, Goldberg et al. 2013). The second mechanism of Heparanase action is the regulation of gene transcription through phosphorylation of Src, p38 and Akt, leading to the induction of EGFR and VEGF expression (Zetser, Bashenko et al. 2006; Cohen-Kaplan, Doweck et al. 2008). *HPSE* is expressed in various tumors, including gliomas (Hong, Nelson et al. 2010). Here I show that GAMs are the primary source for *HPSE* in glioma.

The *IL1RN* encodes for interleukin-1 receptor antagonist (termed IL1RA), a protein that is structurally related to IL1α and IL1β. The secreted form can bind to the IL1 receptor without activating it and thereby acts as an antagonist to IL1α and IL1β (Touzani, Boutin et al. 1999). An intracellular variant of IL1RA has also been described (Dinarello 1996). *IL1RN* has been shown to be expressed by different cell types, such as immune cells (including microglia and monocytes), epithelial cells, skin keratinocytes, hepatocytes, and adipocytes (Perrier, Darakhshan et al. 2006). *IL1RN* expression can be induced by pro-inflammatory cytokines such as IL1 or IFNγ (Perrier, Darakhshan et al. 2006) and is implicated to counteract pro-inflammatory signaling, as it has been shown that *IL1RN* knockout mice exhibit increased neuronal injury size induced by transient cerebral ischemia compared to wildtype animals

(Pinteaux, Rothwell et al. 2006). The influence of high *IL1RN* expression on tumor growth is controversial and contradictory results have been published in different tumor models. Upregulation of *Il1rn* expression has been shown to suppress tumor growth in a melanoma mouse model (Song, Park et al. 2012). In contrast, the expression of *IL1RN* was implicated in supporting the growth of glioma cell lines *in vitro* by repressing an inhibitory autocrine IL1 loop (Oelmann, Kraemer et al. 1997). In addition, *IL1RN* expression has been implicated in supporting the growth of pancreatic tumor models by contributing to chemo resistance and antagonizing senescence (Yang, Ding et al. 2013; Di Mitri, Toso et al. 2014).

In conclusion, these findings show that GAMs produce factors that have been shown to support tumor growth in different tumors, including glioma. Our results are in accordance with previous reports that investigated the expression of selected target genes in GAMs via qRT-PCR (Markovic, Vinnakota et al. 2009; Gabrusiewicz, Ellert-Miklaszewska et al. 2011; Li and Graeber 2012), and markers known for tumor-associated macrophages in peripheral tumors. Several genes that are implicated in angiogenesis (*Vegfa*, *Hgf*), suppression of immunity (*Arg1, Tgfb3*), and tumor invasion (*Mmp2*, *Mmp14*, *Ctgf*) and had previously been linked to GAMs were also highly expressed in our GAMs data set (Table 6) (Mantovani, Sica et al. 2004; Hao, Lu et al. 2012; Li and Graeber 2012).

Taken together, these findings show that GAMs are polarized toward a phenotype that is distinct from the M1 or M2a, M2b, and M2c phenotypes. Furthermore, I identified GAMs as the predominant source for the pro-tumorigenic factors *GPNMB* and *SPP1* in murine and human malignant glioma – highlighting the importance of macrophages and microglia as therapeutic targets in anti-tumor treatment regimes.

5.1.3. Comparison to other studies

Two studies have previously performed screens of freshly-isolated GAMs. I used these data sets to investigate the expression of *Gpnmb, Spp1*, *Hpse*, *Trem1*, *CD300lf*, *Il1rn*, *Isg20*, *Cxcr4*, *Tgfbi*, and *Clec7a* in these studies (Table 8). Huang *et al*. performed a screen of mouse GFP^+ chimeric GL261-associated and naïve bone-marrow-derived myeloid cells in the brain. Using this approach they did not target the brain-resident microglia population that is also present in the tumor (Data set: E-GEOD-38283) (Huang, Hoffman et al. 2014). All of the investigated genes, except *Cxcr4*, were also upregulated in the study of Huang *et al*. – however to a lesser degree. Murat *et al*. performed a microarray experiment on a paired sample of human GAMs and whole tumor lysate from the same patient (Data set: GSE16119) (Murat, Migliavacca et al. 2009). All of the 10 genes were higher expressed in GAMs when compared to the whole tumor lysate. However, it should also be noted that the whole tumor lysate was not depleted of GAMs. None of these studies performed a more detailed analysis of the microarray data. These results indicate that the gene expression changes I found in our screen are consistent across different studies.

Table 8 – A comparison showing the regulation of selected genes in our study and two different studies performing microarrays on GAMs (Murat, Migliavacca et al. 2009; Huang, Hoffman et al. 2014).

	This study	Huang et al. 2014	Murat et al. 2009
	mouse GL261-associated $CD11b^+$ microglia/macrophages vs. naïve microglia and peritoneal macrophages	mouse GL261-associated GFP^+ bone marrow-derived vs. naive GFP^+ bone-marrow	human GAMs vs. matched whole tumor extract (1 patient)
Gpnmb	36-fold upreg.	2.7-fold upreg.	1.3-fold upreg.
Spp1	27.2-fold upreg.	2.3-fold upreg.	18.4-fold upreg.
Trem1	12.6-fold upreg.	1.4-fold upreg.	3-fold upreg.
Cd300lf	6.8-fold upreg.	3.2-fold upreg.	2.8-fold upreg.
Hpse	2.6-fold upreg.	2.1-fold upreg.	3.1-fold upreg.
Il1rn	14.8-fold upreg.	1.9-fold upreg.	3.3-fold upreg.
Isg20	3.4-fold upreg.	1.5-fold upreg.	2.3-fold upreg.
Clec7a	4.7-fold upreg.	1.4-fold upreg.	9.8-fold upreg.
Tgfbi	3.3-fold upreg.	1.1-fold upreg.	16.1-fold upreg.
Cxcr4	10.6-fold upreg.	1.1-fold downreg.	3.5-fold upreg.

5.1.4. Outlook

There are several drawbacks in the design of our study that leave space for future studies investigating the transcriptome of GAMs. The first and possibly largest drawback was the sorting method applied for the samples used for the microarray itself. Using only CD11b as a marker for sorting GAMs from the GL261 mouse gliomas did not enable us to distinguish between various $CD11b^+$ cell types in the glioma tissue, such as brain-intrinsic microglia, invading monocytes/macrophages, but also invading dendritic cells and natural killer cells. I started with the experiments for the microarray when the more sophisticated sorting methods were not established in our lab. Later on I used them for our validation studies. Using a FACS-based sorting approach to distinguish between these cells, either by antibody staining for CD11b, CD45, Ly6C, and Ly6G or by using the *Cx3cr1*$^{GFP/wt}$ *Ccr2*$^{RFP/wt}$ mouse would greatly enhance the impact of a future genome-wide screen. In this way, relatively pure populations of microglia and invading macrophages/monocytes, absent of natural killer cells and dendritic cells, could be collected and the gene expression signatures of these populations could be compared, extending the small set of markers I used for our validation study. Three big studies performed screens of naïve microglia and monocytes and compared the gene expression signatures of these cell types and identified cell-specific gene signatures and markers (Hickman, Kingery et al. 2013; Pong, Walker et al. 2013; Butovsky, Jedrychowski et al. 2014). Using this technique it would be possible to identify genes and factors that are primarily expressed by each cell type on a large scale and to better describe the roles of these distinct cell populations in the tumor.

In addition, a screen based on GAMs isolated from a larger set of human samples would be necessary to validate how the results from mouse models can be translated into the human setting. A problem with human samples is the higher diversity between samples when compared to (inbred) mice that show little variability between animals. This would make it necessary to perform such a screen on a higher number of samples. Another problem is the heterogeneity of the tumors. Several subtypes of GBM have been proposed (classical, mesenchymal, proneural, neural, primary/secondary GBM) which would make it necessary to group samples according to the tumor subtype (Verhaak, Hoadley et al. 2010). However, recent studies have postulated that even within the same tumor different subtypes exist side by side, depending on the area of biopsy in the tumor (Sottoriva, Spiteri et al. 2013; Gill,

Pisapia et al. 2014; Patel, Tirosh et al. 2014). Therefore, GAMs might also be differentially activated and reprogrammed according to the location within the tumor. In order to get an insight into the different phenotype of GAMs in different subtypes it could be feasible to use the mouse RCAS tumor models. Using this system it is possible to model mouse gliomas that recapitulate the different subtypes of human GBM (Holland, Celestino et al. 2000; Uhrbom, Kastemar et al. 2005; Hambardzumyan, Amankulor et al. 2009; Lindberg, Jiang et al. 2014), however with lesser intra-tumorigenic heterogeneity.

Recent advances in sequencing technology made it possible to perform whole genome analysis by RNA sequencing even on a single-cell scale. This approach would allow us to address the topic of GAMs heterogeneity within the tumor and could help to answer the question how diverse GAMs are in the light of polarization. If there is a more homogeneous population or – more likely – if some GAMs are polarized a more M1-like state, whereas other GAMs, maybe depending on the location in the tumor, are polarized to a more M2-like, an M1/M2-independent state, or are deactivated.

In addition, it is necessary to also investigate the role of miRNAs in GAMs. For example, Xu *et al*. recently performed a miRNA screen on human GAMs versus matched control peripheral monocytes and found that the expression of miR-142-3p was significantly downregulated in GAMs (Xu, Wei et al. 2014). They found that lower expression of this miRNA correlated with a more M2-like phenotype *in vitro*. Lastly, the application of miR-142-3p to mice suffering from intracranial GL261 tumors significantly reduced tumor burden and prolonged the survival time of treated animals. This study highlights the importance of miRNAs in the polarization and function of GAMs.

A proteomics screen would help to validate the findings of a genomic screen on a large scale. However, the requirements of material input for such a screen would make it necessary to provide larger quantities of freshly sorted cells, as the protein yield from these sorted cells is generally low.

Lastly, we will further investigate the role and function of potential pro-tumorigenic genes that were identified in this study. I identified several promising target genes that are expressed in GAMs and will try to elucidate the function of these genes in GAMs and glioma.

5.2. Project 2: Effect of *Cx3cr1*-loss on GAMs in an organotypic brain slice model

The function of the fractalkine receptor (CX3CR1) has been studied extensively under physiological conditions and in different diseases. It has also been shown to play a role in glioma. One study reported that a single nucleotide polymorphism in the human *CX3CR1* gene resulted in decreased myeloid cell infiltration and longer survival of patients that underwent surgery (Rodero, Marie et al. 2008). Another study using the GL261 glioma model reported that the loss of CX3CR1 in the recipient mouse leads to a slight decrease of survival of glioma-bearing mice, whereas the number of glioma-infiltrating immune cells was unaltered (Liu, Luo et al. 2008). In contrast, data from a mouse model of low-grade glioma indicates that decreased expression of *Cx3cr1* negatively impacted on tumor growth and led to a decreased infiltration of microglia into the tumor tissue (Pong, Higer et al. 2013), suggesting that the impact of CX3CR1/CX3CL1-signaling on tumor growth might depend on tumor grade.

In vivo data using the RCAS-*PDGFb* glioma model (Feng X. et al., manuscript submitted), indicate that the lack of *Cx3cr1* expression resulted in increased tumor growth, shorter survival times of animals, along with an increased infiltration of peripheral Ly6C^{high} monocytes. Using the organotypic brain slice model I was able to investigate the *Cx3cr1*-dependent role of microglia on glioma-growth in a monocyte-free system. To investigate the role of *Cx3cr1* expression in the microglia-glioma interplay I employed the *Fractalkine-GFP* knockin mouse. In this mouse the *Cx3cr1* gene allels are replaced by the *GFP* sequence. As microglia are the only source of *Cx3cr1* expression in the naïve brain, this model is a feasible tool to study the effect of *Cx3cr1*-loss in microglia.

Tumors implanted into slices from P14-P16 *Cx3cr1*$^{GFP/GFP}$ mice were significantly larger than tumors implanted into slices from *Cx3cr1*$^{GFP/wt}$ and *Cx3cr1*$^{wt/wt}$ littermates. There was no significant difference in tumor size between *Cx3cr1*$^{GFP/wt}$ and *Cx3cr1*$^{wt/wt}$ slices. Based on the results from these organotypic slice culture experiments it can be assumed that in GL261 tumors the loss of *Cx3cr1* expression significantly impacts the microglia-dependent support of tumor growth observed in animals lacking *Cx3cr1* expression. In *Cx3cr1*$^{GFP/GFP}$ slices I observed a non-significant trend toward a higher infiltration of microglia into the GL261 peritumoral areas when compared to *Cx3cr1*$^{GFP/wt}$ slices. This indicates that *Cx3cr1* expression attenuates a GL261 glioma-directed migration of microglia and subsequent glioma-

supporting functions of these cells. In turn, loss of *Cx3cr1* expression prevents this inhibition, leading to a higher infiltration of microglia into the tumor and subsequent exertion of tumor-promoting functions.

In the RCAS-*PDGFb* tumor model the microglia-dependent effect on tumor growth upon loss of *Cx3cr1* expression is less pronounced. Although also in the RCAS-*PDGFb* tumor model a trend toward larger tumors could be observed in slices from *Cx3cr1*$^{GFP/GFP}$ mice, the effect was less strong than in the GL261 model and did not reach significance. However, similar to the GL261 model, in *Cx3cr1*$^{GFP/GFP}$ slices a non-significant trend toward a higher infiltration of microglia into the peritumoral areas could be observed, when compared to *Cx3cr1*$^{GFP/wt}$ slices.

This indicates that invading Ly6C^{high} monocytes might play a more prominent role in tumor promotion than brain-resident microglia in the RCAS-*PDGFb* model, when compared to the GL261 model.

6. Summary

Malignant glioma belong to the most aggressive neoplasms in humans with no successful treatment available. Patients suffering from glioblastoma multiforme (GBM), the highest-grade glioma, have an average survival time of only 12-15 months after diagnosis. Both microglia and peripheral macrophages/monocytes accumulate within and around glioma, but fail to exert effective anti-tumor activity and even support tumor growth. Here I investigated the properties and functions of glioma-associated microglia/macrophages (GAMs) using different molecular and experimental approaches.

In the first project I used microarray analysis to compare the expression profiles of GAMs and naive control cells. Samples were generated from $CD11b^+$ MACS-isolated cells from naïve and GL261-implanted C57BL/6 mouse brains. Around 1000 genes were more than 2-fold up- or downregulated in GAMs when compared to control cells. Comparison to published data sets of M1/M2a,b,c-polarized macrophages revealed a gene expression pattern that has only partial overlap with any of the M1 or M2 gene expression patterns. Samples for the qRT-PCR validation of selected M1 and M2a,b,c-specific genes were generated from two different glioma mouse models and isolated by flow cytometry to distinguish between resident microglia and invading macrophages/monocytes. In both models the unique GAMs phenotype including a mixture of M1 and M2a,b,c-specific genes could be confirmed. To validate the expression of these genes in human samples, I MACS-isolated $CD11b^+$ microglia/macrophages from glioblastoma multiforme (GBM), lower grade brain tumors, and control specimens. Apart from the M1/M2 gene analysis, I demonstrate that *Gpnmb* and *Spp1* are highly expressed in both murine and human GAMs. High expression of these genes has been associated with worsened prognosis in human GBM, as indicated by patient outcome linked to gene expression data. I also show that GAMs are the predominant source of these transcripts in murine and human GBM.

In the second project, I investigated the role of *Cx3cr1* in the microglia-dependent support of glioma growth by employing a monocyte-free organotypic brain slice model. In $Cx3cr1^{GFP/GFP}$ slices, lacking *Cx3cr1* expression, the growth of GL261 tumors was significantly enhanced, when compared to $Cx3cr1^{GFP/wt}$ or $Cx3cr1^{wt/wt}$ slices. In another glioma model the loss of *Cx3cr1* did not significantly impact tumor

growth when compared to *Cx3cr1*$^{GFP/wt}$ or *Cx3cr1*$^{wt/wt}$ slices. In both models a trend toward a higher microglia migration toward tumors could be observed in *Cx3cr1*$^{GFP/GFP}$ slices when compared to *Cx3cr1*$^{GFP/wt}$. This indicates that CX3CR1 signaling attenuates a glioma-directed migration of microglia and subsequent glioma-supporting functions of these cells.

The findings of my thesis provide new insights in the phenotype and function of GAMs and will help to better understand their role for glioma development and progression and to define new potential targets for future anti-glioma therapy.

7. Zusammenfassung

Maligne Gliome gehören zu den aggressivsten Neoplasmen im Menschen und zur Zeit gibt es für diese Tumore keine wirksame Therapieform. Patienten die an einem Glioblastoma multiforme (GBM), der hochgradigsten Form der Gliome, erkrankt sind besitzen nur eine durchschnittliche Lebenserwartung von 12-15 Monate nach der Diagnose. Sowohl Mikroglia, als auch aus der Periphärie invasierende Makrophagen und Monozyten, sammeln sich in und um die Tumormasse an. Diese Zellen entfalten jedoch keine effektive Immunantwort die sich gegen den Tumor richtet, sondern unterstützen sogar das Tumorwachstum. In dieser Arbeit untersuchte ich die Eigenschaften und Funktionen der Gliom-assoziierten Mikroglia/Makrophagen (GAMs) in zwei verschiedenen Projekten.

In dem ersten Projekt habe ich ein Mikroarrayexperiment durchgeführt um die Expressionsprofile von GAMs und naiven Kontrollzellen zu vergleichen. Als Proben wurden $CD11b^+$ Zellen verwendet, welche mittels MACS aus naiven und GL261-implantierten C57BL/6 Maushirnen isoliert wurden. Im Vergleich zu den Kontrollzellen waren in GAMs ungefähr 1000 Gene mehr als 2-fach hoch- oder runterreguliert. Ein Vergleich mit publizierten Datensätzen von M1/M2a,b,c-polarisierten Makrophagen zeigte, dass GAMs ein Genexpressionsmuster besitzen, welches nur eine teilweise Überlappung mit M1 oder M2 Expressionsmustern aufweist. Die Proben für die qRT-PCR Validierung von ausgewählten M1 und M2a,b,c-spezifischen Genen wurden in zwei verschiedenen Gliommodellen erzeugt und mittels Durchflusszytometrie aufgereinigt. Dies ermöglichte es für diese Proben zwischen hirneigenen Mikroglia und invasierenden Makrophagen/Monozyten zu unterscheiden. Ich konnte die Expression ausgewählter M1/M2a,b,c-spezifischer Gene in beiden Tumormodellen in GAMs bestätigen. Desweiteren habe ich mittels MACS $CD11b^+$ Mikroglia/Makrophagen aus humanen Proben (GBM, niedergradige Hirntumore und Kontrollproben) aufgereinigt, um die Expression ausgewählter Gene auch in humanen Proben zu untersuchen. Abgesehen von der M1/M2 Analyse, demonstriere ich in dieser Arbeit, dass die Expression von *Gpnmb* und *Spp1* in murinen und humanen GAMs stark hochreguliert ist. Eine erhöhte Expression dieser Gene ist mit einer schlechteren Lebenserwartung für Patienten mit GBM assoziiert. Ich zeige weiterhin, dass GAMs die Hauptquelle für diese beiden Transkripte in murinen und humanen GBMs sind.

In einem zweiten Projekt untersuchte ich mit Hilfe eines Monozyten-freien organotypischen Hirnschnittkulturmodells die Rolle von *Cx3cr1* in der Mikroglia-abhängigen Unterstützung des Gliomwachstums. GL261 Tumore die in *Cx3cr1*$^{GFP/GFP}$ Schnitte injiziert wurden – welche keine *Cx3cr1* Expression besitzen – waren signifikant größer als GL261 Tumore welche in *Cx3cr1*$^{GFP/wt}$ or *Cx3cr1*$^{wt/wt}$ Schnitte injiziert wurden. In einem weiteren Tumormodell hatte das Fehlen der *Cx3cr1* Expression keinen signifikanten Einfluss auf das Tumorwachstum. In beiden Tumormodellen gab es einen Trend hin zu einer höheren Mikrogliamigration in die peritumoralen Bereiche in *Cx3cr1*$^{GFP/GFP}$ Schnitten (im Vergleich zu *Cx3cr1*$^{GFP/wt}$ Schnitten). Dies deutet darauf hin, dass der CX3CR1 Signalweg einen inhibierenden Einfluss auf die Gliom-gerichetete Migration und anschließende Gliom-unterstützende Funktionen dieser Zellen hat.

Die Ergebnisse meiner Arbeit liefern neue Einsichten in den Phänotyp und die Funktion von GAMs und werden bei der weiteren Charakterisierung dieser Zellen helfen, um neue potentielle Ansatzpunkte für zukünftige Antigliomtherapien zu finden.

8. References

Akbasak, A., E. H. Oldfield, et al. (1991). "Expression and modulation of major histocompatibility antigens on murine primary brain tumor in vitro." J Neurosurg **75**(6): 922-929.

Alcantara Llaguno, S., J. Chen, et al. (2009). "Malignant astrocytomas originate from neural stem/progenitor cells in a somatic tumor suppressor mouse model." Cancer Cell **15**(1): 45-56.

Alterman, R. L. and E. R. Stanley (1994). "Colony stimulating factor-1 expression in human glioma." Mol Chem Neuropathol **21**(2-3): 177-188.

Amantea, D., G. Nappi, et al. (2009). "Post-ischemic brain damage: pathophysiology and role of inflammatory mediators." FEBS J **276**(1): 13-26.

Auffinger, B., A. U. Ahmed, et al. (2013). "Oncolytic virotherapy for malignant glioma: translating laboratory insights into clinical practice." Front Oncol **3**: 32.

Ausman, J. I., W. R. Shapiro, et al. (1970). "Studies on the chemotherapy of experimental brain tumors: development of an experimental model." Cancer Res **30**(9): 2394-2400.

Bachoo, R. M., E. A. Maher, et al. (2002). "Epidermal growth factor receptor and Ink4a/Arf: convergent mechanisms governing terminal differentiation and transformation along the neural stem cell to astrocyte axis." Cancer Cell **1**(3): 269-277.

Badie, B. and J. Schartner (2001). "Role of microglia in glioma biology." Microsc Res Tech **54**(2): 106-113.

Bajetto, A., R. Bonavia, et al. (1999). "Expression of chemokine receptors in the rat brain." Ann N Y Acad Sci **876**: 201-209.

Bajetto, A., R. Bonavia, et al. (1999). "Glial and neuronal cells express functional chemokine receptor CXCR4 and its natural ligand stromal cell-derived factor 1." J Neurochem **73**(6): 2348-2357.

Bao, S., Q. Wu, et al. (2006). "Glioma stem cells promote radioresistance by preferential activation of the DNA damage response." Nature **444**(7120): 756-760.

Bazan, J. F., K. B. Bacon, et al. (1997). "A new class of membrane-bound chemokine with a CX3C motif." Nature **385**(6617): 640-644.

Biber, K., H. Neumann, et al. (2007). "Neuronal 'On' and 'Off' signals control microglia." Trends Neurosci **30**(11): 596-602.

Bleau, A. M., D. Hambardzumyan, et al. (2009). "PTEN/PI3K/Akt pathway regulates the side population phenotype and ABCG2 activity in glioma tumor stem-like

cells." Cell Stem Cell **4**(3): 226-235.

Brennan, C., H. Momota, et al. (2009). "Glioblastoma subclasses can be defined by activity among signal transduction pathways and associated genomic alterations." PloS one **4**(11): e7752.

Brennan, C. W., R. G. Verhaak, et al. (2013). "The somatic genomic landscape of glioblastoma." Cell **155**(2): 462-477.

Brown, L. F., A. Papadopoulos-Sergiou, et al. (1994). "Osteopontin expression and distribution in human carcinomas." The American journal of pathology **145**(3): 610-623.

Butovsky, O., M. P. Jedrychowski, et al. (2014). "Identification of a unique TGF-beta-dependent molecular and functional signature in microglia." Nat Neurosci **17**(1): 131-143.

Cardona, A. E., E. P. Pioro, et al. (2006). "Control of microglial neurotoxicity by the fractalkine receptor." Nat Neurosci **9**(7): 917-924.

Cerami, E., J. Gao, et al. (2012). "The cBio cancer genomics portal: an open platform for exploring multidimensional cancer genomics data." Cancer Discov **2**(5): 401-404.

Chang, C. N., Y. C. Huang, et al. (2011). "A phase I/II clinical trial investigating the adverse and therapeutic effects of a postoperative autologous dendritic cell tumor vaccine in patients with malignant glioma." J Clin Neurosci **18**(8): 1048-1054.

Charles, N. A., E. C. Holland, et al. (2011). "The brain tumor microenvironment." Glia **59**(8): 1169-1180.

Chen, J., Y. Li, et al. (2012). "A restricted cell population propagates glioblastoma growth after chemotherapy." Nature **488**(7412): 522-526.

Chen, J., R. M. McKay, et al. (2012). "Malignant glioma: lessons from genomics, mouse models, and stem cells." Cell **149**(1): 36-47.

Chinot, O. L., W. Wick, et al. (2014). "Bevacizumab plus radiotherapy-temozolomide for newly diagnosed glioblastoma." N Engl J Med **370**(8): 709-722.

Chiocca, E. A., L. K. Aguilar, et al. (2011). "Phase IB study of gene-mediated cytotoxic immunotherapy adjuvant to up-front surgery and intensive timing radiation for malignant glioma." J Clin Oncol **29**(27): 3611-3619.

Choi, B. D., C. T. Kuan, et al. (2013). "Systemic administration of a bispecific antibody targeting EGFRvIII successfully treats intracerebral glioma." Proc Natl Acad Sci U S A **110**(1): 270-275.

Chow, K. K., S. Naik, et al. (2013). "T cells redirected to EphA2 for the immunotherapy of glioblastoma." Mol Ther **21**(3): 629-637.

Chung, D. S., H. J. Shin, et al. (2014). "A New Hope in Immunotherapy for Malignant

Gliomas: Adoptive T Cell Transfer Therapy." J Immunol Res **2014**: 326545.

Chung, J. S., M. Bonkobara, et al. (2009). "The DC-HIL/syndecan-4 pathway inhibits human allogeneic T-cell responses." European journal of immunology **39**(4): 965-974.

Chung, J. S., I. Dougherty, et al. (2007). "Syndecan-4 mediates the coinhibitory function of DC-HIL on T cell activation." Journal of immunology **179**(9): 5778-5784.

Chung, J. S., K. Sato, et al. (2007). "DC-HIL is a negative regulator of T lymphocyte activation." Blood **109**(10): 4320-4327.

Cohen-Kaplan, V., I. Doweck, et al. (2008). "Heparanase augments epidermal growth factor receptor phosphorylation: correlation with head and neck tumor progression." Cancer research **68**(24): 10077-10085.

Davalos, D., J. Grutzendler, et al. (2005). "ATP mediates rapid microglial response to local brain injury in vivo." Nat Neurosci **8**(6): 752-758.

De Vleeschouwer, S., S. Fieuws, et al. (2008). "Postoperative adjuvant dendritic cell-based immunotherapy in patients with relapsed glioblastoma multiforme." Clin Cancer Res **14**(10): 3098-3104.

Dean, M., T. Fojo, et al. (2005). "Tumour stem cells and drug resistance." Nat Rev Cancer **5**(4): 275-284.

Denes, A., S. Ferenczi, et al. (2008). "Role of CX3CR1 (fractalkine receptor) in brain damage and inflammation induced by focal cerebral ischemia in mouse." J Cereb Blood Flow Metab **28**(10): 1707-1721.

Di Mitri, D., A. Toso, et al. (2014). "Tumour-infiltrating Gr-1 myeloid cells antagonize senescence in cancer." Nature.

Dinarello, C. A. (1996). "Biologic basis for interleukin-1 in disease." Blood **87**(6): 2095-2147.

Dolecek, T. A., J. M. Propp, et al. (2012). "CBTRUS statistical report: primary brain and central nervous system tumors diagnosed in the United States in 2005-2009." Neuro Oncol **14 Suppl 5**: v1-49.

Donnelly, D. J., E. E. Longbrake, et al. (2011). "Deficient CX3CR1 signaling promotes recovery after mouse spinal cord injury by limiting the recruitment and activation of Ly6Clo/iNOS+ macrophages." J Neurosci **31**(27): 9910-9922.

Du, R., K. V. Lu, et al. (2008). "HIF1alpha induces the recruitment of bone marrow-derived vascular modulatory cells to regulate tumor angiogenesis and invasion." Cancer Cell **13**(3): 206-220.

Dunay, I. R., R. A. Damatta, et al. (2008). "Gr1(+) inflammatory monocytes are required for mucosal resistance to the pathogen Toxoplasma gondii." Immunity **29**(2): 306-317.

Eichler, G. S., S. Huang, et al. (2003). "Gene Expression Dynamics Inspector (GEDI): for integrative analysis of expression profiles." Bioinformatics **19**(17): 2321-2322.

El Andaloussi, A., Y. Han, et al. (2006). "Prolongation of survival following depletion of CD4+CD25+ regulatory T cells in mice with experimental brain tumors." J Neurosurg **105**(3): 430-437.

Engler, J. R., A. E. Robinson, et al. (2012). "Increased microglia/macrophage gene expression in a subset of adult and pediatric astrocytomas." PLoS One **7**(8): e43339.

Fecci, P. E., D. A. Mitchell, et al. (2006). "Increased regulatory T-cell fraction amidst a diminished CD4 compartment explains cellular immune defects in patients with malignant glioma." Cancer Res **66**(6): 3294-3302.

Fong, Y. C., S. C. Liu, et al. (2009). "Osteopontin increases lung cancer cells migration via activation of the alphavbeta3 integrin/FAK/Akt and NF-kappaB-dependent pathway." Lung cancer **64**(3): 263-270.

Francis, J. M., C. Z. Zhang, et al. (2014). "EGFR Variant Heterogeneity in Glioblastoma Resolved through Single-Nucleus Sequencing." Cancer Discov **4**(8): 956-971.

Gabrusiewicz, K., A. Ellert-Miklaszewska, et al. (2011). "Characteristics of the alternative phenotype of microglia/macrophages and its modulation in experimental gliomas." PloS one **6**(8): e23902.

Gao, J., B. A. Aksoy, et al. (2013). "Integrative analysis of complex cancer genomics and clinical profiles using the cBioPortal." Sci Signal **6**(269): pl1.

Garton, K. J., P. J. Gough, et al. (2001). "Tumor necrosis factor-alpha-converting enzyme (ADAM17) mediates the cleavage and shedding of fractalkine (CX3CL1)." J Biol Chem **276**(41): 37993-38001.

Gautier, L., L. Cope, et al. (2004). "affy--analysis of Affymetrix GeneChip data at the probe level." Bioinformatics **20**(3): 307-315.

Gilbert, C. A. and A. H. Ross (2009). "Cancer stem cells: cell culture, markers, and targets for new therapies." J Cell Biochem **108**(5): 1031-1038.

Gilbert, M. R., J. J. Dignam, et al. (2014). "A randomized trial of bevacizumab for newly diagnosed glioblastoma." N Engl J Med **370**(8): 699-708.

Gill, B. J., D. J. Pisapia, et al. (2014). "MRI-localized biopsies reveal subtype-specific differences in molecular and cellular composition at the margins of glioblastoma." Proc Natl Acad Sci U S A.

Gratchev, A., J. Kzhyshkowska, et al. (2005). "Interleukin-4 and dexamethasone counterregulate extracellular matrix remodelling and phagocytosis in type-2 macrophages." Scandinavian journal of immunology **61**(1): 10-17.

Guan, X., J. Vengoechea, et al. (2014). "Molecular subtypes of glioblastoma are

relevant to lower grade glioma." PLoS One **9**(3): e91216.

Hambardzumyan, D., N. M. Amankulor, et al. (2009). "Modeling Adult Gliomas Using RCAS/t-va Technology." Translational oncology **2**(2): 89-95.

Hanisch, U. K. and H. Kettenmann (2007). "Microglia: active sensor and versatile effector cells in the normal and pathologic brain." Nature neuroscience **10**(11): 1387-1394.

Hao, N. B., M. H. Lu, et al. (2012). "Macrophages in tumor microenvironments and the progression of tumors." Clinical & developmental immunology **2012**: 948098.

Harrison, J. K., Y. Jiang, et al. (1998). "Role for neuronally derived fractalkine in mediating interactions between neurons and CX3CR1-expressing microglia." Proc Natl Acad Sci U S A **95**(18): 10896-10901.

Hickman, S. E., N. D. Kingery, et al. (2013). "The microglial sensome revealed by direct RNA sequencing." Nat Neurosci **16**(12): 1896-1905.

Holland, E. C. (2000). "Glioblastoma multiforme: the terminator." Proc Natl Acad Sci U S A **97**(12): 6242-6244.

Holland, E. C., J. Celestino, et al. (2000). "Combined activation of Ras and Akt in neural progenitors induces glioblastoma formation in mice." Nat Genet **25**(1): 55-57.

Hong, X., K. K. Nelson, et al. (2010). "Heparanase expression of glioma in human and animal models." Journal of neurosurgery **113**(2): 261-269.

Hu, F., M. C. Ku, et al. (2014). "Glioma-associated microglial MMP9 expression is upregulated by TLR2 signaling and sensitive to minocycline." Int J Cancer.

Hu, X., A. K. Liou, et al. (2014). "Neurobiology of microglial action in CNS injuries: Receptor-mediated signaling mechanisms and functional roles." Prog Neurobiol.

Huang, Y., C. Hoffman, et al. (2014). "Oligodendrocyte progenitor cells promote neovascularization in glioma by disrupting the blood-brain barrier." Cancer Res **74**(4): 1011-1021.

Immonen, A., M. Vapalahti, et al. (2004). "AdvHSV-tk gene therapy with intravenous ganciclovir improves survival in human malignant glioma: a randomised, controlled study." Mol Ther **10**(5): 967-972.

Irizarry, R. A., B. M. Bolstad, et al. (2003). "Summaries of Affymetrix GeneChip probe level data." Nucleic Acids Res **31**(4): e15.

Jacobs, J. F., A. J. Idema, et al. (2010). "Prognostic significance and mechanism of Treg infiltration in human brain tumors." J Neuroimmunol **225**(1-2): 195-199.

Jan, H. J., C. C. Lee, et al. (2010). "Osteopontin regulates human glioma cell invasiveness and tumor growth in mice." Neuro-oncology **12**(1): 58-70.

Jones, T. S. and E. C. Holland (2012). "Standard of care therapy for malignant glioma and its effect on tumor and stromal cells." Oncogene **31**(16): 1995-2006.

Kanazawa, N., T. Nakamura, et al. (1999). "Fractalkine and macrophage-derived chemokine: T cell-attracting chemokines expressed in T cell area dendritic cells." Eur J Immunol **29**(6): 1925-1932.

Katz, A. M., N. M. Amankulor, et al. (2012). "Astrocyte-specific expression patterns associated with the PDGF-induced glioma microenvironment." PLoS One **7**(2): e32453.

Kees, T., J. Lohr, et al. (2012). "Microglia isolated from patients with glioma gain antitumor activities on poly (I:C) stimulation." Neuro-oncology **14**(1): 64-78.

Keller, M., J. Mazuch, et al. (2009). "A circadian clock in macrophages controls inflammatory immune responses." Proceedings of the National Academy of Sciences of the United States of America **106**(50): 21407-21412.

Kerber, M., Y. Reiss, et al. (2008). "Flt-1 signaling in macrophages promotes glioma growth in vivo." Cancer research **68**(18): 7342-7351.

Kesavabhotla, K., C. D. Schlaff, et al. (2012). "Phase I/II study of oral erlotinib for treatment of relapsed/refractory glioblastoma multiforme and anaplastic astrocytoma." J Exp Ther Oncol **10**(1): 71-81.

Kettenmann, H., U. K. Hanisch, et al. (2011). "Physiology of microglia." Physiol Rev **91**(2): 461-553.

Kigerl, K. A., J. C. Gensel, et al. (2009). "Identification of two distinct macrophage subsets with divergent effects causing either neurotoxicity or regeneration in the injured mouse spinal cord." The Journal of neuroscience : the official journal of the Society for Neuroscience **29**(43): 13435-13444.

Ku, M. C., S. A. Wolf, et al. (2013). "GDNF mediates glioblastoma-induced microglia attraction but not astrogliosis." Acta Neuropathol **125**(4): 609-620.

Kuan, C. T., K. Wakiya, et al. (2011). "Affinity-matured anti-glycoprotein NMB recombinant immunotoxins targeting malignant gliomas and melanomas." Int J Cancer **129**(1): 111-121.

Langfelder, P. and S. Horvath (2007). "Eigengene networks for studying the relationships between co-expression modules." BMC systems biology **1**: 54.

Lawrence, T. and G. Natoli (2011). "Transcriptional regulation of macrophage polarization: enabling diversity with identity." Nat Rev Immunol **11**(11): 750-761.

Li, A. (2013). "mogene10sttranscriptcluster.db: Affymetrix Mouse Gene 1.0-ST Array Transcriptcluster Revision 8 annotation data (chip mogene10sttranscriptcluster)."

Li, W. and M. B. Graeber (2012). "The molecular profile of microglia under the

influence of glioma." Neuro-oncology **14**(8): 958-978.

Lindberg, N., Y. Jiang, et al. (2014). "Oncogenic signaling is dominant to cell of origin and dictates astrocytic or oligodendroglial tumor development from oligodendrocyte precursor cells." J Neurosci **34**(44): 14644-14651.

Liu, C., D. Luo, et al. (2008). "CX3CL1 and CX3CR1 in the GL261 murine model of glioma: CX3CR1 deficiency does not impact tumor growth or infiltration of microglia and lymphocytes." J Neuroimmunol **198**(1-2): 98-105.

Liu, C., J. C. Sage, et al. (2011). "Mosaic analysis with double markers reveals tumor cell of origin in glioma." Cell **146**(2): 209-221.

Liu, G., X. Yuan, et al. (2006). "Analysis of gene expression and chemoresistance of CD133+ cancer stem cells in glioblastoma." Mol Cancer **5**: 67.

Liu, L., J. Wu, et al. (2010). "Astrocyte elevated gene-1 upregulates matrix metalloproteinase-9 and induces human glioma invasion." Cancer Res **70**(9): 3750-3759.

Lohr, J., T. Ratliff, et al. (2011). "Effector T-cell infiltration positively impacts survival of glioblastoma patients and is impaired by tumor-derived TGF-beta." Clin Cancer Res **17**(13): 4296-4308.

Louis, D. N., H. Ohgaki, et al. (2007). "The 2007 WHO classification of tumours of the central nervous system." Acta Neuropathol **114**(2): 97-109.

Lowther, D. E. and D. A. Hafler (2012). "Regulatory T cells in the central nervous system." Immunol Rev **248**(1): 156-169.

Lu, D. Y., W. L. Yeh, et al. (2012). "Osteopontin increases heme oxygenase-1 expression and subsequently induces cell migration and invasion in glioma cells." Neuro-oncology **14**(11): 1367-1378.

Mantovani, A., A. Sica, et al. (2004). "The chemokine system in diverse forms of macrophage activation and polarization." Trends in immunology **25**(12): 677-686.

Markovic, D. S., K. Vinnakota, et al. (2009). "Gliomas induce and exploit microglial MT1-MMP expression for tumor expansion." Proceedings of the National Academy of Sciences of the United States of America **106**(30): 12530-12535.

Markovic, D. S., K. Vinnakota, et al. (2011). "Minocycline reduces glioma expansion and invasion by attenuating microglial MT1-MMP expression." Brain, behavior, and immunity **25**(4): 624-628.

Marsh, J. C., J. Goldfarb, et al. (2013). "Current status of immunotherapy and gene therapy for high-grade gliomas." Cancer Control **20**(1): 43-48.

Meirovitz, A., R. Goldberg, et al. (2013). "Heparanase in inflammation and inflammation-associated cancer." The FEBS journal **280**(10): 2307-2319.

Miller, J. A., C. Cai, et al. (2011). "Strategies for aggregating gene expression data:

the collapseRows R function." BMC Bioinformatics **12**: 322.

Mok, S., R. C. Koya, et al. (2014). "Inhibition of CSF-1 receptor improves the antitumor efficacy of adoptive cell transfer immunotherapy." Cancer Res **74**(1): 153-161.

Morford, L. A., L. H. Elliott, et al. (1997). "T cell receptor-mediated signaling is defective in T cells obtained from patients with primary intracranial tumors." J Immunol **159**(9): 4415-4425.

Mosser, D. M. and J. P. Edwards (2008). "Exploring the full spectrum of macrophage activation." Nat Rev Immunol **8**(12): 958-969.

Murat, A., E. Migliavacca, et al. (2009). "Modulation of angiogenic and inflammatory response in glioblastoma by hypoxia." PLoS One **4**(6): e5947.

Naumovski, L. and J. R. Junutula (2010). "Glembatumumab vedotin, a conjugate of an anti-glycoprotein non-metastatic melanoma protein B mAb and monomethyl auristatin E for the treatment of melanoma and breast cancer." Curr Opin Mol Ther **12**(2): 248-257.

Nimmerjahn, A., F. Kirchhoff, et al. (2005). "Resting microglial cells are highly dynamic surveillants of brain parenchyma in vivo." Science **308**(5726): 1314-1318.

Ning, J. and H. Wakimoto (2014). "Oncolytic herpes simplex virus-based strategies: toward a breakthrough in glioblastoma therapy." Front Microbiol **5**: 303.

Nishiyori, A., M. Minami, et al. (1998). "Localization of fractalkine and CX3CR1 mRNAs in rat brain: does fractalkine play a role in signaling from neuron to microglia?" FEBS Lett **429**(2): 167-172.

Oelmann, E., A. Kraemer, et al. (1997). "Autocrine interleukin-1 receptor antagonist can support malignant growth of glioblastoma by blocking growth-inhibiting autocrine loop of interleukin-1." Int J Cancer **71**(6): 1066-1076.

Ohgaki, H. and P. Kleihues (2009). "Genetic alterations and signaling pathways in the evolution of gliomas." Cancer Sci **100**(12): 2235-2241.

Okada, M., M. Saio, et al. (2009). "Tumor-associated macrophage/microglia infiltration in human gliomas is correlated with MCP-3, but not MCP-1." Int J Oncol **34**(6): 1621-1627.

Olah, M., D. Raj, et al. (2012). "An optimized protocol for the acute isolation of human microglia from autopsy brain samples." Glia **60**(1): 96-111.

Pan, Y., C. Lloyd, et al. (1997). "Neurotactin, a membrane-anchored chemokine upregulated in brain inflammation." Nature **387**(6633): 611-617.

Paolicelli, R. C., G. Bolasco, et al. (2011). "Synaptic pruning by microglia is necessary for normal brain development." Science **333**(6048): 1456-1458.

Papadopoulos, E. J., C. Sassetti, et al. (1999). "Fractalkine, a CX3C chemokine, is

expressed by dendritic cells and is up-regulated upon dendritic cell maturation." Eur J Immunol **29**(8): 2551-2559.

Papavasiliou, A. K., M. F. Mehler, et al. (1997). "Paracrine regulation of colony-stimulating factor-1 in medulloblastoma: implications for pathogenesis and therapeutic interventions." Neurosurgery **41**(4): 916-923.

Patel, A. P., I. Tirosh, et al. (2014). "Single-cell RNA-seq highlights intratumoral heterogeneity in primary glioblastoma." Science.

Perrier, S., F. Darakhshan, et al. (2006). "IL-1 receptor antagonist in metabolic diseases: Dr Jekyll or Mr Hyde?" FEBS Lett **580**(27): 6289-6294.

Phillips, H. S., S. Kharbanda, et al. (2006). "Molecular subclasses of high-grade glioma predict prognosis, delineate a pattern of disease progression, and resemble stages in neurogenesis." Cancer cell **9**(3): 157-173.

Pietras, A., A. M. Katz, et al. (2014). "Osteopontin-CD44 signaling in the glioma perivascular niche enhances cancer stem cell phenotypes and promotes aggressive tumor growth." Cell Stem Cell **14**(3): 357-369.

Pinteaux, E., N. J. Rothwell, et al. (2006). "Neuroprotective actions of endogenous interleukin-1 receptor antagonist (IL-1ra) are mediated by glia." Glia **53**(5): 551-556.

Platten, M., A. Kretz, et al. (2003). "Monocyte chemoattractant protein-1 increases microglial infiltration and aggressiveness of gliomas." Ann Neurol **54**(3): 388-392.

Pollard, J. W. (2004). "Tumour-educated macrophages promote tumour progression and metastasis." Nature reviews. Cancer **4**(1): 71-78.

Pong, W. W., S. B. Higer, et al. (2013). "Reduced microglial CX3CR1 expression delays neurofibromatosis-1 glioma formation." Ann Neurol **73**(2): 303-308.

Pong, W. W., J. Walker, et al. (2013). "F11R is a novel monocyte prognostic biomarker for malignant glioma." PLoS One **8**(10): e77571.

Pyonteck, S. M., L. Akkari, et al. (2013). "CSF-1R inhibition alters macrophage polarization and blocks glioma progression." Nature medicine **19**(10): 1264-1272.

R Development Core Team (2010). "R: A language and environment for statistical computing."

Rahmathulla, G., E. J. Hovey, et al. (2013). "Bevacizumab in high-grade gliomas: a review of its uses, toxicity assessment, and future treatment challenges." Onco Targets Ther **6**: 371-389.

Raizer, J. J., L. E. Abrey, et al. (2010). "A phase II trial of erlotinib in patients with recurrent malignant gliomas and nonprogressive glioblastoma multiforme postradiation therapy." Neuro Oncol **12**(1): 95-103.

Ransohoff, R. M. (2011). "Microglia and monocytes: 'tis plain the twain meet in the brain." Nat Neurosci **14**(9): 1098-1100.

Reinartz, S., T. Schumann, et al. (2014). "Mixed-polarization phenotype of ascites-associated macrophages in human ovarian carcinoma: correlation of CD163 expression, cytokine levels and early relapse." Int J Cancer **134**(1): 32-42.

Ripoll, V. M., K. M. Irvine, et al. (2007). "Gpnmb is induced in macrophages by IFN-gamma and lipopolysaccharide and acts as a feedback regulator of proinflammatory responses." Journal of immunology **178**(10): 6557-6566.

Riquelme, P., S. Tomiuk, et al. (2013). "IFN-gamma-induced iNOS expression in mouse regulatory macrophages prolongs allograft survival in fully immunocompetent recipients." Molecular therapy : the journal of the American Society of Gene Therapy **21**(2): 409-422.

Rodero, M., Y. Marie, et al. (2008). "Polymorphism in the microglial cell-mobilizing CX3CR1 gene is associated with survival in patients with glioblastoma." J Clin Oncol **26**(36): 5957-5964.

Rodriguez, P. C., D. G. Quiceno, et al. (2007). "L-arginine availability regulates T-lymphocyte cell-cycle progression." Blood **109**(4): 1568-1573.

Rodriguez, P. C., D. G. Quiceno, et al. (2004). "Arginase I production in the tumor microenvironment by mature myeloid cells inhibits T-cell receptor expression and antigen-specific T-cell responses." Cancer Res **64**(16): 5839-5849.

Roszman, T. L. and W. H. Brooks (1980). "Immunobiology of primary intracranial tumours. III. Demonstration of a qualitative lymphocyte abnormality in patients with primary brain tumours." Clin Exp Immunol **39**(2): 395-402.

Russell, S. J., K. W. Peng, et al. (2012). "Oncolytic virotherapy." Nat Biotechnol **30**(7): 658-670.

Saederup, N., A. E. Cardona, et al. (2010). "Selective chemokine receptor usage by central nervous system myeloid cells in CCR2-red fluorescent protein knock-in mice." PloS one **5**(10): e13693.

Sampson, J. H., A. B. Heimberger, et al. (2010). "Immunologic escape after prolonged progression-free survival with epidermal growth factor receptor variant III peptide vaccination in patients with newly diagnosed glioblastoma." J Clin Oncol **28**(31): 4722-4729.

Sandmair, A. M., S. Loimas, et al. (2000). "Thymidine kinase gene therapy for human malignant glioma, using replication-deficient retroviruses or adenoviruses." Hum Gene Ther **11**(16): 2197-2205.

Sarkar, S., A. Doring, et al. (2014). "Therapeutic activation of macrophages and microglia to suppress brain tumor-initiating cells." Nature neuroscience **17**(1): 46-55.

Schumacher, T., L. Bunse, et al. (2014). "A vaccine targeting mutant IDH1 induces antitumour immunity." Nature.

Seligman, A. M. and M. J. Shear (1939). "Experimental production of brain tumors in mice with methylcholanthrene." Studies in Carcinogenesis.

Sica, A., T. Schioppa, et al. (2006). "Tumour-associated macrophages are a distinct M2 polarised population promoting tumour progression: potential targets of anti-cancer therapy." European journal of cancer **42**(6): 717-727.

Singh, S. K., I. D. Clarke, et al. (2003). "Identification of a cancer stem cell in human brain tumors." Cancer Res **63**(18): 5821-5828.

Singh, S. K., C. Hawkins, et al. (2004). "Identification of human brain tumour initiating cells." Nature **432**(7015): 396-401.

Song, J. K., M. H. Park, et al. (2012). "Deficiency of C-C chemokine receptor 5 suppresses tumor development via inactivation of NF-kappaB and upregulation of IL-1Ra in melanoma model." PLoS One **7**(5): e33747.

Sontheimer, H. (2008). "A role for glutamate in growth and invasion of primary brain tumors." J Neurochem **105**(2): 287-295.

Sottoriva, A., I. Spiteri, et al. (2013). "Intratumor heterogeneity in human glioblastoma reflects cancer evolutionary dynamics." Proceedings of the National Academy of Sciences of the United States of America **110**(10): 4009-4014.

Sreekanthreddy, P., H. Srinivasan, et al. (2010). "Identification of potential serum biomarkers of glioblastoma: serum osteopontin levels correlate with poor prognosis." Cancer Epidemiol Biomarkers Prev **19**(6): 1409-1422.

Strik, H. M., M. Stoll, et al. (2004). "Immune cell infiltration of intrinsic and metastatic intracranial tumours." Anticancer Res **24**(1): 37-42.

Stupp, R., W. P. Mason, et al. (2005). "Radiotherapy plus concomitant and adjuvant temozolomide for glioblastoma." N Engl J Med **352**(10): 987-996.

Sukhdeo, K., D. Hambardzumyan, et al. (2011). "Glioma development: where did it all go wrong?" Cell **146**(2): 187-188.

Szatmari, T., K. Lumniczky, et al. (2006). "Detailed characterization of the mouse glioma 261 tumor model for experimental glioblastoma therapy." Cancer Sci **97**(6): 546-553.

Takano, T., J. H. Lin, et al. (2001). "Glutamate release promotes growth of malignant gliomas." Nat Med **7**(9): 1010-1015.

TheCancerGenomeAtlas (2008). "Comprehensive genomic characterization defines human glioblastoma genes and core pathways." Nature **455**(7216): 1061-1068.

Touzani, O., H. Boutin, et al. (1999). "Potential mechanisms of interleukin-1 involvement in cerebral ischaemia." J Neuroimmunol **100**(1-2): 203-215.

Tse, K. F., M. Jeffers, et al. (2006). "CR011, a fully human monoclonal antibody-auristatin E conjugate, for the treatment of melanoma." Clin Cancer Res **12**(4):

1373-1382.

Uhrbom, L., M. Kastemar, et al. (2005). "Cell type-specific tumor suppression by Ink4a and Arf in Kras-induced mouse gliomagenesis." Cancer Res **65**(6): 2065-2069.

Umemura, N., M. Saio, et al. (2008). "Tumor-infiltrating myeloid-derived suppressor cells are pleiotropic-inflamed monocytes/macrophages that bear M1- and M2-type characteristics." Journal of leukocyte biology **83**(5): 1136-1144.

Verhaak, R. G., K. A. Hoadley, et al. (2010). "Integrated genomic analysis identifies clinically relevant subtypes of glioblastoma characterized by abnormalities in PDGFRA, IDH1, EGFR, and NF1." Cancer Cell **17**(1): 98-110.

Vinnakota, K., F. Hu, et al. (2013). "Toll-like receptor 2 mediates microglia/brain macrophage MT1-MMP expression and glioma expansion." Neuro-oncology **15**(11): 1457-1468.

Visvader, J. E. (2011). "Cells of origin in cancer." Nature **469**(7330): 314-322.

Wainwright, D. A., A. L. Chang, et al. (2014). "Durable therapeutic efficacy utilizing combinatorial blockade against IDO, CTLA-4 and PD-L1 in mice with brain tumors." Clin Cancer Res.

Wake, H., A. J. Moorhouse, et al. (2009). "Resting microglia directly monitor the functional state of synapses in vivo and determine the fate of ischemic terminals." J Neurosci **29**(13): 3974-3980.

Wang, J., D. Duncan, et al. (2013). "WEB-based GEne SeT AnaLysis Toolkit (WebGestalt): update 2013." Nucleic Acids Res **41**(Web Server issue): W77-83.

Wang, Y., J. Yang, et al. (2009). "Expression of mutant p53 proteins implicates a lineage relationship between neural stem cells and malignant astrocytic glioma in a murine model." Cancer Cell **15**(6): 514-526.

Warnes, G. R., B. Bolker, et al. (2013). "gplots: Various R programming tools for plotting data. Retrieved from http://cran.r-project.org/package=gplots."

Watters, J. J., J. M. Schartner, et al. (2005). "Microglia function in brain tumors." Journal of neuroscience research **81**(3): 447-455.

Weathers, S. P. and M. R. Gilbert (2014). "Advances in treating glioblastoma." F1000Prime Rep **6**: 46.

Wen, P. Y. and S. Kesari (2008). "Malignant gliomas in adults." The New England journal of medicine **359**(5): 492-507.

Wilson, T. A., M. A. Karajannis, et al. (2014). "Glioblastoma multiforme: State of the art and future therapeutics." Surg Neurol Int **5**: 64.

Xu, S., J. Wei, et al. (2014). "Effect of miR-142-3p on the M2 macrophage and therapeutic efficacy against murine glioblastoma." J Natl Cancer Inst **106**(8).

Xue, J., S. V. Schmidt, et al. (2014). "Transcriptome-based network analysis reveals a spectrum model of human macrophage activation." Immunity **40**(2): 274-288.

Yamanaka, R., J. Homma, et al. (2005). "Clinical evaluation of dendritic cell vaccination for patients with recurrent glioma: results of a clinical phase I/II trial." Clin Cancer Res **11**(11): 4160-4167.

Yang, D. R., X. F. Ding, et al. (2013). "Increased chemosensitivity via targeting testicular nuclear receptor 4 (TR4)-Oct4-interleukin 1 receptor antagonist (IL1Ra) axis in prostate cancer CD133+ stem/progenitor cells to battle prostate cancer." J Biol Chem **288**(23): 16476-16483.

Ye, X. Z., S. L. Xu, et al. (2012). "Tumor-associated microglia/macrophages enhance the invasion of glioma stem-like cells via TGF-beta1 signaling pathway." Journal of immunology **189**(1): 444-453.

Ye, Z. C. and H. Sontheimer (1999). "Glioma cells release excitotoxic concentrations of glutamate." Cancer Res **59**(17): 4383-4391.

Young, G. R., U. Eksmond, et al. (2012). "Resurrection of endogenous retroviruses in antibody-deficient mice." Nature **491**(7426): 774-778.

Yung, W. K., J. J. Vredenburgh, et al. (2010). "Safety and efficacy of erlotinib in first-relapse glioblastoma: a phase II open-label study." Neuro Oncol **12**(10): 1061-1070.

Zetser, A., Y. Bashenko, et al. (2006). "Heparanase induces vascular endothelial growth factor expression: correlation with p38 phosphorylation levels and Src activation." Cancer research **66**(3): 1455-1463.

Zhang, B., S. Kirov, et al. (2005). "WebGestalt: an integrated system for exploring gene sets in various biological contexts." Nucleic Acids Res **33**(Web Server issue): W741-748.

Zhang, L., D. Alizadeh, et al. (2009). "Stat3 inhibition activates tumor macrophages and abrogates glioma growth in mice." Glia **57**(13): 1458-1467.

Zhou, L. T., F. Y. Liu, et al. (2012). "Gpnmb/osteoactivin, an attractive target in cancer immunotherapy." Neoplasma **59**(1): 1-5.

9. Eidesstattliche Erklärung

Hiermit erkläre ich, dass ich die vorliegende Dissertation mit dem Thema „Investigating the properties of glioma-associated microglia/macrophages" eigenständig und ohne unerlaubte Hilfe angefertigt habe. Es wurden von mir ausschließlich die angegebene Quellen und Hilfen in Anspruch genommen.

Des Weiteren versichere ich, dass die vorliegende Arbeit nie in dieser oder einer anderen Form Gegenstand eines früheren Promotionsverfahrens war.

Berlin, den 3.12.2014

_____

Frank Szulzewsky

10.Curriculum vitae

Der Lebenslauf ist in der Online-Version aus Gründen des Datenschutzes nicht enthalten

11.Appendix

11.1. Publications

Georgieva, P.B., **Szulzewsky, F.**, Pannell, M., Kettenmann, H., Wolf, S.A. Microglia from a mouse model of schizophrenia show an impaired response in ATP dependent functions. In preparation.

Feng, X., **Szulzewsky, F.**, Yerevanyan, A., Hainzmann, D., Alvarez-Garcia, V., Zhou, H., Li, H., Kettenmann, H., Ransohoff, R., and Hambardzumyan, D. Loss of *Cx3cr1* increases migration of circulating Ly-6C^{hi} "inflammatory" monocytes into the CNS, enhances the glioma stem cell phenotype and promotes gliomagenesis. Accepted in Oncotarget.

Hoffmann, C.J., Harms, U., Rex, A., **Szulzewsky, F.**, Wolf, S.A., Sendtner, M., Kettenmann, H., Dirnagl, U., Endres, M., Harms, C. Vascular Stat3 Promotes Angiogenesis and Neuroplasticity Long-Term After Stroke. Circulation. 2015 Mar 20. pii: CIRCULATIONAHA.114.013003.

Szulzewsky F, Pelz A, Feng X, Synowitz M, Markovic D, Langmann T, Holtman IR, Wang X, Eggen BJ, Boddeke HW, Hambardzumyan D, Wolf SA, Kettenmann H. Glioma-associated microglia/macrophages display an expression profile different from M1 and M2 polarization and highly express *GPNMB* and *SPP1.* PLoS One. 2015 Feb 6;10(2):e0116644.

Pannell M, Meier MA, **Szulzewsky** F, Matyash V, Endres M, Kronenberg G, Prinz V, Waiczies S, Wolf SA, Kettenmann H. The subpopulation of microglia expressing functional muscarinic acetylcholine receptors expands in stroke and Alzheimer's disease. Brain Struct Funct. 2014 Dec 19.

Preissler, J., Grosche, A., Lede, V., Le Duc, D., Krugel, K., Matyash, V., **Szulzewsky, F.**, Kallendrusch, S., Immig, K., Kettenmann, H.*, et al*. Altered microglial phagocytosis in GPR34-deficient mice. Glia. 2015 Feb;63(2):206-15.

Vinnakota, K., Hu, F., Ku, M.C., Georgieva, P.B., **Szulzewsky, F.**, Pohlmann, A., Waiczies, S., Waiczies, H., Niendorf, T., Lehnardt, S.*, et al*. Toll-like receptor 2 mediates microglia/brain macrophage MT1-MMP expression and glioma expansion. Neuro Oncol. 2013 Nov;15(11):1457-68.

Bulavina, L., **Szulzewsky, F.**, Rocha, A., Krabbe, G., Robson, S.C., Matyash, V., and Kettenmann, H. NTPDase1 activity attenuates microglial phagocytosis. Purinergic Signal. 2013 Jun;9(2):199-205.

11.2. Abstracts/Talks

Szulzewsky, F., Pelz, A., Feng, X., Synowitz, M., Holtman, I.R., Boddeke, H.W.G.M., Hambardzumyan, D., Wolf, S.A., Kettenmann, H. Glioma-associated microglia/ macrophages display an expression profile distinct from M1 and M2 polarization. TMEN Junior Investigator Meeting 2014, Washington D.C., USA.

11.3. Abstracts/Posters

Szulzewsky, F., Pelz, A., Synowitz, M., Holtman, I.R., Boddeke, H.W.G.M., Wolf, S.A., Kettenmann, H. Identification of regulated genes in glioma-associated microglia/macrophages using microarray. Berlin Brain Days 2013, Berlin, Germany.

Szulzewsky, F., Pelz, A., Synowitz, M., Holtman, I.R., Boddeke, H.W.G.M., Wolf, S.A., Kettenmann, H. Identification of regulated genes in glioma-associated microglia/macrophages using microarray. SFB TRR 43 Symposium 2013, Goettingen, Germany.